Linear Stability Analyses of Poiseuille Flows of Viscoelastic Liquids

A thesis submitted for the degree of

Philosophiae Doctor of the University of Wales

December 2007

Alison Palmer

Institute of Mathematical and Physical Sciences

The University of Wales

Aberystwyth

Summary

The linear stability of the Giesekus and linear Phan-Thien Tanner (PTT) fluid models is investigated for a number of planar Poiseuille flows in single, double and triple layered configurations. The Giesekus and PTT models involve parameters that can be used to fit shear and extensional data, thus making them suitable for describing both polymer solutions and melts. The base flow is determined using a Chebyshev-tau method. The linear stability equations are also discretized using Chebyshev approximations to furnish a generalized eigenvalue problem which is then solved using the QZ-algorithm.

The eigenspectra are shown to comprise of continuous parts and discrete parts. The theoretical and numerical results are validated for the Oldroyd-B model, which is a simplified case of the Giesekus and PTT models, by comparing with results in the literature. The continuous and discrete parts of the eigenspectra are determined using a purely numerical scheme to solve the discretized eigenvalue problem. The continuous spectra are then more accurately determined using a semi-analytical scheme which uses an analytical solution of the Orr-Sommerfeld equation alongside a numerical solution for the base flow.

A comprehensive survey of the effect of each shear thinning and extensional fluid parameter is undertaken and an instability is found for particular parameter values for the Giesekus fluid. A preliminary investigation of this instability is undertaken whereby the unstable discrete eigenvalue is investigated using an Orthonormal Runge-Kutta scheme within a shooting method which uses the results from the Chebyshev-QZ scheme as a starting point. The linear PTT fluid is found to be stable to infinitesimal disturbances within the range of shear-thinning and extensional parameters considered. The computational efficiency and accuracy of the numerical methods are also investigated.

Declaration

This work has not previously been accepted in substance for any degree and is not being concurrently submitted in candidature for any degree.
Signed .....(candidate)
Date .....

Statement 1

This thesis is the result of my own investigations, except where otherwise stated. Other sources are acknowledged by citations giving explicit references. A bibliography is appended.
Signed .....(candidate)
Date .....

Statement 2

I hereby give consent for my thesis, if accepted, to be available for photocopying and for inter-library loan, and for the title and summary to be made available to outside organisations.
Signed .....(candidate)
Date .....

E-Thesis Deposit Agreement

Details of the Work

I would like to deposit the following item in the digital repository maintained by the University of Wales, Aberystwyth, or any other authorized for use by the University of Wales, Aberystwyth:

Linear Stability Analyses of Poiseuille Flows of Viscoelastic Liquids

This item is a product of my own research endeavours and is covered by the agreement below in which the item is referred to as "the Work". It is identical in content to that deposited in the Library.

Non-exclusive Rights

Rights granted to the digital repository through this agreement are entirely non-exclusive. I am free to publish the Work in its present version or future versions elsewhere.

I agree that the University of Wales, Aberystwyth may electronically store, copy or translate the Work to any approved medium or format for the purpose of future preservation and accessibility. The University of Wales, Aberystwyth is not under any obligation to reproduce or display the Work in the same formats or resolutions in which it was originally deposited.

UWA Digital Repository

I understand that work deposited will be accessible to a wide variety of people and institutions, including automated agents and search engines via the World Wide Web.

I understand that once the Work is deposited, metadata will be incorporated into public access catalogues.

I agree as follows:

- That I am the author and do hereby give the University of Wales, Aberystwyth the right to make available the Work in the way described above.
- That the electronic copy of the Work deposited in the digital repository and covered by this agreement, is identical to the paper copy of the Work deposited in the Library of the University of Wales, Aberystwyth.
- That I have exercised reasonable care to ensure that the Work is original, and to the best of my knowledge, does not breach any laws including those relating to defamation, libel and copyright.
- That I have, in instances where the intellectual property of other authors or copyright holders is included in the Work, gained explicit permission for the inclusion of that material in the Work and in the electronic form of the Work as accessed through the open digital repository, *or* that I have identified that material for which adequate permission has not been obtained and which will be inaccessible via the digital repository.
- That the University of Wales, Aberystwyth does not hold any obligation to take legal action on behalf of the Depositor, or other rights holders, in the event of a breach of intellectual property rights, or any other right, in the material deposited.
- That I undertake to indemnify the University of Wales, Aberystwyth against all actions, suits, proceedings, claims, demands and costs occasioned by the University in consequence of any breach of this agreement.

Signed ..... Date .....

Acknowledgements

Thanks to...

- Prof Tim Phillips for being my supervisor, for being knowledgeable, encouraging and above all, patient.

- The *EPSRC* for providing a Research Studentship, without which none of this would have ever been possible.

- The *Numerical Algorithms Group* (*NAG*) for the temporary licence.

- My examiners, Dr Rob Douglas and Prof Sean McKee, for their informative discussions.

- The many people, too many to name them all, who have encouraged me to persevere and have kept me alive whilst I tried to do so.

- My family: Mum, Dad, Simon, Zuzana (and the next generation), for their unwavering love and support, for answering the phone at all hours and for caring enough to interfere even when I didn't want them to.

- My partner Jeff for helping me through the tough and stressful last days, for staying up all night with me and for getting me drunk when it is all over.

- and James for making me laugh and educating me on the importance of Wrestling, *Haribos* and *GTA*.

Contents

List of Figures

Chapter 1

Introduction

1.1 Viscoelastic Liquids

Viscoelastic liquids have both viscous and elastic properties. Considering the extreme cases of a perfectly elastic solid which obeys Hooke's law, and a perfectly viscous liquid which obeys Newton's law (a Newtonian liquid), then a viscoelastic liquid could be considered to lie somewhere in between. In the case of a perfectly elastic solid the stress experienced by the solid is directly proportional to the strain. For a perfectly viscous liquid the stress is directly proportional to the rate of strain. Therefore, in the case of viscoelastic liquids, the stress is neither directly proportional to the strain nor the rate of strain, but the relationship is more complex [24].

It is due to these complex relationships between stress, strain and rate of strain that viscoelastic liquids have many useful properties, and so there is a need to study such materials. This area of fluid dynamics has been increasingly relevant over recent decades with

the advent and growth of the synthetic polymers (plastics) industries and their applications to a variety of roles, from clothing and foods to pharmaceuticals and even bank-notes [3].

To be of any practicable use, however, it is often necessary to process these viscoelastic fluids before they can be incorporated into the final product. A common process is *extrusion* whereby the polymer is forced through a 'die' under pressure. The 'extrudate', the polymer which exits the die, is then taken as the final product, or onto the next stage of processing as required. Examples of extrudates are copper piping, titanium aircraft components (seat tracks, engine rings), pasta and road markings (see [4]). *Co-extrusion* is also increasingly common for situations where a combination of materials is required so as to incorporate the different properties of each component.

A major criteria for the success of extrusion and co-extrusion processes is the quality of the extrudate. It is generally accepted that any deformities or irregularities in the extrudate (for example, melt fractures [49, 50]) can be explained by instabilities in the flow within the die. For obvious reasons, these irregularities and ways of controlling them are important areas of research.

It is the aim in this thesis to make some headway into a further understanding of these features. The die is modelled as a one-dimensional planar channel through which the viscoelastic fluid experiences pressure driven Poiseuille flow. Two viscoelastic fluid models, the Giesekus and linear Phan-Thien Tanner (PTT) models, are investigated in one-, two- and three-layered flows and the eigenspectra are sought, with the intention of investigating any instabilities which arise.

There has been much work on channel flows of viscoelastic fluids in the literature. Poiseuille flow, and its frequent companion Couette flow are often used as benchmark tests for new constitutive equations [29, 33, 46, 63] and there has been much interest in instabilities in Couette flow of viscoelastic liquids (see [11, 32, 35, 36, 44, 55, 56, 57, 58, 59]) since Gorodtsov and Leonov [30] calculated two modes in 1967. Poiseuille flows however, do not appear to have been so comprehensively covered, although some features of the literature are discussed in the next Section. This is not intended to be a full literature survey, rather it is intended that the main issues which are relevant to the investigations in this thesis are discussed.

1.2 Poiseuille Flows

Planar Poiseuille flow of a Newtonian fluid is an elementary mathematical problem. Instabilities in multilayered Poiseuille flows are another matter however. In 1967 Yih showed that viscosity stratification across two Newtonian fluids in Poiseuille flow can cause an instability [69]. The unstable modes were discovered to be in the region of a previously known neutral mode for the single fluid case, hence implying the importance of an investigation of the full eigenspectrum as opposed to considering only unstable modes. Two-layered Poiseuille flows of Newtonian fluids were still being studied as (relatively) recently as 1989 when Y. Renardy performed a weakly-nonlinear analysis and gave details of the resulting bifurcations [59]. In the following year Anturkar *et al.* took a new approach to an old problem and undertook a comprehensive linear stability analysis of n-layered Poiseuille flow [7].

A stability analysis of planar Poiseuille flow of a non-Newtonian fluid was performed by

Porteous and Denn in 1972 [53, 54]. The viscoelastic fluid models of a second-order fluid and a Maxwell fluid were investigated and a new 'elastic' mode of the Orr-Sommerfeld equation was determined. Elasticity was found to be destabilizing for finite disturbances.

Purely elastic interfacial instabilities were further examined by Su and Khomami [62] in 1992 and the cause of the instabilities was found to be a jump in the first normal stress difference across the interface. They also proposed that elastic instabilities would have a greater impact in experimental situations than instabilities which are driven wholly or in part by viscosity. The later experimental investigations of Khomami and Su [39] and Khomami *et al.* [38] were able to provide observations of purely elastic and purely viscous instabilities for the first time. Their experimental results showed good correlation to their theoretical calculations for Boger fluids and again, elasticity was determined to play a major role in the stability of these flows, corroborating the predictions of Su and Khomami [62].

The linear stability of two- and three-layered Poiseuille flows of Oldroyd-B fluids was investigated by Laure *et al.* using a longwave and moderate wavelength analysis [42]. They found that for the case of three symmetric layers (identical to that shown in Fig. 3.4) the critical wavelength is dependent on the thickness ratio between the fluid layers. For the two layered flow the critical wavelength is only weakly dependent on the thickness ratio.

Almost simultaneously Wilson and Rallison [64] considered specifically the effects of elasticity on the symmetric three-layered Poiseuille flow of Oldroyd-B and UCM fluids. A short wave disturbance was found and investigated and for dilute Oldroyd-B fluids, where there is a small concentration of the viscometric solute (see Section 2.2.2), this was found

to be unstable with a maximum growth rate at moderate elasticity and a decreasing growth rate when elasticity is high in at least one fluid. For UCM fluids the disturbance was found to be unstable, but restabilises if the elasticity stratification is high.

The analyses of three-layered Poiseuille flow was continued by Scotto and Laure [61] who considered a non-symmetric flow geometry. They determined that the most dangerous modes were in the short wavelength limit at large Weissenberg numbers.

An in depth study of the form of the full eigenspectra for a UCM and an Oldroyd-B fluid in single layered Poiseuille flow has been undertaken by Wilson *et al.* [65]. This study is frequently referred to in this thesis and the work contained herein can be considered an extension of parts of Wilson *et al.*'s investigation. Their findings for the structure of the eigenspectra are similar to those given in Chapter 6, and a fuller discussion is provided there. A similar study of the structure of the eigenspectra was performed by Grillet *et al.* [31] for a Giesekus and an exponential Phan-Thien Tanner fluid. Again, these results correspond well with those given in Chapter 6 and again, this is discussed in more detail there.

Studies of more rheologically complex fluids are becoming more common in recent years. For example, the work of Bogaerds *et al.* for the eXtended Pom-Pom model [9] and Kwon's work on the Doi-Edwards model [40], a derivation of which is shown in Chapter 2 along with the derivations of the Giesekus and Phan-Thien Tanner models which are to be used in the investigations shown in later Chapters.

Chapter 2

Viscoelastic Constitutive Equations

The work contained in this thesis is chiefly concerned with the flows of Giesekus and linear Phan-Thien Tanner (PTT) fluids. These are two models for viscoelastic fluids which are described by constitutive equations which are required to be solved alongside the conservation equations in order to elucidate any information about the flows in question. Both of these constitutive equations are derived from macro-molecular considerations of polymer melts and polymer solutions in Newtonian solvents. What follows is an overview of the derivations of these constitutive equations as well as some details of other fluid models considered to be of relevance.

2.1 The Navier-Stokes Equations

Firstly, the Navier Stokes equations are described. These are the mathematical statements of the conservation of momentum,

$$\rho\frac{\mathrm{D}\mathbf{u}}{\mathrm{D}t} = -\nabla p + \nabla.\mathbf{T}, \tag{2.1}$$

and the conservation of mass,

$$\nabla.\mathbf{u} = 0. \tag{2.2}$$

When the fluid in question is viscoelastic the polymeric part of the stress tensor $\boldsymbol{\tau}$ may be separated from the Newtonian part so that

$$\mathbf{T} = \boldsymbol{\tau} + \eta_s\left(\nabla\mathbf{u} + (\nabla\mathbf{u})^{\mathrm{T}}\right).$$

The equation for conservation of momentum can then be written in the form

$$\rho\frac{\mathrm{D}\mathbf{u}}{\mathrm{D}t} = -\nabla p + \nabla.\boldsymbol{\tau} + \eta_s\nabla^2\mathbf{u}. \tag{2.3}$$

Here $\mathrm{D}/\mathrm{D}t$ is the material derivative and is given by

$$\frac{\mathrm{D}\mathbf{u}}{\mathrm{D}t} = \frac{\partial\mathbf{u}}{\partial t} + (\mathbf{u}.\nabla)\mathbf{u}.$$

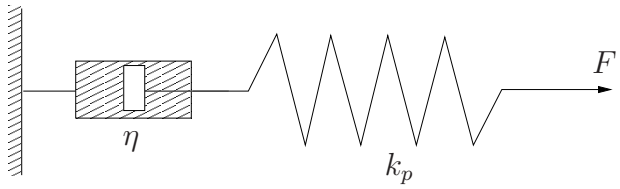

Figure 2.1: The spring and dashpot of the Maxwell model.

Clearly **u** represents the fluid velocity vector, t is time and p is the fluid pressure. The solvent viscosity η_s and the fluid density ρ are the only material parameters required for the calculation of flows of Newtonian fluids. For non-Newtonian fluids where a polymeric viscosity is present the polymeric stress $\boldsymbol{\tau}$ is non-zero and an additional constitutive equation is required for the solution of flow problems. The following Sections describe the derivation of some constitutive equations relevant to the work in later Chapters of this thesis.

2.2 Basic Viscoelastic Models

2.2.1 The Upper-Convected Maxwell Model

The upper-convected Maxwell (UCM) model is derived by representing a viscoelastic fluid as a spring and dashpot in series as shown in Fig. 2.1. The spring obeys Hooke's law for solids and the dashpot obeys the Newtonian law for viscosity. Hence a model can be derived which incorporates both fluid and solid properties and is a likely representation of a viscoelastic fluid. Together the spring and dashpot are known as a Maxwell element. The parameter k_p is the spring constant, defined as the ratio of force acting on the spring to the displacement of the spring. The parameter η is the viscosity of the Maxwell fluid. The rate

of change of displacement of the element can be expressed as the sum of the individual rates of change of the displacement of the spring and dashpot. Applying the subscripts 1 to the spring and 2 to the dashpot the total rate of displacement is expressed as

$$\frac{\mathrm{d}\gamma}{\mathrm{d}t} = \frac{\mathrm{d}\gamma_1}{\mathrm{d}t} + \frac{\mathrm{d}\gamma_2}{\mathrm{d}t} = \frac{\mathrm{d}}{\mathrm{d}t}\left(\frac{F_1}{k_p}\right) + \frac{F_2}{\eta}.$$

The forces F_1 and F_2 are equal since the spring and dashpot are in series. Hence, putting $F_1 = F_2 = F$, the total rate of displacement becomes

$$\frac{\mathrm{d}\gamma}{\mathrm{d}t} = \frac{1}{k_p}\frac{\mathrm{d}F}{\mathrm{d}t} + \frac{F}{\eta}.$$

Regarding the force F as the total stress in the fluid, the rate of displacement $\mathrm{d}\gamma/\mathrm{d}t$ as the rate of deformation of the fluid and introducing the relaxation time $\tau_{\mathrm{UCM}} = \frac{\eta}{k_p}$ (the time taken for the molecules to relax after experiencing an instantaneous stretch due to a step strain being applied on the fluid) leads to the following tensor equation

$$\mathbf{T} + \tau_{\mathrm{UCM}}\frac{\partial \mathbf{T}}{\partial t} = 2\eta\mathbf{d} \tag{2.4}$$

where $\mathbf{T}$ is the total stress and the rate of deformation tensor $\mathbf{d}$ is defined as

$$\mathbf{d} = \frac{1}{2}\left(\nabla\mathbf{u} + (\nabla\mathbf{u})^{\mathrm{T}}\right).$$

A final adjustment is required before the UCM equation is derived. The time derivative

here is indifferent to changes of reference frame, hence the Eulerian time derivative $\partial/\partial t$ is replaced by an invariant derivative. In general form, the invariant derivative of a tensor $\mathbf{A}$ is

$$\frac{\delta \mathbf{A}}{\delta t} = \frac{D\mathbf{A}}{Dt} - \mathbf{G}.\mathbf{A} - \mathbf{A}.\mathbf{G}^{\mathrm{T}}$$

where D/Dt is the material derivative as defined in the previous Section. The tensor $\mathbf{G}$ is defined by

$$\mathbf{G} = \left(1 - \frac{\varphi}{2}\right) \nabla \mathbf{u} - \frac{\varphi}{2} \left(\nabla \mathbf{u}\right)^{\mathrm{T}}.$$

This invariant time derivative is also known as the Johnson-Segalman derivative and is described in a later Section. A special case of this invariant derivative is when $\varphi = 0$. This is known as the upper-convected derivative

$$\overset{\triangledown}{\mathbf{A}} = \frac{D\mathbf{A}}{Dt} - \left(\nabla \mathbf{u}\right).\mathbf{A} - \mathbf{A}.\left(\nabla \mathbf{u}\right)^{\mathrm{T}}.$$

This is the most frequently used form of the invariant derivative since the UCM model predicts physically relevant results, in particular it gives a positive first normal stress difference and a zero second normal stress difference which is in qualitative agreement with experimental data.

By employing the upper-convected derivative into the Maxwell model, equation (2.4) becomes

$$\mathbf{T} + \tau_{\mathrm{UCM}} \overset{\triangledown}{\mathbf{T}} = 2\eta \mathbf{d} \tag{2.5}$$

where the upper-convected derivative of the stress tensor is

$$\overset{\triangledown}{\mathbf{T}} = \frac{\partial \mathbf{T}}{\partial t} + \mathbf{u}.\nabla\mathbf{T} - (\nabla\mathbf{u}).\mathbf{T} - \mathbf{T}.(\nabla\mathbf{u})^{\mathrm{T}}.$$

The UCM model for viscoelastic equations is one of the most important models in rheological research since many other more complicated or more recent models are extensions of this model. Although there have been several different approaches to the mechanical theories behind the derivations of viscoelasic fluid models, many successful models have been shown to reduce to the UCM model for certain parameter values. Thus a study of the UCM model is an obvious first step in much rheological research.

2.2.2 The Oldroyd-B Model

The Oldroyd-B model is an extension of the UCM model which considers fluids consisting of a viscoelastic solute dissolved within a Newtonian solvent. Hence the fluid is considered in two parts, a polymeric part with viscosity η_p which is well described by the UCM model and a Newtonian part with viscosity η_s for which extra terms are necessary. The leads to a choice for the conservation of momentum equation as given by equation (2.3), as opposed to that given by equation (2.1). The constitutive equation includes an extra term for the Newtonian part of the fluid and an extra constant, referred to as the retardation time. Thus the Oldroyd-B constitutive equation is

$$\mathbf{T} + \tau_{\mathrm{UCM}}\overset{\triangledown}{\mathbf{T}} = 2\eta_t\left(\mathbf{d} + \tau_{\mathrm{O-B}}\overset{\triangledown}{\mathbf{d}}\right), \tag{2.6}$$

where $\tau_{\mathrm{O-B}}$ is the retardation time of the solvent part of the fluid and $\eta_t = \eta_s + \eta_p$ is the total viscosity. Splitting the stress tensor as in Section 2.1

$$\mathbf{T} = \boldsymbol{\tau} + 2\eta_s \mathbf{d}$$

the constitutive equation (2.6) can be written in terms of the polymeric stress only. Also the viscosities and relaxation times of the two parts of the fluid are related thus;

$$\frac{\tau_{\mathrm{O-B}}}{\tau_{\mathrm{UCM}}} = \frac{\eta_s}{\eta_s + \eta_p}.$$

Hence the Oldroyd-B constitutive equation becomes

$$\boldsymbol{\tau} + \tau_{\mathrm{UCM}} \overset{\triangledown}{\boldsymbol{\tau}} = 2\eta_p \mathbf{d}. \tag{2.7}$$

2.2.2.1 The Jeffreys Model

The Jeffreys model is a spring dashpot representation of the Oldroyd-B model and is shown in Fig. 2.2. From this physical representation the addition of a second dashpot in parallel has been used to add the effect of a Newtonian solvent into the fluid model. A derivation similar to that undertaken to derive the UCM model gives rise to the Oldroyd-B equations as given above.

As previously mentioned both the UCM and Oldroyd-B models give qualitatively accurate results for the stress differences, however these are not quantitatively accurate since

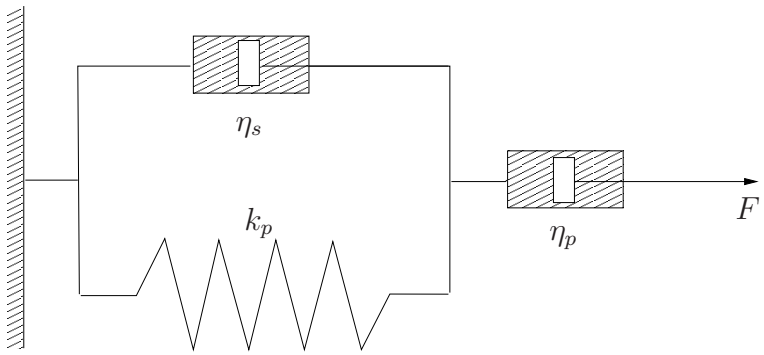

Figure 2.2: The spring and dashpot of the Jeffreys model, an illustrative example of an Oldroyd-B fluid.

experiments predict opposite signs for the first and second normal stress differences. These models also predict an infinite extensional viscosity when a critical extensional strain rate is exceeded in steady shearing flows. They also neglect shear-thinning effects which is a poor assumption for some viscoelastic fluids.

In the next Section a different approach to the derivation of constitutive equations is described, which relies on specific assumptions at the molecular level. A number of relevant models are introduced and their relationship to the UCM and Oldrold-B models is explained.

2.3 Molecular Considerations

The derivation of constitutive equations can be based either on continuum mechanics, mathematics (rational continuum mechanics), molecular physics or thermodynamics. The models in the previous Section are derived under a continuum assumption, i.e. that any molecular interactions are averaged out at a larger scale. This is not necessarily true for many viscoelastic liquids however. The stresses in a polymeric liquid are associated with the

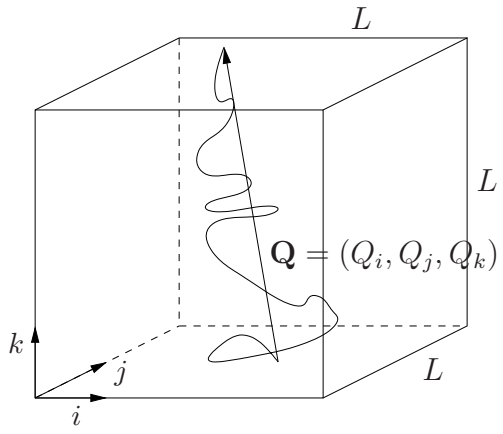

Figure 2.3: A volume element of volume L^3, containing a number of polymer chains of which one is shown.

configurations of the polymer molecules, the forces carried by the molecule and, in the cases of branched polymers, by the different forces acting on different parts of the molecules. Thus, the molecular physics method is the most favoured in recent years since most rheological constants can be derived from molecular parameters e.g. molecular weight, end-to-end length etc. In the following Sections molecular physics is used to consider intra- or inter- molecular dynamics as some common models for polymer molecules are described.

2.3.1 Polymer Chains

Many constitutive equations have been developed from the assumption that a polymer molecule can be modelled as a chain or as a number of subchains with links between them. Considering a number of polymer chains in a volume element of volume L^3, as shown in Fig. 2.3, then the total stress is found by summing all of the contributions from each subchain in the volume. Denoting the end-to-end vector of one of these subchains by $\mathbf{Q}$ and the force

carried by that subchain as **F** then the probability that this chain will cut the j-plane in the volume element is Q_j/L and so the contribution to the stress **T** from this particular subchain is F_iQ_j/L^3. The average number of subchains of molecular weight M_c in the volume element is $\rho L^3/M_c$. Summing over all of the subchains in the volume element gives

$$T_{ij} = \frac{\rho N_A}{M_c} < F_iQ_j > \tag{2.8}$$

where $< . >$ denotes an averaging over the volume, or an 'ensemble average', ρ represents the density of the fluid and N_A is Avogadro's constant (the number of molecules in a quantity of that molecule whose mass is equivalent to that molecule's molecular weight: $N_A = 6.02214199 \times 10^{23}$ per mole [2]).

2.3.1.1 Gaussian Chains

A possible assumption for a chain model of a polymer molecule is that it can be modelled as a number of Gaussian chains. This means that the equilibrium orientation of each chain is random. Consider a chain with N_c links of length b. Assuming that each link aligns itself independently of the orientation of any of the other links then, in the absence of flow, the configuration of the polymer chain is essentially a random walk. Thus, from the theory of random walks, the end-to-end length of the entire polymer chain is $b\sqrt{N_c}$.

The entropic force in the polymer chain arises from the Brownian motion of the chain as it attempts to restore itself to its equilibrium configuration. For small departures from

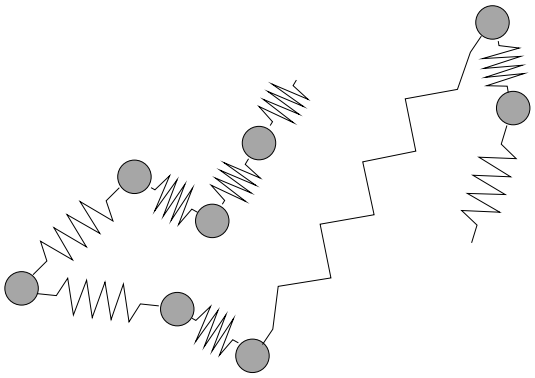

Figure 2.4: The Rouse spring and bead model for a polymer molecule.

equilibrium the force in a subchain of N_c links obeys Hookes law such that

$$\mathbf{F} = \frac{3kT_a}{N_c b^2}\mathbf{Q} \tag{2.9}$$

where k is Boltzmann's constant ($1.3807 \times 10^{-23}\text{JK}^{-1}$ [1]), T_a is the absolute temperature and $\mathbf{Q}$ is the end-to-end vector of the polymer chain which was introduced in the previous Section. Substituting equation (2.9) into equation (2.8) leads to an expression for the total stress on the molecule as

$$\mathbf{T} = \frac{3\rho R_g T_a}{M_c} < \frac{\mathbf{QQ}}{N_c b^2} >, \tag{2.10}$$

where $R_g = N_A k$ is the gas constant and again, $< . >$ denotes an ensemble average.

2.3.1.2 The Rouse Model: Springs and Beads

The main assumption of the Rouse model [60] is to consider the polymer chain to be a 'necklace' of N_R beads connected together by springs of length b as shown in Fig 2.4. Rouse

assumes that each bead experiences a frictional resistance of $\zeta_R \mathbf{u}_{\text{rel}}$, where $\mathbf{u}_{\text{rel}}$ is the relative velocity between the fluid and the bead and the friction coefficient ζ_R is proportional to the solvent viscosity η_s. This leads to a prediction for the relaxation modulus $G(t)$,

$$G(t) = \frac{\rho Q T_a}{M} \sum_{n=1}^{\infty} e^{-\frac{2n^2 t}{\tau_R}},$$

where M is the molecular weight of the whole chain and

$$\tau_R = \frac{\zeta N^2 b^2}{3\pi^2 k T_a}$$

is the Rouse relaxation time.

2.3.1.3 Kramers Bead and Rod Model

A Kramers freely jointed bead-rod chain is shown in Fig. 2.5. This chain consists of N identical beads of mass m, linked linearly by $N-1$ massless rigid rods of length b. This is the molecular model chosen by Curtiss and Bird [15, 16] for their analysis which is discussed in Section 2.4.2.

Unit vectors associated with the kth rod are the triad $\hat{\mathbf{u}}_k$, $\hat{\mathbf{v}}_k$ and $\hat{\mathbf{w}}_k$ and are shown in Fig. 2.5. Here $\hat{\mathbf{v}}_k$ lies on the plane which passes through the point P and the beads k and

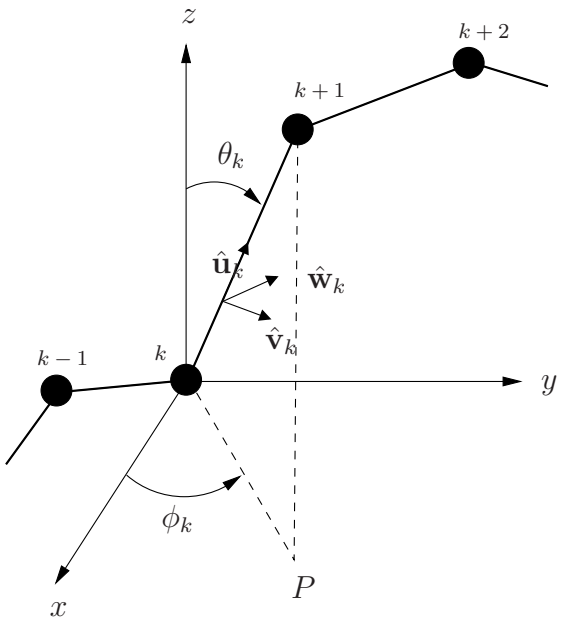

Figure 2.5: The Kramers bead and rod model for a polymer molecule. Figure taken from [15].

$k+1$, and $\hat{\mathbf{w}}_k$ is perpendicular to the same plane. These are defined by

$$\hat{\mathbf{u}}_k = (\sin\theta_k \cos\phi_k, \sin\theta_k \sin\phi_k, \cos\theta_k)\,,$$

$$\hat{\mathbf{v}}_k = (\cos\theta_k \cos\phi_k, \cos\theta_k \sin\phi_k, -\sin\theta_k)\,,$$

$$\hat{\mathbf{w}}_k = (-\sin\phi_k, \cos\phi_k, 0)\,.$$

The orientation of the kth rod, between beads k and $k+1$, is described by the unit vector $\hat{\mathbf{u}}_k$, or alternatively by θ_k and ϕ_k, the two polar angles associated with $\mathbf{u}_k$. The location of the nth bead can be expressed by the position vector $\mathbf{r}_n$ with respect to an arbitrary coordinate system, or by the vector $\mathbf{R}_n = \mathbf{r}_n - \mathbf{r}_c$ with respect to the position of the centre of mass of

the molecule, $\mathbf{r}_c$ given by

$$\mathbf{r}_c = \frac{1}{N}\sum_n \mathbf{r}_n.$$

The bead coordinates and rod orientation vectors are thus related by the following expressions:

$$b\hat{\mathbf{u}}_k = \mathbf{r}_{k+1} - \mathbf{r}_k = \sum_n \bar{B}_{kn}\mathbf{r}_n,$$

$$\mathbf{R}_n = \mathbf{r}_n - \mathbf{r}_c = b\sum_k B_{nk}\hat{\mathbf{u}}_k.$$

Here

$$\bar{B}_{kn} = \delta_{k+1,n} - \delta_{kn},$$

$$B_{nk} = \begin{cases} \frac{k}{N} & \text{for } k < n \\ \frac{k}{N} - 1 & \text{when } k \geq n \end{cases}$$

In their analysis Curtiss and Bird [15, 16] employ the Kramers matrix

$$C_{ij} = \sum_n B_{ni}B_{nj} = \begin{cases} \frac{i(N-j)}{N} & \text{if } i \leq j, \\ \frac{j(N-i)}{N} & \text{if } j \geq i, \end{cases}$$

and the Rouse matrix

$$A_{ij} = \sum_n \bar{B}_{in}\bar{B}_{jn} = \begin{cases} 2 & \text{if } i = j, \\ -1 & \text{if } i = j \pm 1, \\ 0 & \text{otherwise,} \end{cases}$$

which are inverse to one another. A modified Rouse matrix with components

$$\tilde{A}_{ij} = A_{ij}\left(\hat{\mathbf{u}}_i - \hat{\mathbf{u}}_j\right)$$

and the inverse of this, a modified Kramers matrix with components $\tilde{C}_{ij}$ are also defined, as well as a set of 'Kramers tensors'

$$\mathbf{K}_{ij} = C_{ij}\delta - \tilde{C}_{ij}\hat{\mathbf{u}}_i\hat{\mathbf{u}}_j.$$

The above definitions provide the basis from which Curtiss and Bird re-derived the Doi-Edwards constitutive equations [18, 19, 20, 21, 22] using their own phase-space theory [14]. These models are discussed in further detail in Section 2.4.

2.3.2 The Concept of Reptation

The concept of reptation describes the fact that the motion of a polymer molecule, when surrounded by other molecules, is often restricted, and frequently to such an extent that the possible movements of the molecule are reduced to snake-like movements along the

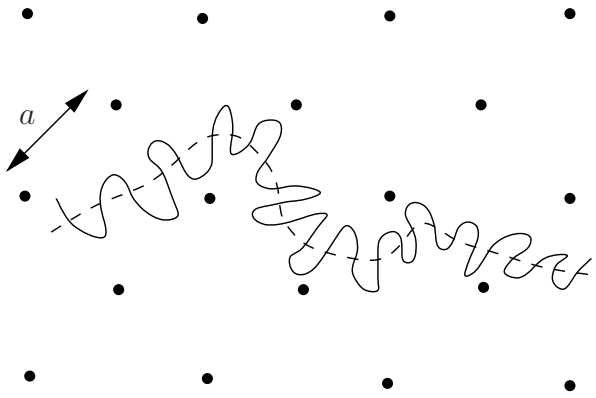

Figure 2.6: The cage model. Here the primitive chain is denoted by the dashed line.

orientation of the molecule. The name reptation was first proposed by DeGennes [17] as a metaphor for this snake-like type of motion. The following three equivalent molecular models consider this idea in more detail.

2.3.2.1 The Cage Model

A schematic illustration of the cage model is shown in Fig. 2.6. Here the polymer molecule under consideration is regarded as being contained within a fixed 'cage field' of mesh size a, an averaged representation of the surrounding molecules. The movements of the molecule are restricted within a tube-like boundary around the molecule, the central line of which is taken to be the 'primitive chain' to which a suitable chain model may be applied. Clearly the assumption that the surrounding cage field is fixed can be brought to question. Since the cage is an averaged representation of the surrounding molecules, then it must fluctuate as the surrounding molecules move. However, in the case of high concentrations of long chains any fluctuation within the cage is unlikely to be on the same scale as the individual polymer

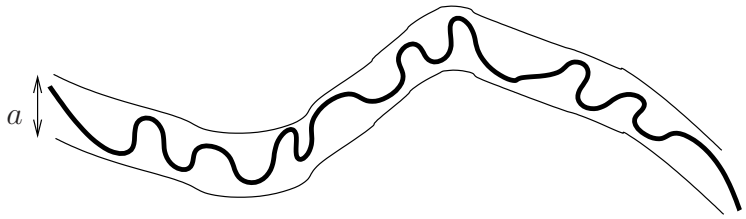

Figure 2.7: The tube model. The polymer molecule is confined within a tube of diameter a.

chain since such a fluctuation would entail unrealistically large movements of a large number of long chains. For lower concentrations and for shorter polymer molecules, other models would be recommended, since the assumption of the fixed cage field is less suitable in these cases.

2.3.2.2 The Tube Model

The theory of tube models is based upon the assumption that a polymer chain is restricted in its configuration and movements by the surrounding polymer molecules, similarly to the cage model. It is assumed that each individual polymer molecule can be considered to be essentially confined within an imaginary tube of diameter a, the value of which is defined by the positions of the surrounding molecules as shown in Fig. 2.7. This idea was first introduced by Edwards [23] and is used in the derivation of the Doi-Edwards constitutive equation [18, 19, 20, 21, 22] which is discussed in Section 2.4.1. This tube assumption enables each polymer molecule to be considered independently and is particularly useful when modelling highly entangled polymers, since without this assumption it would be necessary to simultaneously take into account the dynamics of a large number of interacting polymer

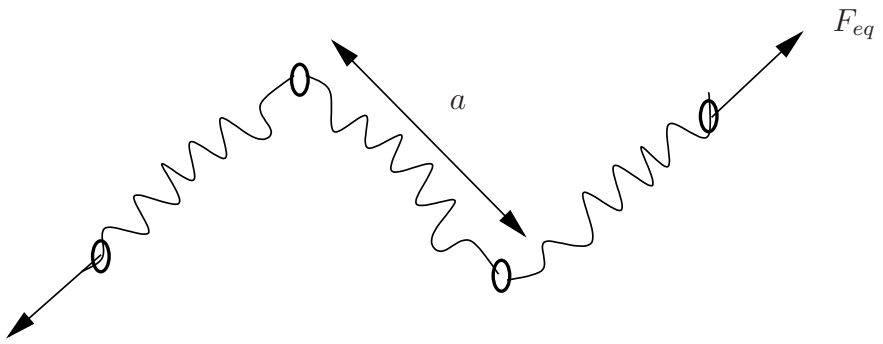

Figure 2.8: The slip-link network model.

molecules, making the derivation of constitutive equations highly difficult.

2.3.2.3 The Slip-Link Network Model

Fig. 2.8 shows the slip-link network model for a polymer molecule. In this network the junctions are small rings through which a chain can pass freely, and the molecule is also allowed to move freely between the slip-links. In an equilibrium state these links are separated by a distance a which can be regarded to be equivalent to the cage mesh size in Section 2.3.2.1 or the tube diameter in Section 2.3.2.2. In this model the line segment between two slip-links is defined as the primitive chain.

Since the only constraint on the polymer molecule is that it passes through the points at the slip-links an additional constraint is required to prevent shrinkage of the end-to-end length by lateral expansion, as shown in the situation in Fig. 2.9. Applying the assumption that there exist two Maxwell 'demons' pulling outwards on the chain at the chain ends with a constant tensile force F_{eq} (shown in Fig. 2.8). Following elementary statistical mechanical theory of chains a force of magnitude $3kTl_{sl}/nb^2$ is required to keep the chain segment in the

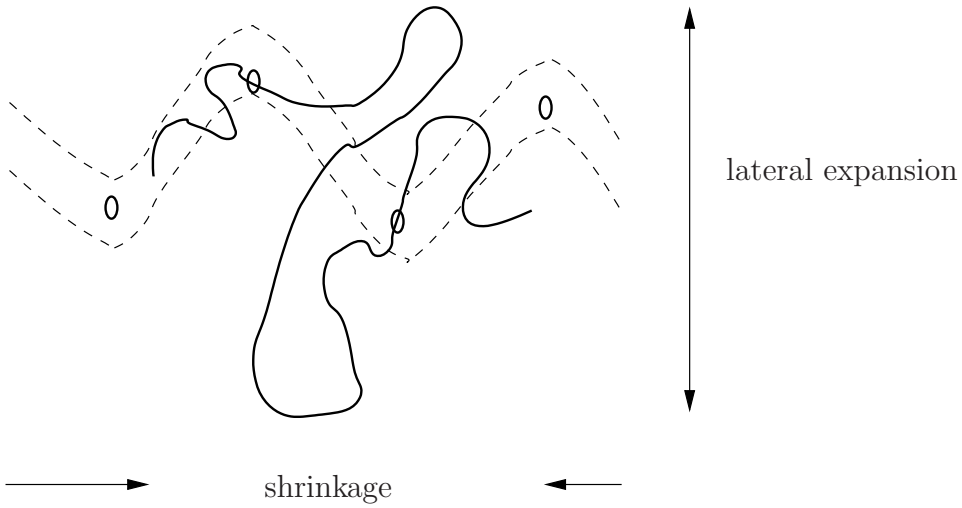

Figure 2.9: The potential for shrinkage due to lateral expansion in an unconstrained slip-link model (shown by the solid line) and the alternative spacial restriction imposed by the tube model (shown by the dashed lines).

form of n monomers at relative distance l_{sl}. The arc length of the polymer chain in question is $L_{sl} = N_0 b^2/a$ where N_0 is the degree of polymerization. Hence the magnitude of the force exerted by each of the Maxwell demons is [20]

$$F_{eq} = \frac{3kTL_{sl}}{N_0 b^2} = \frac{3kT}{a}.$$

This slip-link network model provides a simple molecular mechanism for the break-up and creation of links within the chain of monomers through the simple sliding of the chain through the slip-links. This also allows for n, the number of monomers in the chain, to be changeable. Doi and Edwards showed that this element of the model could be used to explain the non-Gaussian elastic reponse of a polymeric liquid [20].

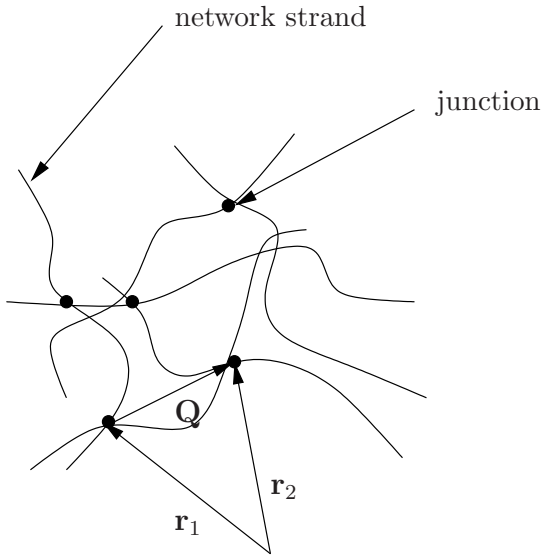

Figure 2.10: A network of polymer molecules. The end-to-end vector of a 'network strand' is denoted by $\mathbf{Q}$, and $\mathbf{r}_i$ are the position vectors of 'junctions' with respect to an arbitrary coordinate system.

2.3.3 Lodge-Yamamoto Network Theory

In the previous Sections the models which have been examined are of individual polymer molecules within the fluids in question. In the Lodge-Yamamoto network theory described in this Section the fluid is considered as a network of entangled polymer molecules such that the interactions of several molecules within the fluid can be considered simultaneously. This temporary network of polymer molecules contains junctions at the points where molecules are entangled as shown in Fig. 2.10. These junctions are allowed to move within the fluid and can also be created and destroyed. The junctions are allowed to slip so that the strand stretching and total motion of the fluid are not necessarily related by an affine transformation. Each 'network strand' is represented by an end-to-end vector $\mathbf{Q}$.

Considering the motion of an arbitrary junction with position vector $\mathbf{r}(t)$ over time $\triangle t$

then

$$\mathbf{r}(t+\triangle t) = \mathbf{r}(t) + \mathbf{L}\mathbf{r}\triangle t + \boldsymbol{\alpha}_s \triangle t$$

where $\boldsymbol{\alpha}_s$ is the 'slip' vector and $\mathbf{L} = \nabla\mathbf{u}$ is the velocity gradient tensor. It is assumed that $\mathrm{tr}(\mathbf{L}) = 0$ and hence this model applies only to incompressible flows, i.e. liquids.

For each network strand

$$\begin{aligned}\mathbf{Q}(t+\triangle t) =& \mathbf{r}_2(t+\triangle t) - \mathbf{r}_1(t+\triangle t)\\ =& \mathbf{Q}(t) + \mathbf{L}\mathbf{Q}\triangle t + \left(\boldsymbol{\alpha}_s(\mathbf{r}_2) - \boldsymbol{\alpha}_s(\mathbf{r}_1)\right)\triangle t.\end{aligned}$$

To first order this is

$$\dot{\mathbf{Q}}(t) = \mathbf{L}\mathbf{Q} + \frac{\partial \boldsymbol{\alpha}_s}{\partial \mathbf{r}}\mathbf{Q}. \tag{2.11}$$

When the slip tensor, $\partial\boldsymbol{\alpha}_s/\partial\mathbf{r}$ is equated to zero then this is the affine transformation which was customarily assumed before the derivation of the PTT model (which is given in Section 2.4.4). Alternatively, assuming that the slip tensor is a tensor-valued function of the stretching rate $\mathbf{d}_{\mathrm{PTT}}$ and the end-to-end vector $\mathbf{Q}$ then it can be shown, using a representation theorem [43] that equation (2.11) can be written as

$$\dot{\mathbf{Q}} = \mathbf{L}\mathbf{Q} - \chi\mathbf{Q} - \xi_\alpha \mathbf{d}_{\mathrm{PTT}}\mathbf{Q}, \tag{2.12}$$

where

$$\mathbf{d}_{\mathrm{PTT}} = \frac{1}{2}\left(\mathbf{L} + \mathbf{L}^{\mathrm{T}}\right)$$

and χ and ξ_α are constants.

An alternative to equation (2.11) was proposed by Phan-Thien [51] whereby the relative motion of the junctions is described by the equation

$$\dot{\mathbf{Q}} - \boldsymbol{\omega}\mathbf{Q} = \mathcal{F}\left(\mathbf{d}_{\mathrm{PTT}}, \mathbf{Q}\right), \tag{2.13}$$

which considers the individual network strands as opposed to considering the motion of the network as a whole. Here $\boldsymbol{\omega}$ is the vorticity tensor and $\mathcal{F}$ is an isotropic vector function of the stretching rate and the end-to-end vector. Using the same representation theorem as was previously employed [43] it can be shown that this alternative equation can be written as

$$\dot{\mathbf{Q}} = \mathbf{L}\mathbf{Q} - \chi\mathbf{Q} - \xi_\omega \mathbf{d}\mathbf{Q}, \tag{2.14}$$

which matches equation (2.12) with the exception that ξ_ω is not considered to be a constant, but is a function of $\mathbf{\Pi}_{\mathbf{d}_{\mathrm{PTT}}}$, the second invariant of $\mathbf{d}_{\mathrm{PTT}}$.

Considering now the probability distribution function f_J of the junctions such that $f_J V$ denotes the number of junctions in the volume V (here $V = \mathrm{d}^3\mathbf{Q}\mathrm{d}^3\mathbf{r}$). Total differentiation of f_J gives

$$\frac{\mathrm{d}f_J}{\mathrm{d}t} = \frac{\partial f_J}{\partial t} + \mathbf{v}.\frac{\partial f_J}{\partial \mathbf{r}} + \dot{\mathbf{Q}}.\frac{\partial f_J}{\partial \mathbf{Q}} = (\text{rate of creation} - \text{rate of destruction}) \text{ of junctions} \tag{2.15}$$

or

$$\frac{\mathrm{d}f_J}{\mathrm{d}t} = g - hf_J \tag{2.16}$$

where g is the rate of creation of junctions and hf_J is the rate of destruction of junctions. Incorporating equations (2.12) and (2.14) into equations (2.15) and (2.16), the conservation equation for f_J is then

$$\frac{\partial f_J}{\partial t} + \mathbf{v}.\frac{\partial f_J}{\partial \mathbf{r}} + (\mathbf{LQ} - \chi\mathbf{Q} - \xi_{\alpha,\omega}\mathbf{dQ}).\frac{\partial f_J}{\partial \mathbf{Q}} = g - hf_J \tag{2.17}$$

where g and h are functions of the end-to-end vector $\mathbf{Q}$. Assuming a Gaussian network (see [45, 66, 67, 68] and Section 2.3.1.1) then the stress tensor $\mathbf{T}$ is given by the following integral

$$\begin{aligned} \mathbf{T} &= \frac{3kT_a}{Na^2}\iiint \mathbf{QQ}f_J \mathrm{d}^3\mathbf{Q} \\ &= \frac{3kT_a}{Na^2} < \mathbf{QQ} > \end{aligned} \tag{2.18}$$

where T_a is the absolute temperature, k is Boltzmann's constant, $(Na^2)^{1/2}$ is the equilibrium extension of the network strand and $< . >$ denotes averaging over the configuration space ($\mathbf{Q}$-space in this instance). The discussion of the theory surrounding this network model is extended further in order to derive the Phan-Thien Tanner constitutive equations in Section 2.4.4.

2.4 Constitutive Equations

2.4.1 The Doi-Edwards Model

Although the Doi-Edwards model [18, 19, 20, 21, 22] is not used in this thesis an explanation of the derivation of this constitutive equation will serve to elucidate some of the main principles of other models which will be discussed in later Sections. The Doi-Edwards fluid model considers polymers whose molecules are simple chains. Doi and Edwards based the development of their model on the concept of reptation. They employ the cage, tube and slip-link network models described earlier, equivalently and interchangeably [20].

Consider a polymer molecule consisting of N links between chains of length b and confined within a tube of diameter a. For length scales smaller than a the chain has sufficient room within the tube to behave as a Gaussian chain. Defining the 'entanglement molecular weight', M_e, as the molecular weight of a polymer chain with mean end-to-end distance equal to a, then

$$a^2 \sim 3\frac{M_e}{M}Nb^2,$$

where M is the mass of the whole molecule. By dividing the chain into $s = M/M_e$ segments, each segment will perform as an unentangled Gaussian chain and so the relaxation time of the whole polymer chain is

$$\tau_e = \frac{\zeta N_e^2 b^2}{3\pi^2 k T_a},$$

where $N_e = N/s$ and ζ is a friction coefficient.

If the polymer was unentangled then $M = M_e$ and the relaxation time would be equal to

the Rouse time τ_R, as defined in Section 2.3.1.2. The entanglement of the polymer, however, causes the molecule to relax in two separate stages. Initially the polymer will relax on length scales smaller than a and this causes the ends of the chain to be pulled inwards along the length of the tube. This part of the relaxation occurs in a time of the order of the Rouse relaxation time.

The polymer is now at the correct length, however it is still required to relax further since it is not in its equilibrium orientation. This part of the relaxation is achieved by the process of reptation whereby the polymer moves lengthwise along the tube. The reptation relaxation time is found by calculating the time taken for the polymer to diffuse a distance of sa along the tube. This is

$$\tau_{\text{rep}} \sim \frac{s^2 a^2}{2D} \sim s^3 \tau_e,$$

where D is the coefficient of diffusion and is given by the Einstein relationship

$$D = \frac{kT_a}{N\zeta}.$$

In order to calculate the stress exerted by the polymer chain, consider the case when the tube is of length sa and the subchains are sections of the chain with molecular mass M_e. The stress is then determined only by the orientation of the tube segments. Using the earlier theory of Gaussian chains (see Section 2.3.1.1) the stress is given by

$$T_{ij} = \frac{\rho N_A}{M_e} < F_i Q_j >, \tag{2.19}$$

where

$$F_i = \frac{3kT_a}{N_e b^2} Q_i,$$

and $\mathbf{Q}$ is the end-to-end vector of the polymer molecule. Since each segment is of length $a = b\sqrt{N_e}$, then it is required that

$$< Q_i Q_j >= \frac{a^2}{3} S_{ij}$$

where $\mathbf{S}$ is the orientation tensor denoting the orientations of the tube segments. Thus the stress becomes

$$\mathbf{T} = G_0 \mathbf{S} \tag{2.20}$$

where

$$G_0 = \frac{\rho R_g T_a}{M_e}$$

is the plateau modulus.

To complete this formulation Doi and Edwards derive the stress tensor for their primitive chain as [21]

$$T_{ij} = \frac{3ckT}{a} \int_0^{L_{DE}} \mathrm{d}s < \hat{u}_i(s,t)\hat{u}_j(s,t) - \frac{1}{3}\delta_{ij} > + P\delta_{ij}. \tag{2.21}$$

Here c is the number of chains in a unit volume, L_{DE} is the full length of the molecule and P is the dynamic pressure. The vector $\hat{\mathbf{u}}(s,t)$ is the unit vector tangent to the primitive chain at arc length coordinate s and time t and as before $< . >$ denotes the mean value.

2.4.2 The Modified Reptation Model of Curtiss and Bird

Shortly after the publication of the Doi-Edwards model [18, 19, 20, 21, 22] in 1978-79, Curtiss and Bird used their own phase-space theory [14], published in 1976, to rederive the same model with some adjustments [15, 16]. The main aim of this 1981 work was to avoid a number of, what Curtiss and Bird regarded to be, awkward intricacies of the Doi-Edwards theory. The main stumbling points were

(i) Non-consistency in the choice of molecular models: in the derivation of their orientational distribution function Doi and Edwards employed a model for the polymer molecule which consisted of freely jointed chains with rigid links [21], but used a 'rubber elasticity' expression for the stress tensor [20] thus implying the presence of Gaussian chains. A matching procedure is then used so as to obtain equilibrium forces in the chains and to preserve a constant contour length.

(ii) An 'independent alignment approximation' is used whereby each link in the chain is independently twisted by the fluid and the links are then reassembled. Curtiss and Bird felt this approximation to be unsatisfactory.

Curtiss and Bird tackled these issues by using a Kramers bead and rod model (see Section 2.3.1.3) to describe the polymer molecule and developing a rigorous procedure to handle the reptational movement of the polymer along its backbone. They then derive an expression for the stress tensor in terms of the average forces on the beads as

$$\mathbf{T} = NnkT\left[\frac{1}{3}\delta - \int_0^1 <\hat{\mathbf{u}}\hat{\mathbf{u}}> \mathrm{d}\sigma_{\mathrm{CB}} - \varepsilon\lambda\mathbf{u} : \int_0^1 \sigma_{\mathrm{CB}}\left(1-\sigma_{\mathrm{CB}}\right) <\hat{\mathbf{u}}\hat{\mathbf{u}}\hat{\mathbf{u}}\hat{\mathbf{u}}> \mathrm{d}\sigma_{\mathrm{CB}}\right]. \quad (2.22)$$

Here $\hat{\mathbf{u}}$ is the unit vector along the kth rod as defined in Section 2.3.1.3, $\sigma_{\mathrm{CB}} = j/N$ is the fractional distance along the chain, ε is the 'link tension coefficient', $\lambda = N^{3+j}\zeta a^2/2kT$ is a characteristic time and $\mathbf{u}$ is the velocity vector. Equation (2.22) relates to Doi and Edwards' equivalent expression, equation (2.21), since $\varepsilon = 0$ in the Doi and Edwards theory [16].

2.4.3 The Giesekus Model

In 1962 Giesekus developed a viscoelastic model based on the kinetic theory of dilute polymer solutions [25, 26, 27, 28]. This development is also reiterated (in English) in [8]. Following the introduction of the reptation concept by de Gennes [17] in 1971, Doi, Edwards, Curtiss and Bird developed their models, as are described above, and included the idea that the tensorial drag coefficient is connected to the orientations of the rods and beads used in the molecular models (e.g. the Kramers bead and rod model and the reptation models described in Section 2.3.2). Following these publications in 1978, '79 and '81, Giesekus reintroduced a simplification of his earlier theory which showed another method for the introduction of the tensorial drag coefficient [29]. A synopsis of the theory is given here.

Initially Giesekus defines a sequence of tensors $\mathbf{C}_k$ to characterize the different configurations of the network structures within the fluid. These tensors are connected to the tensor of excess stress, $\mathbf{S}$, by the relation

$$\mathbf{S}_k + \hat{\eta}_k \overset{\triangledown}{\mathbf{C}}_k = 0, \qquad \mathbf{S} = \sum_k \mathbf{S}_k. \tag{2.23}$$

where $\hat{\eta}_k$ is a series of fitted material constants, with the properties of zero viscosity, to be

determined by experiment. Substituting $\mathbf{C}_k = \mathbf{1} + 2\mathbf{E}_k$ into equation (2.23) gives

$$\mathbf{S}_k + 2\hat{\eta}\overset{\triangledown}{\mathbf{E}}_k = 2\hat{\eta}\mathbf{d}_{\mathrm{G}}, \tag{2.24}$$

where the sequence of $\mathbf{E}_k$'s represent the network strains and $\mathbf{1}$ implies a vector with all components equal to one. Also $\mathbf{d}_{\mathrm{G}} = \frac{1}{2}\left(\nabla\mathbf{u} + (\nabla\mathbf{u})^{\mathrm{T}}\right)$ is the rate of strain tensor.

Assuming that the network consists of linear relations to which Hooke's law can be applied, then

$$\mathbf{S}_k = 2\mu_k\mathbf{E}_k \tag{2.25}$$

and equation (2.24) becomes

$$\mathbf{S}_k + \lambda_k\overset{\triangledown}{\mathbf{S}}_k = 2\hat{\eta}_k\mathbf{d}_{\mathrm{G}}, \tag{2.26}$$

where $\lambda_k = \hat{\eta}_k/\mu_k$.

In its current condition this model does not possess a second normal stress difference in simple shear flows. In order to counteract this issue, scalar mobility constants, $\mathbf{B}_k$ say, contained in the constants $\hat{\eta}$, are substituted by non-isotropic mobilities such that $\mathbf{B}_k = \boldsymbol{\beta}_k B_k$. These relative mobility tensors, $\boldsymbol{\beta}_k$ tend to the unit tensor in the limit of the state of rest. Equation (2.23) then becomes

$$\frac{1}{2}\left(\boldsymbol{\beta}_k.\mathbf{S}_k + \mathbf{S}_k.\boldsymbol{\beta}_k\right) + \hat{\eta}\overset{\triangledown}{\mathbf{C}}_k = 0. \tag{2.27}$$

Assuming that the mobility does not depend on the configurations of individual polymer

units, but on an average configuration, then the tensors $\boldsymbol{\beta}_k$ are each functions of the full set of configuration tensors $\mathbf{C}_k$. Thus the sequence of equations (2.27) is coupled. This was not necessarily the case for equation (2.23).

This result can be further reduced to a one mode model by assuming a uniform network structure such that the configuration can be characterized by a single tensor, $\mathbf{C}$. Thus the set of equations (2.27) becomes the single equation

$$\boldsymbol{\beta}.\mathbf{S} + \hat{\eta}\overset{\triangledown}{\mathbf{C}} = 0. \tag{2.28}$$

2.4.4 The Phan-Thien Tanner Network Models

The Phan-Thien Tanner models are derived from a Lodge-Yamamoto network theory as described earlier in Section 2.3.3. The derivations in the following Sections are continuations of this earlier analysis.

The Linear Phan-Thien Tanner Model

In [52] Phan-Thien and Tanner attempted to solve equations (2.17) and (2.18) in order to determine f_J, the probability distribution function of the networks, and the stress tensor. Equations (2.17) and (2.18) can be combined into one constitutive equation for the stress tensor, thus eliminating the need to solve (2.17) explicitly for f_J. Assuming that

$$\lim_{n\to\infty} \mathbf{Q}^n f = 0,$$

then multiplying (2.17) by $\mathbf{QQ}$ and averaging over the configuration space gives

$$\begin{aligned}\frac{\mathrm{d}}{\mathrm{d}t} < \mathbf{QQ} > -\mathbf{L} < \mathbf{QQ} > - < \mathbf{QQ} > \mathbf{L}^{\mathrm{T}} - \xi_l \left(\mathbf{d} < \mathbf{QQ} > + < \mathbf{QQ} > \mathbf{d}\right) \\ +5\chi < \mathbf{QQ} >= \iiint g\mathbf{QQ}\mathrm{d}^3\mathbf{Q} - \iiint h\mathbf{QQ}f_J\mathrm{d}^3\mathbf{Q}\end{aligned} \tag{2.29}$$

Here χ is the constant which was first introduced in equation 2.12.

The elastic energy, or the Helmholtz energy of a network strand is proportional to the average extension of the strand $< Q^2 >$ [45] and so, by taking this to be the important parameter and assuming also

$$g = G(< Q^2 >) \exp\left(\frac{-3Q^2}{2Na^2}\right),$$

and

$$h = h(< Q^2 >),$$

then equation (2.29) becomes

$$\frac{\mathrm{d}\mathbf{T}}{\mathrm{d}t} - \mathcal{L}\mathbf{T} - \mathbf{T}\mathcal{L}^{\mathrm{T}} + H\mathbf{T} = NkT_aG\mathbf{I}, \tag{2.30}$$

where $\mathcal{L} = \mathbf{L} - \xi_l\mathbf{d}$ is the effective velocity gradient and

$$H(< Q^2 >) = h(< Q^2 >) + 5\chi.$$

It is expected that the above approximations are useful over a wide range of flow rates since they hold for both 'weak' (viscometric) flows when h has only a small dependence on $\mathbf{Q}$ as well as for 'strong' (elongational) flows when f_J, the distribution function, is in a form similar to a delta function in the localized $\mathbf{Q}$-space.

By writing (2.29) in convected form it is possible to solve explicitly for the stress tensor

$$\mathbf{T} = NkT_a \int_{-\infty}^{\infty} G(t') e^{\left(-\int_{t'}^{t} H(t'')\mathrm{d}t''\right)} \mathbf{B}(t')\mathrm{d}t', \tag{2.31}$$

where $\mathbf{B}$ is the 'effective' Finger tensor corresponding to the effective velocity gradient $\mathcal{L}$. The functions $G(t)$ and $H(t)$ are expressed as implicit functions of time through $< Q^2 > (t)$. Since

$$\mathrm{tr}(\mathbf{T}) = \frac{3kT_a}{Na^2} < Q^2 >$$

then H and G are functions of $\mathrm{tr}(\mathbf{T})$. Assuming a linear dependence on $\mathrm{tr}(\mathbf{T})$ of H and G then

$$\overset{\square}{\mathbf{T}} + h_0 \left(1 + E'\mathrm{tr}(\mathbf{T})\right) \mathbf{T} = g_0 \left(1 + E'\mathrm{tr}(\mathbf{T})\right) \mathbf{T},$$

where E' is a constant. The same slope has been chosen for the G and H versus $\mathbf{T}$ relationships, for simplicity. Equivalently, this could be written as

$$\tau_0 \overset{\square}{\boldsymbol{\tau}} + \left(1 + E''\mathrm{tr}(\boldsymbol{\tau})\right) \boldsymbol{\tau} = 2\frac{G_0\tau_0}{1-\xi_l} \mathbf{d}_{\mathrm{PTT}}, \tag{2.32}$$

where

$$\overset{\square}{\boldsymbol{\tau}} = \frac{\partial \boldsymbol{\tau}}{\partial t} + (\mathbf{u}.\nabla)\,\boldsymbol{\tau} - \mathcal{L}\boldsymbol{\tau} - \boldsymbol{\tau}\mathcal{L}^{\mathrm{T}},$$

$$\begin{aligned} \mathbf{d}_{\mathrm{PTT}} =& \frac{1}{2}\left(\mathcal{L} + \mathcal{L}^{\mathrm{T}}\right), & \boldsymbol{\tau} =& \mathbf{T} - \frac{g_0}{h_0}\mathbf{I}, \\ \tau_0 =& \frac{1}{h_0}\left(1 + 3E'\frac{g_0}{h_0}\right)^{-1}, & E'' =& \frac{E'}{1 + 3E'\frac{g_0}{h_0}}, \\ G_0 =& \frac{g_0}{h_0}\left(1 - \xi\right). \end{aligned}$$

Here $\overset{\square}{\boldsymbol{\tau}}$ is the general convective derivative, or Johnson-Segalman derivative of the extra stress tensor. This was introduced earlier in Section 2.2.1 and reduces to the upper-convected derivative $\overset{\triangledown}{\boldsymbol{\tau}}$ when $\xi_l = 0$, the corotational derivative $\overset{\circ}{\boldsymbol{\tau}}$ when $\xi_l = 1$ and the lower-convective derivative $\overset{\triangle}{\boldsymbol{\tau}}$ when $\xi_l = 2$.

This constitutive equation can be extended to incorporate the complete distribution of relaxation times by performing a spectral decomposition of the stress tensor, thus

$$\begin{cases} \boldsymbol{\tau} = \sum_i \boldsymbol{\tau}^{(i)}, \\ \tau_{0i}\overset{\square}{\boldsymbol{\tau}}^{(i)} + \boldsymbol{\tau}^{(i)}\left(1 + \frac{\epsilon_l}{G_i}\mathrm{tr}(\boldsymbol{\tau}^{(i)})\right) = 2\frac{G_i\tau_i}{1-\xi_l}\mathbf{d}_{\mathrm{PTT}}. \end{cases}$$

It is noted that there are only two adjustable parameters, ϵ_l and ξ_l, and both of these are nondimensional.

The Exponential Phan-Thien Tanner Model

An alternative approach is given in [51] whereby the integral (2.18) is transformed to a reference configuration and the total derivative of the stress tensor is incorporated to obtain

$$\frac{\mathrm{d}\mathbf{T}}{\mathrm{d}t} = \frac{3kT_a}{Na^2}\iiint_o \left(\left(\dot{\mathbf{Q}}\mathbf{Q} + \mathbf{Q}\dot{\mathbf{Q}}\right) f_J J + \mathbf{Q}\mathbf{Q}\frac{\mathrm{d}f_J}{\mathrm{d}t}J + \mathbf{Q}\mathbf{Q}f_J\frac{\mathrm{d}J}{\mathrm{d}t}\right)\mathrm{d}^3\mathbf{Q}_o, \tag{2.33}$$

where the subscript o denotes the reference configuration and

$$J = \left|\frac{\partial \mathbf{Q}}{\partial \mathbf{Q}_o}\right|, \qquad \frac{\mathrm{d}J}{\mathrm{d}t} = J\mathrm{tr}\left(\frac{\partial \dot{\mathbf{Q}}}{\partial \mathbf{Q}}\right)$$

Using equations (2.14), (2.16) and (2.33) it is possible to obtain

$$\frac{\mathrm{d}\mathbf{T}}{\mathrm{d}t} - \mathcal{L}\mathbf{T} - \mathbf{T}\mathcal{L}^{\mathrm{T}} + 5\chi\mathbf{T} = \frac{3kT_a}{Na^2}\iiint \left(\left(g - hf_J\right)\mathbf{Q}\mathbf{Q}\right)\mathrm{d}^3\mathbf{Q},$$

where $\mathcal{L} = \mathbf{L} - \xi_e\mathbf{d}_{\mathrm{PTT}}$ is the effective velocity gradient as before. Again, ξ_ω is a function of $\mathbf{\Pi_d}$. Here $< Q^2 >$ is again taken as the important parameter which governs the rheological behaviour of the network. The following is also assumed

$$g = g_1(< Q^2 >, T_a)e^{\left(\frac{-3\mathbf{Q}^2}{2Na^2}\right)},$$

and

$$h = h(< Q^2 >, T_a).$$

Then

$$\frac{\mathrm{d}\mathbf{T}}{\mathrm{d}t} - \mathcal{L}\mathbf{T} - \mathbf{T}\mathcal{L}^{\mathrm{T}} + H\mathbf{T} = G_1\mathbf{I}, \tag{2.34}$$

where

$$H = 5\chi + h(< Q^2 >),$$

$$G_1 = NkT_a g_1(< Q^2 >).$$

As in the derivation of the linear model, these approximations can be shown to be useful over a wide range of flow rates. The solution to (2.34) is

$$\mathbf{T} = \int_{-\infty}^{t} G_1(t') e^{\left(-\int_{t'}^{t} H(t'')\mathrm{d}t''\right)} \mathbf{B}(t')\mathrm{d}t', \tag{2.35}$$

which is similar to equation (2.31) but with a temperature dependence inside the integral. As before $\mathbf{B}$ is the effective Finger tensor corresponding to the effective velocity gradient $\mathcal{L}$ and the functions $G_1(t)$ and $H(t)$ are expressed as implicit functions of time through the time dependence of $< Q^2 > (t)$.

As for the linear model

$$\mathrm{tr}(\mathbf{T}) = \frac{3kT_a}{Na^2} < Q^2 >$$

and hence H and G_1 are functions of $\mathrm{tr}(\mathbf{T})$ and the temperature T_a. Assuming that $G_1 \propto H$ with constant of proportionality G then by eliminating the isotropic tensor, equation (2.34) becomes

$$\tau \overset{\square}{\mathcal{T}} + Y(\mathrm{tr}(\mathcal{T}), \theta)\mathcal{T} = 2\lambda G\mathbf{d}$$

where τ is a time constant and Y is a dimensionless function of $\mathrm{tr}(\mathcal{T})$ and T_a. Also

$$\mathbf{T} = \mathcal{T} + G\mathbf{I}\,(1-\xi)\,, \qquad Y = \tau H,$$

$$G_1 = GH\,(1-\xi)\,, \qquad \overset{\square}{\mathcal{T}} = \frac{\partial \mathcal{T}}{\partial t} + (\mathbf{v}.\nabla)\,\mathcal{T} - \mathcal{L}\mathcal{T} - \mathcal{T}\mathcal{L}^{\mathrm{T}}.$$

As before this can be extended to incorporate the full spectrum of relaxation times by performing a spectral decomposition of the stress tensor such that

$$\begin{cases} \mathcal{T} = \sum_i \mathcal{T}^{(i)}, \\ \tau_i \overset{\square}{\mathcal{T}}^{(i)} + Y(\mathrm{tr}(\mathcal{T}^{(i)}), T_a)\mathcal{T}^{(i)} = G_i\tau_i\mathbf{d}. \end{cases}$$

It can be shown that the τ_i are relaxation times and the G_i are relaxation moduli. These parameters are not adjustable since they are taken from the equilibrium relaxation spectrum $H(\tau)$. Thus there is only one adjustable parameter in ξ_ω which is a function of $\mathbf{\Pi_d}$ and the unknown function Y which is to be determined by the 'time-temperature superposition principle' [51].

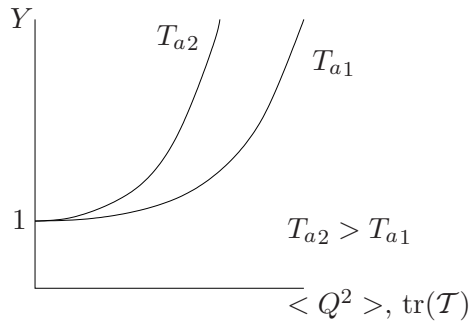

Figure 2.11: The expected relationship between the function Y, temperature T_a and the average extension of the network $< Q^2 >$. (Taken from [51].)

The function Y is essentially a description of the rate of the destruction of the network junctions and it would be expected that Y will increase as temperature increases and similarly as the average extension of the network ($< Q^2 >$) increases. Hence a relationship like that shown in Fig. 2.11 could be expected.

Assuming that the function Y is of the form

$$Y(\mathrm{tr}(\mathcal{T}^{(i)}), T_a) = \phi(T_a) K(\mathrm{tr}(\mathcal{T}^{(i)})), \qquad \phi(T_r) = 1,$$

where T_r is the reference temperature (where the relaxation spectrum is measured) then the constitutive equation becomes

$$\tau_i \overset{\square}{\mathcal{T}}^{(i)} + \phi(T_a) K(\mathrm{tr}(\mathcal{T}^{(i)})) \mathcal{T}^{(i)} = 2 G_i \tau_i \mathbf{d}_{\mathrm{PTT}}.$$

Changing the time scale according to $t' = \phi t$ eliminates ϕ so that

$$\tau_i \overset{\square\,'}{\mathcal{T}}{}^{(i)} + K(\mathrm{tr}(\mathcal{T}^{(i)}))\mathcal{T}^{(i)} = 2G_i\tau_i \mathbf{d}'_{\mathrm{PTT}},$$

is the same as would be obtained by setting $T_a = T_r$. Here $\overset{\square\,'}{\mathbf{A}}{}^{(i)}$ is the Johnson-Segalman derivative of $\mathbf{A}^{(i)}$ and $\mathbf{d}'_{\mathrm{PTT}}$ is the stretching rate, both calculated with respect to the new time scale, t'. Hence for a non-isothermal field the constitutive equations are

$$\begin{cases} \mathcal{T} = \sum_i \mathcal{T}^{(i)}, \\ \tau_i \overset{\square}{\mathcal{T}}{}^{(i)} - \mathcal{T}^{(i)} \frac{\mathrm{d}}{\mathrm{d}t}(\ln T_a) + \phi(T_a) K(\mathrm{tr}(\mathcal{T}^{(i)}))\mathcal{T}^{(i)} = 2G_i\tau_i \mathbf{d}_{\mathrm{PTT}}. \end{cases}$$

It remains to propose an expression for $K(\mathrm{tr}(\mathcal{T}^{(i)}))$ and the suggested form is

$$K(\mathrm{tr}(\mathcal{T}^{(i)})) = e^{(\epsilon_\omega/G_i)\mathrm{tr}(\mathcal{T}^{(i)})},$$

where $\epsilon_\omega \sim 0.01$ is a constant.

Governing Equations

In more familiar notation, which will be used for the remainder of this thesis, these two constitutive equations derived above can be expressed as

$$\tau_p \overset{\square}{\boldsymbol{\tau}} + f(\boldsymbol{\tau})\boldsymbol{\tau} = 2\eta_p \mathbf{d}, \tag{2.36}$$

where the function $f(\boldsymbol{\tau})$ can take either a linear or an exponential form. In what follows the linear form

$$f(\boldsymbol{\tau}) = \frac{\epsilon\tau_p}{\eta_p}\mathrm{tr}(\boldsymbol{\tau}) + 1, \tag{2.37}$$

is considered and comparisons are made with the results of Grillet *et al.* [31] for the exponential form of the model which is defined by

$$f(\boldsymbol{\tau}) = \exp\left(\frac{\epsilon\tau_p}{\eta_p}\mathrm{tr}(\boldsymbol{\tau})\right).$$

The linear PTT model could be considered to be a linearization of its exponential equivalent.

Here the general convective derivative of the polymeric stress tensor $\overset{\square}{\boldsymbol{\tau}}$ is defined as earlier. The relationship between strand stretching and fluid motion is expressed through the effective velocity gradient $\mathcal{L} = \mathbf{L} - \xi\mathbf{d}$ where $\mathbf{d}$ is the rate of strain and $\mathbf{L}$ is the velocity gradient as before. The physical parameters of the system are the relaxation time of the polymer solute, τ_p, and the solvent and polymer viscosities, η_s and η_p, respectively, which can be added to give the total viscosity, $\eta_t = \eta_s + \eta_p$. The parameters ξ and ϵ are parameters specific to a PTT fluid and are determined experimentally by fitting the model to data for elongational and shearing flows, respectively. Thus these parameters will be referred to as the extensional, ξ, and shear thinning, ϵ, parameters. The parameter ξ can be measured from the dynamic viscosity - shear viscosity shift,

$$\eta'(x) = \eta\left(\frac{x}{\sqrt{\xi\,(2-\xi)}}\right),$$

where η' is the dynamic viscosity and η is the shear viscosity. A reasonable constant value of ξ for polymer melts is of the order 0.1. The parameter ϵ indicates the susceptibility of the fluid to shear-thinning and is a constant of order 0.01 [51].

The PTT model reduces to the Oldroyd-B model when $\xi = \epsilon = 0$. Thus, the PTT model can be regarded as an extension to and an improvement on the Oldroyd-B fluid model. The PTT model incorporates shear-thinning which the Oldroyd-B model neglects. The PTT model also gives a bounded extensional viscosity, although it does not give a non-zero second normal stress difference [41].

In the next Chapter the constitutive equations for the Giesekus and linear PTT models will be applied to the specific channel geometries that will be investigated in this thesis.

Chapter 3

Single and Multilayered Planar Poiseuille Flow

In this Chapter the flow geometries which are to be investigated in this thesis will be introduced. The non-dimensionalizations, boundary conditions and other flow restrictions that these geometries impart on the Navier-Stokes equations and constitutive equations will be discussed. The base flow equations and linearized stability equations will be derived in preparation for the application of the numerical methods as described in Chapter 4. There are four different flow geometries under investigation in this thesis: non-symmetric planar Poiseuille flow of one fluid; symmetric planar Poiseuille flow of one fluid; planar Poiseuille flow of two immiscible fluids, one lying over the other, within the same channel; and a three layer configuration whereby one fluid occupies a central layer and another, immiscible fluid, occupies two outer layers with all three layers within one channel.

3.1 Non-Dimensionalizations

It is necessary to non-dimensionalize the governing equations which were derived in Chapter 2, thus removing any units of measurement, before any attempts at a solution can be made. This also reduces the number of adjustable parameters and hence simplifies the analysis of the solutions. The method of non-dimensionalization will be slightly different for each of the flow geometries under consideration due to the differences in boundary positions, the number of fluids, channel widths and the fluids involved.

3.1.1 Single Fluid Flows

Fig. 3.1 shows the flow configuration for *non-symmetric* planar Poiseuille flow. Here the fluid is confined within a channel bounded by solid, impermeable walls at $y = 0$ and $y = L$. Fig. 3.2 shows the flow configuration for *symmetric* planar Poiseuille flow where the channel is bounded by solid walls at $y = \pm L$. The velocities and stresses are independent of the channel-lengthwise variable, x, and the pressure gradient in this direction is a nontrivial constant. The schematic velocity profiles shown are in the forms of negative parabolas, as is consistent with Poiseuille flows, and is the expected result of future calculations.

In order to pursue the non-dimensionalization the following non-dimensional variables are introduced:

$$\mathbf{u}^* = \frac{\mathbf{u}}{U}, \qquad p^* = \frac{Lp}{\eta_t U}, \qquad \boldsymbol{\tau}^* = \frac{L\boldsymbol{\tau}}{\eta_t U},$$
$$\mathbf{x}^* = \frac{\mathbf{x}}{L}, \qquad t^* = \frac{Ut}{L},$$

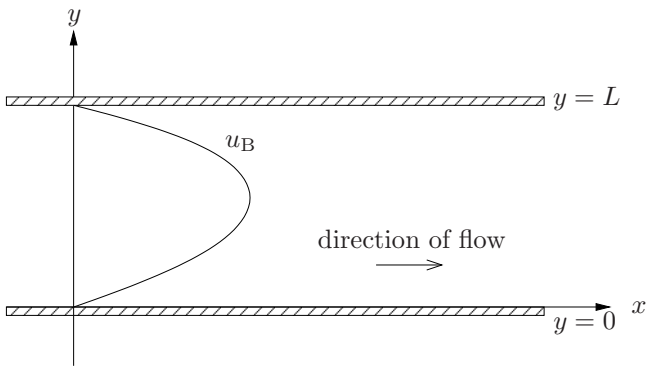

Figure 3.1: The flow configuration for non-symmetric planar Poiseuille flow of a single fluid.

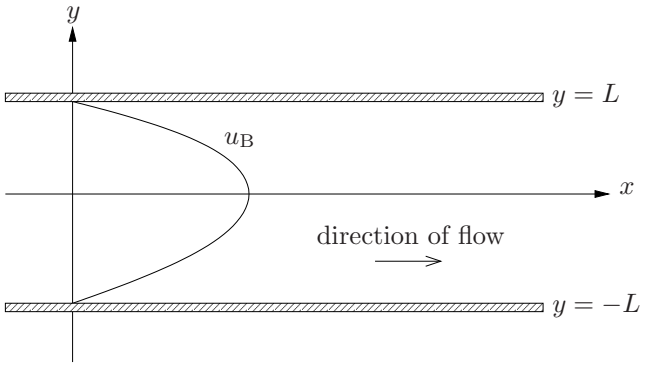

Figure 3.2: The flow configuration for symmetric planar Poiseuille flow of a single fluid.

where U and L are characteristic velocity and lengths, respectively, and an asterisk denotes a non-dimensonal variable.

For one-dimensional planar Poiseuille flow the characteristic velocity U is chosen to be the flow velocity at the centre of the channel, which is fixed at unity by a choice of the pressure gradient. The characteristic length scale L is chosen to be equal to the full channel width for the non-symmetric case, and equal to half the channel width for the symmetric case. Hence the non-dimensional problems that have been derived consider Poiseuille flow of a fluid confined within a non-symmetric channel defined by $y \in [0, 1]$, or within a symmetric channel defined by $y \in [-1, 1]$.

It is also necessary to define the following non-dimensional parameters:

$$R = \frac{\rho U L}{\eta_t}, \qquad W = \frac{\lambda U}{L}, \qquad \beta = \frac{\eta_s}{\eta_t} = \frac{\eta_s}{\eta_s + \eta_p}.$$

Here R is known as the Reynolds number and W as the Weissenberg number. The solvent to total viscosity ratio is represented by β, and λ is the relaxation time of the fluid. It is noted that the shear-thinning parameter, ϵ, and the Phan-Thien Tanner extensional parameter, ξ, are already non-dimensional in the derivations of the Giesekus and Phan-Thien Tanner models and hence they need not be modified here.

3.1.2 Multiple Fluid Flows

Fig. 3.3 shows the two fluid flow configuration. The two fluids within the channel are of the same constitutive type, i.e. they are either both Giesekus fluids or both PTT fluids,

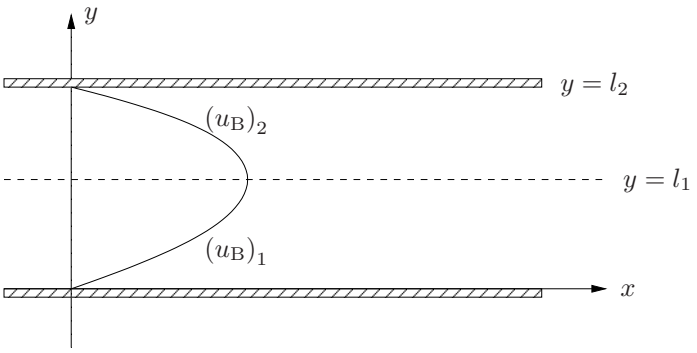

Figure 3.3: The flow configuration for planar Poiseuille flow of two immiscible fluids.

and are immiscible. They are confined within solid, impermeable channel walls at $y = 0$ and $y = l_2$ with fluid 1 occupying the lower layer, $y \in [0, l_1]$, and fluid 2 occupying the upper layer, $y \in [l_1, l_2]$. Each fluid obeys its own set of governing equations and these equations differ between the two fluids only in the values of the non-dimensional fluid parameters. The two fluids meet at the fluid-fluid interface, $y = l_1$ where interfacial conditions involving the velocities and stresses of each fluid come into play. It is noted that this is a non-symmetric flow configuration and that the special cases where fluid 1 and fluid 2 are identical are equivalent to the non-symmetric single fluid flows with the same parameter values.

Fig. 3.4 shows the flow geometry for the three-layered flow problem. Here, fluid 1 occupies the inner layer, $y \in [-l_1, l_1]$, and fluid 2 occupies the two outer layers, $y \in [-l_2, -l_1] \cup [l_1, l_2]$. Again, both fluids are of the same constitutive type and each fluid obeys its own set of governing equations which differ only in the values of the fluid parameters. The fluids meet at two fluid-fluid interfaces, at $y = \pm l_1$, where the velocities and stresses obey interfacial conditions.

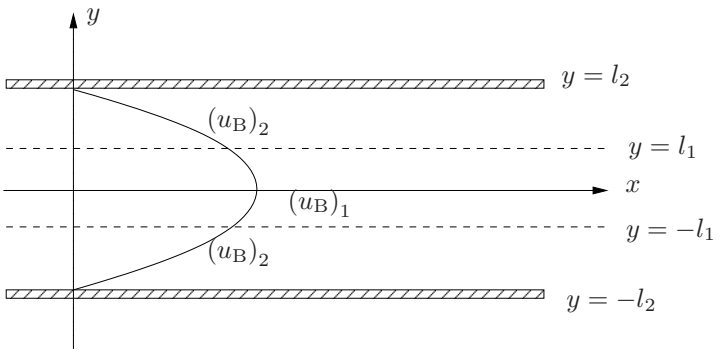

Figure 3.4: The flow configuration for three-layer planar Poiseuille flow of two immiscible fluids.

Due to the symmetry of this configuration it makes sense to reduce the problem to take into account only the upper half of the channel. Hence fluid 1 occupies the channel at $y \in [0, l_1]$ and fluid 2 occupies the channel at $y \in [l_1, l_2]$. This also reduces the number of fluid-fluid interfaces to one and hence the problem is greatly simplified. It is also clear from this simplification that special cases of this three-layered configuration, where both fluids are identical, are equivalent to the symmetric case of a single fluid with the same parameter values.

Mathematically, as opposed to physically, this three-layered problem is very similar to the two fluid problem described earlier. The only difference, albeit a critical difference, is that the lower boundary of the geometry is not a solid boundary, but one of symmetry, and the boundary conditions required to give a full solution will reflect this.

The non-dimensionalizations required for these two multiple fluid flow problems are almost identical. The following dimensionless variables (again denoted by asterisks) are intro-

duced;

$$\mathbf{u}_j^* = \frac{\mathbf{u}_j}{U}, \qquad p_j^* = \frac{l_2 p_j}{\eta_{t1} U}, \qquad \boldsymbol{\tau}_j^* = \frac{l_2 \boldsymbol{\tau}_j}{\eta_{t1} U},$$
$$\mathbf{x}^* = \frac{\mathbf{x}}{l_2}, \qquad t^* = \frac{Ut}{l_2}.$$

The following dimensionless parameters are also defined,

$$R_j = \frac{\rho_j U l_2}{\eta_{tj}}, \qquad W_j = \frac{\lambda_j U}{l_2}, \qquad \beta_j = \frac{\eta_{sj}}{\eta_{tj}} = \frac{\eta_{sj}}{\eta_{sj} + \eta_{pj}}.$$

The subscript $j = 1, 2$ denotes the fluid to which the parameters correspond. As for the single fluid problems, R_j are the Reynolds numbers and W_j are the Weissenberg numbers. The parameters β_j denote the ratios of solvent viscosity to total viscosity and λ_j are the relaxation times.

Two final non-dimensional parameters are required particularly for these multiple fluid problems. They are

$$m_j = \frac{\eta_{tj}}{\eta_{t1}}, \qquad l = \frac{l_1}{l_2},$$

where clearly, $m_1 = 1$. Also, m_2 is linked to β_j and this is to be considered before conclusions can be made about the effects of varying either m_2 or β_j. Again the shear-thinning parameters, ϵ_j, and the Phan-Thien Tanner extensional parameters, ξ_j, are already non-dimensional.

For the two fluid geometry the characteristic velocity U is chosen to be the velocity at the fluid-fluid interface and this will be set to unity as a condition for the choice of the pressure gradient. The characteristic length l_2 is the width of the whole channel, similar to the characteristic length for the non-symmetric single fluid configuration.

For the three-layered flow problem the characteristic velocity U is chosen to be the velocity at centre of the channel, at $y = 0$, and this again will be set to unity as a condition for the choice of the pressure gradient. The characteristic length is chosen as half the width of the channel, l_2, similarly to the characteristic length chosen for the symmetric single fluid configuration.

When the governing equations are expressed in terms of the above non-dimensional parameters, either for a single fluid configuration or for a multiple fluid configuration, the resulting equations are identical, with the exception of the subscripts which denote which fluid is being referred to. Omitting the asterisks these non-dimensional governing equations are as follows:

The Navier-Stokes equations: the conservation of momentum

$$R_j \frac{\mathrm{D}\mathbf{u}_j}{\mathrm{D}t} = -\nabla p_j + \nabla.\boldsymbol{\tau}_j + m_j\beta_j \nabla^2\mathbf{u}_j, \tag{3.1}$$

and the conservation of mass

$$\nabla.\mathbf{u}_j = 0. \tag{3.2}$$

The Giesekus constitutive equation:

$$W_j \overset{\triangledown}{\boldsymbol{\tau}}_j + \boldsymbol{\tau}_j + \frac{\epsilon_j W_j}{m_j\,(1-\beta_j)} \boldsymbol{\tau}_j . \boldsymbol{\tau}_j = 2m_j(1-\beta_j)\mathbf{d}_j. \tag{3.3}$$

The linear PTT constitutive equation:

$$W_j \overset{\square}{\boldsymbol{\tau}}_j + \boldsymbol{\tau}_j + \frac{\epsilon_j W_j}{m_j\,(1-\beta_j)} \mathrm{tr}(\boldsymbol{\tau}_j)\boldsymbol{\tau}_j = 2m_j(1-\beta_j)\mathbf{d}_j. \tag{3.4}$$

For application to the single fluid problems the subscripts, j, may be dropped and the parameters m_j may be fixed at $m_1 = m_2 = 1$.

These governing equations are written in Cartesian coordinates. The third spatial dimension is neglected since the geometries under consideration are two-dimensional. The full set of non-dimensional governing equations are as follows:

The Navier-Stokes equations: conservation of momentum

$$R_j \left(\frac{\partial u_j}{\partial t} + u_j \frac{\partial u_j}{\partial x} + v_j \frac{\partial u_j}{\partial y} \right) = -\frac{\partial p_j}{\partial x} + \frac{\partial \tau_{xx\,j}}{\partial x} + \frac{\partial \tau_{xy\,j}}{\partial y} + m_j \beta_j \left(\frac{\partial^2 u_j}{\partial x^2} + \frac{\partial^2 u_j}{\partial y^2} \right), \tag{3.5}$$

$$R_j \left(\frac{\partial v_j}{\partial t} + u_j \frac{\partial v_j}{\partial x} + v_j \frac{\partial v_j}{\partial y} \right) = -\frac{\partial p_j}{\partial y} + \frac{\partial \tau_{xy\,j}}{\partial x} + \frac{\partial \tau_{yy\,j}}{\partial y} + m_j \beta_j \left(\frac{\partial^2 v_j}{\partial x^2} + \frac{\partial^2 v_j}{\partial y^2} \right), \tag{3.6}$$

and conservation of mass

$$\frac{\partial u_j}{\partial x} + \frac{\partial v_j}{\partial y} = 0. \tag{3.7}$$

The Giesekus constitutive equation

$$W_j\left[\frac{\partial \tau_{xx_j}}{\partial t}+u_j\frac{\partial \tau_{xx_j}}{\partial x}+v_j\frac{\partial \tau_{xx_j}}{\partial y}-2\left(\frac{\partial u_j}{\partial x}\tau_{xx_j}+\frac{\partial v_j}{\partial x}\tau_{xy_j}\right)\right] + \tau_{xx_j}+\frac{\epsilon_j W_j}{m_j\left(1-\beta\right)}\left(\tau_{xx_j}^2+\tau_{xy_j}^2\right)=2m_j\left(1-\beta_j\right)\frac{\partial u_j}{\partial x}, \quad (3.8)$$

$$W_j\left[\frac{\partial \tau_{xy_j}}{\partial t}+u_j\frac{\partial \tau_{xy_j}}{\partial x}+v_j\frac{\partial \tau_{xy_j}}{\partial y}-\tau_{xy_j}\left(\frac{\partial u_j}{\partial x}+\frac{\partial v_j}{\partial y}\right)-\tau_{xx_j}\frac{\partial u}{\partial y}-\tau_{yy}\frac{\partial v}{\partial x}\right] + \tau_{xy_j}+\frac{\epsilon_j W_j}{m_j\left(1-\beta\right)}\left(\tau_{xx_j}+\tau_{yy_j}\right)\tau_{xy_j}=m_j\left(1-\beta_j\right)\left(\frac{\partial u_j}{\partial y}+\frac{\partial v_j}{\partial x}\right), \quad (3.9)$$

$$W_j\left[\frac{\partial \tau_{yy_j}}{\partial t}+u_j\frac{\partial \tau_{yy_j}}{\partial x}+v_j\frac{\partial \tau_{yy_j}}{\partial y}-2\left(\frac{\partial v_j}{\partial y}\tau_{yy_j}+\frac{\partial u_j}{\partial y}\tau_{xy_j}\right)\right] + \tau_{yy_j}+\frac{\epsilon_j W_j}{m_j\left(1-\beta\right)}\left(\tau_{xy_j}^2+\tau_{yy_j}^2\right)=2m_j\left(1-\beta_j\right)\frac{\partial v_j}{\partial y}, \quad (3.10)$$

and the PTT constitutive equation

$$W_j\left[\frac{\partial \tau_{xx_j}}{\partial t}+u_j\frac{\partial \tau_{xx_j}}{\partial x}+v_j\frac{\partial \tau_{xx_j}}{\partial y}-2\left(\frac{\partial u_j}{\partial x}\tau_{xx_j}+\frac{\partial v_j}{\partial x}\tau_{xy_j}\right)\right] + W_j\xi_j\left[\left(\frac{\partial u_j}{\partial y}+\frac{\partial v_j}{\partial x}\right)\tau_{xy_j}+2\frac{\partial u_j}{\partial x}\tau_{xx_j}\right] + \tau_{xx_j}+\frac{\epsilon_j W_j}{m_j\left(1-\beta\right)}\left(\tau_{xx_j}+\tau_{yy_j}\right)\tau_{xx_j}=2m_j\left(1-\beta_j\right)\frac{\partial u_j}{\partial x}, \quad (3.11)$$

$$W_j\left[\frac{\partial\tau_{xy_j}}{\partial t}+u_j\frac{\partial\tau_{xy_j}}{\partial x}+v_j\frac{\partial\tau_{xy_j}}{\partial y}-\frac{\partial u_j}{\partial y}\tau_{xx_j}-\left(\frac{\partial u_j}{\partial x}+\frac{\partial v_j}{\partial y}\right)\tau_{xy_j}-\frac{\partial v}{\partial x}\tau_{yy_j}\right]$$
$$+\frac{W_j\xi_j}{2}\left[\left(\frac{\partial u_j}{\partial y}+\frac{\partial v_j}{\partial x}\right)\left(\tau_{xx_j}+\tau_{yy_j}\right)+\tau_{xy_j}\left(\frac{\partial u_j}{\partial x}+\frac{\partial v_j}{\partial y}\right)\right]+\tau_{xy_j}$$
$$+\frac{\epsilon_j W_j}{m_j\left(1-\beta\right)}\left(\tau_{xx_j}+\tau_{yy_j}\right)\tau_{xy_j}=m_j\left(1-\beta_j\right)\left(\frac{\partial u_j}{\partial y}+\frac{\partial v_j}{\partial x}\right), \quad (3.12)$$

$$W_j\left[\frac{\partial\tau_{yy_j}}{\partial t}+u_j\frac{\partial\tau_{yy_j}}{\partial x}+v_j\frac{\partial\tau_{yy_j}}{\partial y}-2\left(\frac{\partial u_j}{\partial y}\tau_{xy_j}+\frac{\partial v_j}{\partial y}\tau_{yy_j}\right)\right]$$
$$+W_j\xi_j\left[\left(\frac{\partial u_j}{\partial y}+\frac{\partial v_j}{\partial x}\right)\tau_{xy_j}+2\frac{\partial v_j}{\partial y}\tau_{yy_j}\right]$$
$$+\tau_{yy_j}+\frac{\epsilon_j W_j}{m_j\left(1-\beta\right)}\left(\tau_{xx_j}+\tau_{yy_j}\right)\tau_{yy_j}=2m_j\left(1-\beta_j\right)\frac{\partial v_j}{\partial y}. \quad (3.13)$$

3.2 Base Flow Equations

In order to calculate the steady base flow, which is denoted by the subscript B, it is assumed that all variables are dependent only on the cross channel coordinate, y. The exception to this is pressure, p_{B}, which is also a function of x, the independent variable in the direction of the flow. The form of the pressure function is such that the pressure gradient, $\partial p_{\mathrm{B}}/\partial x$, is a constant. The cross channel velocity component, v_{B}, is zero. By implementing these restrictions the governing equations reduce to the following systems of differential equations.

From the Navier-Stokes equation for continuity of momentum

$$0 = -\frac{\partial p_{\mathrm{B}}}{\partial x} + \frac{\mathrm{d}\left(\tau_{xy_{\mathrm{B}}}\right)_j}{\mathrm{d}y} + m_j\beta_j\frac{\mathrm{d}^2\left(u_{\mathrm{B}}\right)_j}{\mathrm{d}y^2}, \tag{3.14}$$

$$0 = -\frac{\partial\left(p_{\mathrm{B}}\right)_j}{\partial y} + \frac{\mathrm{d}\left(\tau_{yy_{\mathrm{B}}}\right)_j}{\mathrm{d}y}. \tag{3.15}$$

The Giesekus constitutive equation

$$\left(\tau_{xx\mathrm{B}}\right)_j + \frac{\epsilon_j W_j}{m_j\left(1-\beta_j\right)}\left(\left(\tau_{xx\mathrm{B}}\right)_j^2 + \left(\tau_{xy_{\mathrm{B}}}\right)_j^2\right) = 0, \tag{3.16}$$

$$\begin{aligned} -W_j\left(\tau_{xx\mathrm{B}}\right)_j\frac{\mathrm{d}\left(u_{\mathrm{B}}\right)_j}{\mathrm{d}y} + \left(\tau_{xy_{\mathrm{B}}}\right)_j + \frac{\epsilon_j W_j}{m_j\left(1-\beta_j\right)}\left(\left(\tau_{xx\mathrm{B}}\right)_j + \left(\tau_{yy_{\mathrm{B}}}\right)_j\right)\left(\tau_{xy_{\mathrm{B}}}\right)_j \\ = m_j\left(1-\beta_j\right)\frac{\mathrm{d}\left(u_{\mathrm{B}}\right)_j}{\mathrm{d}y}, \end{aligned} \tag{3.17}$$

$$-2W_j\left(\tau_{xy_{\mathrm{B}}}\right)_j\frac{\mathrm{d}\left(u_{\mathrm{B}}\right)}{\mathrm{d}y} + \left(\tau_{yy_{\mathrm{B}}}\right)_j + \frac{\epsilon_j W_j}{m_j\left(1-\beta_j\right)}\left(\left(\tau_{xy_{\mathrm{B}}}\right)_j^2 + \left(\tau_{yy_{\mathrm{B}}}\right)_j^2\right) = 0, \tag{3.18}$$

and the Phan-Thien Tanner constitutive equation

$$-W_j\xi_j\frac{\mathrm{d}\left(u_{\mathrm{B}}\right)_j}{\mathrm{d}y}\left(\tau_{xy_{\mathrm{B}}}\right)_j + \left(\tau_{xx\mathrm{B}}\right)_j + \frac{\epsilon_j W_j}{m_j\left(1-\beta_j\right)}\left(\left(\tau_{xx\mathrm{B}}\right)_j + \left(\tau_{yy_{\mathrm{B}}}\right)_j\right)\left(\tau_{xx\mathrm{B}}\right)_j = 0, \tag{3.19}$$

$$\begin{aligned} -W_j\frac{\mathrm{d}\left(u_{\mathrm{B}}\right)_j}{\mathrm{d}y}\left(\tau_{xx\mathrm{B}}\right)_j + W\frac{\xi}{2}\frac{\mathrm{d}\left(u_{\mathrm{B}}\right)_j}{\mathrm{d}y}\left(\left(\tau_{xx\mathrm{B}}\right)_j + \left(\tau_{yy_{\mathrm{B}}}\right)_j\right) + \left(\tau_{xy_{\mathrm{B}}}\right)_j \\ + \frac{\epsilon_j W_j}{m_j\left(1-\beta_j\right)}\left(\left(\tau_{xx\mathrm{B}}\right)_j + \left(\tau_{yy_{\mathrm{B}}}\right)_j\right)\left(\tau_{xy_{\mathrm{B}}}\right)_j = m_j\left(1-\beta_j\right)\frac{\mathrm{d}\left(u_{\mathrm{B}}\right)_j}{\mathrm{d}y}, \end{aligned} \tag{3.20}$$

$$-W_j\left(2-\xi_j\right)\frac{\mathrm{d}\left(u_{\mathrm{B}}\right)_j}{\mathrm{d}y}\left(\tau_{xy_{\mathrm{B}}}\right)_j+\left(\tau_{yy_{\mathrm{B}}}\right)_j+\frac{\epsilon_j W_j}{m_j\left(1-\beta_j\right)}\left(\left(\tau_{xx\mathrm{B}}\right)_j+\left(\tau_{yy_{\mathrm{B}}}\right)_j\right)\left(\tau_{yy_{\mathrm{B}}}\right)_j=0. \quad (3.21)$$

Equation (3.7), which is derived from continuity, is identically zero. The above system of equations is solvable without equation (3.15) which can be used to find the y-dependence of pressure, although this is not performed in this thesis since it is not necessary as a precursor to a linear stability analysis nor is it necessary for an analysis of the character of these Poiseuille flows. By treating the pressure gradient, $\partial p_{\mathrm{B}}/\partial x$, as an unknown constant the x-dependence is completely removed from the system and this set of equations can then be treated as a set of ordinary differential equations. It is noted here that since the Reynolds number R is not present in the above base flow equations then inertia will have no effect on the base flows. This is discussed further in later Chapters.

3.2.1 Boundary Conditions

For a full solution of this set of ordinary differential equations a corresponding set of boundary conditions are required. These will obviously differ for each of the different flow configurations.

3.2.1.1 Non-Symmetric Planar Poiseuille Flows

The boundary conditions for planar Poiseuille flow are 'no-slip' at the channel walls and since the walls are stationary this dictates that the velocities of the fluids at the boundaries

are all equal to zero. This gives the boundary conditions for the non-symmetric problems as

$$(u_{\mathrm{B}})_j \,|_{y=0,1} = 0, \tag{3.22}$$

where the subscript j denotes whichever fluid is in contact with the channel wall.

3.2.1.2 Symmetric Planar Poiseuille Flows

Applying the 'no-slip' condition to the symmetric flow configurations gives boundary conditions on the upper wall as

$$(u_{\mathrm{B}})_j \,|_{y=1} = 0. \tag{3.23}$$

The lower boundaries of the symmetric problems are axes of symmetry and not fluid-solid boundaries, hence the 'no-slip' criterion cannot be applied. Since this is a symmetric problem then the maximum velocity must be at the centre of the channel, that is, along the axis of symmetry. This then gives the boundary conditions on the axes of symmetry as

$$(u_{\mathrm{B}})'_j \,|_{y=0} = 0. \tag{3.24}$$

3.2.2 Interface Conditions for Multilayered Flows

The presence of the fluid-fluid interface in the multilayered flow configurations requires that forces are balanced across this boundary, i.e. that continuity is preserved. The expression

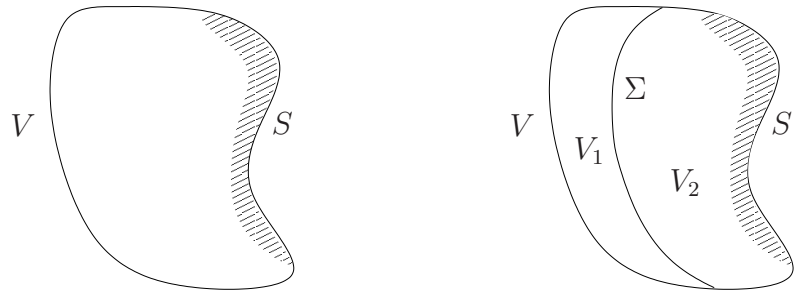

Figure 3.5: The two volume elements used for the derivation of the Navier-Stokes equations: without the interface Σ and with the interface Σ.

for continuity of velocity across the interface is simply the jump equation

$$[[\mathbf{u}]] = 0.$$

Here $[[.]]$ denotes the jump across the interface, i.e. $[[.]] = (.)_1|_{y=l} - (.)_2|_{y=l}$. For the base flow this jump equation reduces to

$$[[u_{\mathrm{B}}]] = 0. \tag{3.25}$$

Expressions for the continuity of shear stresses and normal stresses are obtained by consideration of the conservation of momentum. Whereas the first of the Navier Stokes equations, that for momentum, is derived by considering the balance of momentum within an arbitrary volume V enclosed by the surface S, the conditions for the balance of stresses across an interface can be derived by introducing an interface within V, as illustrated in Fig. 3.5. The interface, denoted by Σ, splits V into two, not necessarily equal parts, V_1 and V_2 such that $V = V_1 \cup V_2$. When an analysis similar to that leading to the derivation of the momentum equation is applied over $V_1 \cup V_2$, the momentum equation is derived as

before, as well as an interface condition. This interface condition describes the balancing of the tangential tractions at the interface and the normal component of the jump across the interface by the surface tension on Σ [37]. In the problems considered in this thesis, surface tension is neglected and this analysis leads to the jump equations

$$[[\hat{\mathbf{t}}.\mathbf{T}.\hat{\mathbf{n}}]] = 0,$$

for shear stresses and

$$[[\hat{\mathbf{n}}.\mathbf{T}.\hat{\mathbf{n}}]] = 0,$$

for normal stresses. The vector $\hat{\mathbf{t}}$ is the unit vector parallel to the interface,

$$\hat{\mathbf{t}} = \frac{1}{\sqrt{1+\left(\frac{\partial H}{\partial x}\right)^2}} \begin{pmatrix} 1 \\ \\ \frac{\partial H}{\partial x} \end{pmatrix},$$

and the vector $\hat{\mathbf{n}}$ is the unit vector normal to the interface,

$$\hat{\mathbf{n}} = \frac{1}{\sqrt{1+\left(\frac{\partial H}{\partial x}\right)^2}} \begin{pmatrix} -\frac{\partial H}{\partial x} \\ \\ 1 \end{pmatrix}.$$

Here H denotes the equation of the interface which for the steady base flow is $h_{\mathrm{B}} = l - y = 0$. The stress tensors $\mathbf{T}_j$ are defined as

$$\mathbf{T}_j = \boldsymbol{\tau}_j + m_j\beta_j\left(\nabla\mathbf{u}_j + (\nabla\mathbf{u}_j)^T\right) - p_j\mathbf{I},$$

where the stress has been split into Newtonian and non-Newtonian parts as in the derivation of the governing equations.

Applying the assumptions for the base flow, the shear stress condition becomes

$$[[\tau_{xy_{\mathrm{B}}} + m\beta u'_{\mathrm{B}}]] = 0. \tag{3.26}$$

The normal stress condition is applicable only with equation (3.15) if the solutions for the pressures are required.

The kinematic free surface condition,

$$\frac{\partial H}{\partial t} + \left((\mathbf{u})_j \mid_{y=l} \right) . \nabla H = 0, \tag{3.27}$$

which expresses the condition that fluids do not flow across free surfaces or interfaces, is also required to hold. For the base flow this is

$$\frac{\partial h_{\mathrm{B}}}{\partial t} + \left((\mathbf{u}_{\mathrm{B}})_j \mid_{y=l} \right) . \nabla h_{\mathrm{B}} = 0, \tag{3.28}$$

which is identically zero for both fluids. These interface conditions are identical for Giesekus and PTT fluids and also for both the two fluid configuration and the three-layered configuration.

3.2.3 Pressure Gradient Conditions

During the nondimensionalizations of the Navier-Stokes equations and the Giesekus and PTT constitutive equations in Section 3.1, it was stated that the velocity scale is imposed by a choice of the value of the pressure gradient which would ensure that the velocity of the fluids at a particular point in the channel is equal to unity. For the single fluid configurations and for the three-layered configuration the location of this criterion for the fluid velocity is at the centre of the channel. For the two fluid configuration this criterion is implemented at the fluid-fluid interface. This leads to the requirement for a so called 'pressure gradient condition' - a rule which dictates the point within the channel where the fluid velocity is to be set equal to unity.

For the single non-symmetric flow configuration this rule is

$$u_{\mathrm{B}}|_{y=\frac{1}{2}} = 1. \tag{3.29}$$

For the two fluid problem either of

$$(u_{\mathrm{B}})_1\,|_{y=l} = 1, \qquad \text{or} \qquad (u_{\mathrm{B}})_2\,|_{y=l} = 1 \tag{3.30}$$

can be used for the pressure gradient condition.

For the symmetric problems the pressure gradient condition is applied at the axis of symmetry. Hence

$$(u_{\mathrm{B}})_1\,|_{y=0} = 1 \tag{3.31}$$

is the required condition for both the single symmetric case and the three-layered case.

The base flow equations (3.14)-(3.21) along with the relevant boundary, interface and pressure gradient conditions form a complete problem set which can be solved to find the base flows for the Giesekus and PTT fluids for each of the four configurations under consideration. These solutions are described and analysed in Chapter 5.

3.3 Linearized Stability Analysis

In order to perform a linear stability analysis of the flows, the effects of arbitrary, infinitesimal disturbances to the base flows are to be considered. These disturbances are written in general form as

$$\tilde{\mathbf{u}}_j = \bar{\mathbf{u}}_j(y)e^{i\psi x+\sigma t}, \qquad \tilde{p}_j = \bar{p}_j(y)e^{i\psi x+\sigma t}, \qquad \tilde{\boldsymbol{\tau}}_j = \bar{\boldsymbol{\tau}}_j(y)e^{i\psi x+\sigma t}, \tag{3.32}$$

where $\tilde{\mathbf{u}}_j = (\tilde{u}_j, \tilde{v}_j)$, $\bar{\mathbf{u}}_j = (\bar{u}_j, \bar{v}_j)$, $\tilde{\boldsymbol{\tau}}_j = \left(\tilde{\tau}_{xx_j}, \tilde{\tau}_{xy_j}, \tilde{\tau}_{yy_j}\right)$, and $\bar{\boldsymbol{\tau}}_j = \left(\bar{\tau}_{xx_j}, \bar{\tau}_{xy_j}, \bar{\tau}_{yy_j}\right)$. The eigenfunctions, $\bar{u}_j$, $\bar{v}_j$,..., $\bar{\tau}_{yy_j}$ are complex functions of y that express the shape of the disturbance mode and all have infinitesimally small magnitudes such that nonlinear terms may be neglected. The wavelength of the disturbances is denoted by the real parameter, ψ, which dictates the propagation of the disturbances along the channel in the x direction. The complex eigenvalue, σ, indicates the stability of the flow and is required to have negative real part for the disturbances to decay and for the base flow to be stable. There will be a number of eigenvalues, forming an eigenspectrum and it is the value of the most unstable

eigenvalue, i.e. that with the most positive real part, which is of most interest in a linear stability analysis. These disturbances are added to the base flow so that the velocity of the fluid is defined as a sum of the base flow and the disturbances, i.e. $\mathbf{u}_j = (\mathbf{u}_{\mathrm{B}})_j + \tilde{\mathbf{u}}_j$ and similarly for the pressure and stresses. For the multilayered problems it is noted that although the pressure gradient is identical across the channel, the pressure itself is not, and so the perturbations to pressure may be different in each fluid as may be the perturbations to the other base flow variables.

Substituting these expressions into the governing equations (3.5)-(3.13) and linearizing, by neglecting second and higher order terms of the disturbance variables, gives the following linearized stability equations:

The Navier-Stokes equations: conservation of momentum

$$R_j \left[i\psi \left(u_{\mathrm{B}}\right)_j + \sigma \right] \bar{u}_j - m_j \beta_j \left(\bar{u}_j'' - \psi^2 \bar{u}_j \right) + R_j \left(u_{\mathrm{B}}\right)_j' \bar{v}_j = i\psi \left(\bar{\tau}_{xx_j} - \bar{p}_j \right) + \bar{\tau}_{xy_j}', \tag{3.33}$$

$$R_j \left[i\psi \left(u_{\mathrm{B}}\right)_j + \sigma \right] \bar{v}_j - m_j \beta_j \left(\bar{v}_j'' - \psi^2 \bar{v}_j \right) = i\psi \bar{\tau}_{xy_j} + \bar{\tau}_{yy_j}' - \bar{p}_j', \tag{3.34}$$

and continuity of mass

$$i\psi \bar{u}_j + \bar{v}_j' = 0. \tag{3.35}$$

The Giesekus constitutive equation

$$W_j\left[\left(i\psi\left(u_{\mathrm{B}}\right)_j+\sigma\right)\bar{\tau}_{xx_j}+\left(\tau_{xx\mathrm{B}}\right)'_j\bar{v}_j-2i\psi\left(\left(\tau_{xx\mathrm{B}}\right)_j\bar{u}_j+\left(\tau_{xy_{\mathrm{B}}}\right)_j\bar{v}_j\right)\right]+\bar{\tau}_{xx_j}$$
$$+2\frac{\epsilon_j W_j}{m_j\left(1-\beta_j\right)}\left(\left(\tau_{xx\mathrm{B}}\right)_j\bar{\tau}_{xx_j}+\left(\tau_{xy_{\mathrm{B}}}\right)_j\bar{\tau}_{xy_j}\right)=2i\psi m_j\left(1-\beta_j\right)\bar{u}_j, \quad (3.36)$$

$$W_j\left[\left(i\psi\left(u_{\mathrm{B}}\right)_j+\sigma\right)\bar{\tau}_{xy_j}+\left(\tau_{xy_{\mathrm{B}}}\right)'_j\bar{v}_j-\left(\tau_{xx\mathrm{B}}\right)_j\bar{u}'_j-\left(u_{\mathrm{B}}\right)'_j\bar{\tau}_{xx_j}-i\psi\left(\tau_{yy_{\mathrm{B}}}\right)_j\bar{v}_j\right]+\bar{\tau}_{xy_j}$$
$$+\frac{\epsilon_j W_j}{m_j\left(1-\beta_j\right)}\left(\left(\tau_{xy_{\mathrm{B}}}\right)_j\left(\bar{\tau}_{xx_j}+\bar{\tau}_{yy_j}\right)+\left(\left(\tau_{xx\mathrm{B}}\right)_j+\left(\tau_{yy_{\mathrm{B}}}\right)_j\right)\bar{\tau}_{xy_j}\right)=m_j\left(1-\beta_j\right)\left(\bar{u}'_j+i\psi\bar{v}_j\right), \quad (3.37)$$

$$W_j\left[\left(i\psi\left(u_{\mathrm{B}}\right)_j+\sigma\right)\bar{\tau}_{yy_j}+\left(\tau_{yy_{\mathrm{B}}}\right)'_j\bar{v}_j-2\left(\tau_{yy_{\mathrm{B}}}\right)_j\bar{v}'_j-2\left(u_{\mathrm{B}}\right)'_j\bar{\tau}_{xy_j}-2\left(\tau_{xy_{\mathrm{B}}}\right)_j\bar{u}'_j\right]+\bar{\tau}_{yy_j}$$
$$+2\frac{\epsilon_j W_j}{m_j\left(1-\beta_j\right)}\left(\left(\tau_{xy_{\mathrm{B}}}\right)_j\bar{\tau}_{xy_j}+\left(\tau_{yy_{\mathrm{B}}}\right)_j\bar{\tau}_{yy_j}\right)=2m_j\left(1-\beta_j\right)\bar{v}'_j. \quad (3.38)$$

The Phan-Thien Tanner constitutive equation

$$W_j\left[\left(i\psi\left(u_{\mathrm{B}}\right)_j+\sigma\right)\bar{\tau}_{xx_j}+\left(\tau_{xx\mathrm{B}}\right)'_j\bar{v}_j-2i\psi\left(\left(\tau_{xx\mathrm{B}}\right)_j\bar{u}_j+\left(\tau_{xy_{\mathrm{B}}}\right)_j\bar{v}_j\right)\right]$$
$$W_j\xi_j\left[i\psi\left(2\left(\tau_{xx\mathrm{B}}\right)_j\bar{u}_j+\left(\tau_{xy_{\mathrm{B}}}\right)_j\bar{v}\right)+\left(\tau_{xy_{\mathrm{B}}}\right)_j\bar{u}'_j+\bar{\tau}_{xy_j}\left(u_{\mathrm{B}}\right)'_j\right]+\bar{\tau}_{xx_j}$$
$$+\frac{\epsilon_j W_j}{m_j\left(1-\beta_j\right)}\left(\left(\tau_{xx\mathrm{B}}\right)_j\left(\bar{\tau}_{xx_j}+\bar{\tau}_{yy_j}\right)+\bar{\tau}_{xx_j}\left(\left(\tau_{xxB}\right)_j+\left(\tau_{yy_B}\right)_j\right)\right)=2i\psi m_j\left(1-\beta_j\right)\bar{u}_j, \quad (3.39)$$

$$W_j\left[\left(i\psi\left(u_{\mathrm{B}}\right)_j+\sigma\right)\bar{\tau}_{xy_j}+\left(\tau_{xy_{\mathrm{B}}}\right)'_j\bar{v}_j-\left(u_{\mathrm{B}}\right)'_j\bar{\tau}_{xx_j}-\left(\tau_{xx\mathrm{B}}\right)_j\bar{u}'_j-i\psi\left(\tau_{yy_{\mathrm{B}}}\right)_j\bar{v}_j\right]$$
$$+\frac{W_j\xi_j}{2}\left[2i\psi\left(\left(\tau_{xx\mathrm{B}}\right)_j+2\left(\tau_{yy_{\mathrm{B}}}\right)_j\right)\bar{v}+\left(u_{\mathrm{B}}\right)'_j\left(\bar{\tau}_{xx_j}+\bar{\tau}_{yy_j}\right)+\left(\left(\tau_{xx\mathrm{B}}\right)_j+\left(\tau_{yy_{\mathrm{B}}}\right)_j\right)\bar{u}'_j\right]+\bar{\tau}_{xy_j}$$
$$+\frac{\epsilon_j W_j}{m_j\left(1-\beta_j\right)}\left(\left(\tau_{xy_{\mathrm{B}}}\right)_j\left(\bar{\tau}_{xx_j}+\bar{\tau}_{yy_j}\right)+\bar{\tau}_{xy_j}\left(\left(\tau_{xx\mathrm{B}}\right)_j+\left(\tau_{yy_{\mathrm{B}}}\right)_j\right)\right)=m_j\left(1-\beta_j\right)\left(\bar{u}'_j+i\psi\bar{v}_j\right), \tag{3.40}$$

$$W_j\left[\left(i\psi\left(u_{\mathrm{B}}\right)_j+\sigma\right)\bar{\tau}_{yy_j}+\left(\tau_{yy_{\mathrm{B}}}\right)'_j\bar{v}_j-2\left(\left(\tau_{yy_{\mathrm{B}}}\right)_j\bar{v}'_j+\left(\tau_{xy_{\mathrm{B}}}\right)_j\bar{u}'+\left(u_{\mathrm{B}}\right)'_j\bar{\tau}_{xy_j}\right)\right]$$
$$+W_j\xi_j\left[2\left(\tau_{yy_{\mathrm{B}}}\right)_j\bar{v}'_j+\left(\tau_{xy_{\mathrm{B}}}\right)_j\bar{u}'_j+\left(u_{\mathrm{B}}\right)'_j\bar{\tau}_{xy_j}+i\psi\left(\tau_{xy_{\mathrm{B}}}\right)_j\bar{v}_j\right]+\bar{\tau}_{yy_j}$$
$$+\frac{\epsilon_j W_j}{m_j(1-\beta_j)}\left(\left(\tau_{yy_{\mathrm{B}}}\right)_j\left(\bar{\tau}_{xx_j}+\bar{\tau}_{yy_j}\right)+\bar{\tau}_{yy_j}\left(\left(\tau_{xx\mathrm{B}}\right)_j+\left(\tau_{yy_{\mathrm{B}}}\right)_j\right)\right)=2m_j\left(1-\beta_j\right)\bar{v}'_j. \tag{3.41}$$

Here, primes have been introduced to denote differentiation with respect to y. Equation (3.34) has been derived in detail in Appendix A.

3.3.1 Boundary Conditions

The boundary conditions for the disturbance quantities are homogeneous to the 'no-slip' boundary conditions which have been applied to the base flow, hence,

$$\bar{u}_j|_{y=0,1}=0 \qquad \text{and} \qquad \bar{v}_j|_{y=0,1}=0, \tag{3.42}$$

for the non-symmetric problems, and

$$\bar{u}_j|_{y=1} = 0, \qquad \bar{v}_j|_{y=0,1} = 0 \qquad \text{and} \qquad \bar{u}_j'|_{y=0} = 0; \tag{3.43}$$

for the symmetric problems.

3.3.2 Interface Conditions for Multilayered flows

The disturbed interface is described by the equation

$$H = h_{\mathrm{B}} + \tilde{h},$$

where $h_{\mathrm{B}} = l - y = 0$ is the interface in the steady base flow and $\tilde{h} = \bar{h}e^{i\psi x+\sigma t}$ is the disturbance to this interface. The eigenfunction $\bar{h}$ has a small magnitude and is treated similarly to the other eigenfunctions, $\bar{u}_j$, $\bar{v}_j$,...,$\bar{\tau}_{yy_j}$, with the exception that $\bar{h}$ is a constant as opposed to being a function of y. The interface conditions are the same as those for the base flow. They reduce to the following jump equations: continuity of velocity

$$\bar{h}[[u_{\mathrm{B}}']] + [[\bar{u}]] = 0, \tag{3.44}$$

$$[[\bar{v}]] = 0, \tag{3.45}$$

continuity of shear stresses

$$-i\psi\bar{h}[[\tau_{xx\mathrm{B}} - \tau_{yy\mathrm{B}}]] + [[\bar{\tau}_{xy}]] + [[m\beta\,(\bar{u}' + i\psi\bar{v})]] = 0, \tag{3.46}$$

continuity of normal stresses

$$[[\bar{\tau}_{yy}]] - [[\bar{p}]] + 2[[m\beta\bar{v}']] = 0, \tag{3.47}$$

and the kinematic free surface condition

$$\bar{h}\,(\sigma + i\psi(u_{\mathrm{B}})_j|_{y=l}) = \bar{v}_j|_{y=l}. \tag{3.48}$$

These linearized stability equations, boundary conditions and interface conditions make up several eigenvalue problems, for the eigenvalue σ, for Giesekus or PTT fluids, for any of the flow configurations under consideration. These systems are to be solved in order to determine the eigenspectra and hence to analyse the stability of the base flows. The resulting eigenspectra are described and analysed in Chapter 6.

Chapter 4

Numerical Methods

In this Chapter the numerical methods which are employed to solve the equations derived in Chapter 3 are explained. There are essentially three methods in all. The first method is the discretization and subsequent solution of the base flow equations in order to derive the base flow. The following two methods employ the linearized stability equations, with the inclusion of the base flow solution, for the application of two different numerical methods in order to derive an eigenspectrum.

4.1 Notation

In the following Sections a large amount of notation is introduced. Therefore, in order to aid understanding and as a reference point, Tables 4.1, 4.2 and 4.3 contain definitions of all notations relevant to this Chapter and are included at the beginning of each relevant Section.

4.2 Calculation of the Base Flow

z	general flow variable
$\hat{z}_n$	nth Chebyshev coefficient in the Chebyshev expansion representing the general flow variable z
T_n	nth Chebyshev polynomial
N	maximum number of Chebyshev polynomials in a truncated expansion
z_i	general flow variable represented by a Chebyshev expansion truncated to i terms
$(\mathbf{f}_{\text{eq}})_j$	vector containing the simultaneous equations for the Chebyshev coefficients relevant to the 'eq' equation where eq is one of: m - the momentum equation ci - the ith constitutive equation ($i = 1, 2, 3$) pg - the pressure gradient condition j refers to either fluid 1 or fluid 2 in multiple fluid flows
$\mathbf{f}_{\text{B}}^{[i]}$	vector containing all the vectors $\mathbf{f}_{\text{eq}}$ in succession as required for the complete base flow of an i-fluid problem
$\mathbf{T}_R$	vector containing the first 0 to R Chebyshev polynomials and then additional terms of T_0 to make up dimension $N + 1$
$\mathbf{x}_n$	vector containing the nth guess for the values of all Chebyshev coefficients during implementation of Newton's method
$\mathbf{f}_{\text{B}}^{[i]'}(\mathbf{x}_n)$	the Jacobean matrix of $\mathbf{f}_{\text{B}}^{[i]}$ evaluated using the values for the Chebyshev coefficients given by $\mathbf{x}_n$

Table 4.1: Table explaining the notation introduced in Section 4.2.

An analytical solution for the planar Poiseuille flow of a Giesekus fluid has not been found and is not known of in the literature, although a semi-analytical solution has been proposed by Cruz and Pinho [12]. (Here, semi-analytical refers to the fact that, whereas

explicit analytical expressions for the principal normal stress and velocity gradient have been determined, numerical integration is required in order to determine the velocity.) A numerical scheme has therefore been devised so as to provide discretized solutions for the base flow of Giesekus fluids in the configurations described in Chapter 3. Analytical solutions for the channel flow of a linear PTT fluid have been derived by Alves *et. al.* [6] and Cruz *et. al.* [13]. These are complicated solutions for a single fluid in a symmetric channel so have limited application to the geometries studied here. Also, since a discrete form of the base flow solution will be required for the calculation of the eigenspectrum it is convenient to compute a numerical solution.

A spectral method is chosen for these numerical computations as these methods require fewer degrees of freedom for a given accuracy than other non-spectral methods, such as finite elements, hence there is less computational expense. The method is described in the following Sections.

4.2.1 Discretization using Chebyshev Polynomials

Discretization using the Chebyshev-tau method is a preferred method in the literature for the computation of the complete eigenspectrum (see [9, 31, 65]) and is the first method used later for the same means. It is logical to apply this method here, in order to find the base flow, since these solutions are required in the later computations of the eigenspectra and use of the same method of discretization will ensure their compatability.

In order to utilize the Chebyshev polynomials in the discretization it is necessary for

the independent variable, y, to have values in the interval $[-1, 1]$. The formulation of the problems given in Chapter 3 dictates that the flow variables for the single fluid problems are dependent on $y \in [0, 1]$. For the two fluid problems the flow variables are dependent on $y \in [0, l]$ for fluid 1 and $y \in [l, 1]$ for fluid 2. It is therefore necessary to transform y as follows: for the single fluid cases

$$\tilde{y} = 2y - 1,$$

and for the two fluid cases

$$\tilde{y}_1 = \frac{2y}{l} - 1,$$
$$\tilde{y}_2 = \frac{2(y-1)}{1-l} + 1.$$

The flow variables can now be easily expressed in terms of Chebyshev polynomial expansions. The relevant equations and boundary, interface and pressure gradient conditions are also modified to correspond to the new independent variables $\tilde{y}_j$.

Applying the above and assuming that [10]

$$z \in L_w^2(-1, 1) = \left\{ z : \int_{-1}^{1} \frac{1}{\sqrt{1-x^2}} z^2 \mathrm{d}x < \infty \right\}$$

where z is any base flow variable, then every base flow variable can be expressed in the form

$$z(y) = \sum_{n=0}^{\infty} \hat{z}_n T_n(y),$$

where $\hat{z}_n$ represents the Chebyshev coefficients. The y-dependence of the flow variables is expressed via the orthogonal polynomials T_n as

$$T_n(y) = \cos n\theta, \qquad \theta = \arccos y, \qquad y \in [-1, 1], \qquad n \in \mathbb{N}. \tag{4.1}$$

Clearly $T_0(y) = 1$ for all y. Given that the correct values of the Chebyshev coefficients, $\hat{z}_n$, are known, this infinite sequence of Chebyshev polynomials is an exact representation of the corresponding flow variables. In order for this representation to have any practical relevance however, and for computational purposes, it is necessary to take an approximation to the variables as

$$z_N = \sum_{n=0}^{N} \hat{z}_n T_n, \tag{4.2}$$

where N is suitably large. Thus the accuracy of the numerical solution is governed by the chosen value of N. This choice of the value of N is discussed later in this Chapter.

Derivative terms of the flow variables are expressible as [10]

$$z'_N = \sum_{n=0}^{N} z_n^{(1)} T_n, \qquad z_n^{(1)} = \frac{2}{c_n} \sum_{\substack{q=n+1 \\ q+n \text{ odd}}}^{N} q\hat{z}_q, \tag{4.3}$$

and for second derivatives

$$z''_N = \sum_{n=0}^{N} z_n^{(2)} T_n, \qquad z_n^{(2)} = \frac{1}{c_n} \sum_{\substack{q=n+2 \\ q+n \text{ even}}}^{N} q(q^2 - n^2)\hat{z}_q, \tag{4.4}$$

where

$$c_n = \begin{cases} 2 & \text{if } n = 0 \\ 1 & \text{if } n \geq 1. \end{cases}$$

The following identity is required for use in the discretization of product terms [10]

$$2T_nT_k = T_{n+k} + T_{|n-k|}. \tag{4.5}$$

In a summation the first term on the right-hand side of (4.5) is neglected by convention when $n + k > N$ so as to be in line with the truncation of other terms.

4.2.1.1 Discretization of the Base Flow Equations

The fully discretized form of equation (3.14) is

$$0 = -\widehat{\left(\frac{\partial p_{\mathrm{B}}}{\partial x}\right)}_0 + \frac{2}{L}\sum_{n=0}^{N}\frac{2}{c_n}\sum_{\substack{q=n+1 \\ q+n\,\text{odd}}}^{N} q\widehat{\left(\tau_{xy_{\mathrm{B}}}\right)}_q T_n + \frac{4}{L^2}m\beta\sum_{n=0}^{N}\frac{1}{c_n}\sum_{\substack{q=n+2 \\ q+n\,\text{even}}}^{N} q(q^2-n^2)\widehat{(u_{\mathrm{B}})}_q T_n, \tag{4.6}$$

where the subscripts denoting the fluid have been neglected. Here

$$L = \begin{cases} l & \text{for fluid 1} \\ 1-l & \text{for fluid 2} \\ 1 & \text{for single fluid flows} \end{cases}$$

Here $\widehat{(\partial p_{\mathrm{B}}/\partial x)}_0$ is the only Chebyshev coefficient required to represent the pressure gradient since this is known to be a constant. The shear stress is represented by a set of $(N + 1)$

Chebyshev coefficients, $\widehat{\left(\tau_{xy_{\mathrm{B}}}\right)}_n$ where $n = 0, 1, \ldots, N$, and similarly for the velocity and other stresses.

Continuing with the example above, equation (3.14), when $N = 3$ equation (4.6) becomes

$$\left[-\widehat{\left(\frac{\partial p_{\mathrm{B}}}{\partial x}\right)}_0 + \frac{2}{L}\widehat{\left(\tau_{xy_{\mathrm{B}}}\right)}_1 + \frac{6}{L}\widehat{\left(\tau_{xy_{\mathrm{B}}}\right)}_3 + m\beta\frac{16}{L^2}\widehat{(u_{\mathrm{B}})}_2\right] T_0 + \left[\frac{8}{L}\widehat{\left(\tau_{xy_{\mathrm{B}}}\right)}_2 + m\beta\frac{96}{L^2}\widehat{(u_{\mathrm{B}})}_3\right] T_1 + \frac{12}{L}\widehat{\left(\tau_{xy_{\mathrm{B}}}\right)}_3 T_2 = 0.$$

This equation can be expressed as the vector equation

$$\begin{pmatrix} T_0 & T_1 & T_2 & T_3 \end{pmatrix} \mathbf{f}_{\mathrm{m}} = 0,$$

where

$$\mathbf{f}_{\mathrm{m}} = \begin{pmatrix} -\widehat{\left(\frac{\partial p_{\mathrm{B}}}{\partial x}\right)}_0 + \frac{2}{L}\widehat{\left(\tau_{xy_{\mathrm{B}}}\right)}_1 + \frac{6}{L}\widehat{\left(\tau_{xy_{\mathrm{B}}}\right)}_3 + m\beta\frac{16}{L^2}\widehat{(u_{\mathrm{B}})}_2 \\ \frac{8}{L}\widehat{\left(\tau_{xy_{\mathrm{B}}}\right)}_2 + m\beta\frac{96}{L^2}\widehat{(u_{\mathrm{B}})}_3 \\ \frac{12}{L}\widehat{\left(\tau_{xy_{\mathrm{B}}}\right)}_3 \\ 0 \end{pmatrix},$$

and the subscript m denotes the momentum equation

Similar equations exist for the discretized forms of the Giesekus and PTT constitutive equations. These are given in full for general N in Appendix B.

4.2.1.2 Discretized Boundary, Interface and Pressure Gradient Conditions

The above vector equations do not include any terms relating to the boundary, interface or pressure gradient conditions. In order for these conditions to be included in the computations, which is essential to determine accurate approximations, they must be discretized and suitably incorporated into the vector equations.

The boundary, interface and pressure gradient conditions can be discretized in a similar manner to the base flow equations, with the exception that a value for the independent variable $\tilde{y}_j$ can be applied to the T_n functions. At the lower boundary, when $\tilde{y}_j = -1$, the Chebyshev polynomial functions reduce as follows:

$$\begin{aligned} T_n(\tilde{y}_j = -1) &= \cos\left(n \arccos\left(-1\right)\right), \\ &= \cos\left(n\left(2i+1\right)\pi\right), \qquad\qquad i \in \mathbb{N}, \\ &= \left(-1\right)^n. \end{aligned}$$

At the upper boundary, when $\tilde{y}_j = 1$, the functions reduce similarly:

$$\begin{aligned} T_n(\tilde{y}_j = 1) &= \cos\left(n \arccos\left(1\right)\right), \\ &= \cos\left(n2i\pi\right), \qquad\qquad i \in \mathbb{N}, \\ &= 1. \end{aligned}$$

The discretized boundary conditions for the non-symmetric problems are therefore

$$\sum_{n=0}^{N}\widehat{\left(\left(u_{\mathrm{B}}\right)_j\right)}_n T_n(-1) = \sum_{n=0}^{N}(-1)^n\widehat{\left(\left(u_{\mathrm{B}}\right)_j\right)}_n = 0, \tag{4.7}$$

$$\sum_{n=0}^{N}\widehat{\left(\left(u_{\mathrm{B}}\right)_j\right)}_n T_n(1) = \sum_{n=0}^{N}\widehat{\left(\left(u_{\mathrm{B}}\right)_j\right)}_n = 0. \tag{4.8}$$

For the symmetric problems the boundary conditions are

$$\frac{2}{L}\sum_{n=0}^{N}\frac{2}{c_n}\sum_{\substack{q=n+1\\ q+n\,\mathrm{odd}}}^{N} q\widehat{\left(\left(u_{\mathrm{B}}\right)_j\right)}_q T_n(-1) = \frac{2}{L}\sum_{n=0}^{N}\frac{2}{c_n}(-1)^n\sum_{\substack{q=n+1\\ q+n\,\mathrm{odd}}}^{N} q\widehat{\left(\left(u_{\mathrm{B}}\right)_j\right)}_q = 0, \tag{4.9}$$

$$\sum_{n=0}^{N}\widehat{\left(\left(u_{\mathrm{B}}\right)_j\right)}_n T_n(1) = \sum_{n=0}^{N}\widehat{\left(\left(u_{\mathrm{B}}\right)_j\right)}_n = 0. \tag{4.10}$$

The discretized velocity interface condition is

$$\sum_{n=0}^{N}\widehat{\left(\left(u_{\mathrm{B}}\right)_1\right)}_n - \sum_{n=0}^{N}\widehat{\left(\left(u_{\mathrm{B}}\right)_2\right)}_n(-1)^n = 0 \tag{4.11}$$

and the discretized shear stress interface condition is

$$\sum_{n=0}^{N}\left(\widehat{\left(\tau_{xy_{\mathrm{B}}}\right)_1}\right)_n + \beta_1\frac{2}{l_1}\sum_{n=0}^{N}\frac{2}{c_n}\sum_{\substack{q=n+1\\ q+n\,\mathrm{odd}}}^{N} q\widehat{\left(\left(u_{\mathrm{B}}\right)_1\right)}_q$$
$$-\sum_{n=0}^{N}\left(\widehat{\left(\tau_{xy_{\mathrm{B}}}\right)_2}\right)_n(-1)^n - m\beta_2\frac{2}{1-l_1}\sum_{n=0}^{N}\frac{2}{c_n}\sum_{\substack{q=n+1\\ q+n\,\mathrm{odd}}}^{N} q\widehat{\left(\left(u_{\mathrm{B}}\right)_2\right)}_q(-1)^n = 0. \tag{4.12}$$

It is also necessary to discretize the pressure gradient conditions. For the single fluid configurations and the three-layered configuration the velocity is set equal to unity in the

centre of the channel. For the non-symmetric single fluid configuration the centre of the channel is at $\tilde{y} = 0$. The value of the Chebyshev polynomials at $\tilde{y} = 0$ is given by

$$\begin{aligned} T_n(\tilde{y} = 0) &= \cos\left(n \arccos\left(0\right)\right), \\ &= \cos\left(n\frac{(2i+1)\,\pi}{2}\right), \qquad\qquad i \in \mathbb{N}, \\ &= \begin{cases} (-1)^{\frac{n}{2}} & \text{if } n \text{ even} \\ 0 & \text{if } n \text{ odd} \end{cases} \end{aligned}$$

So the discretized representation of the pressure gradient condition for the non-symmetric Poiseuille flow of a single fluid is

$$\sum_{n=0}^{N} \widehat{\left(\left(u_{\mathrm{B}}\right)_j\right)}_n T_n(0) = \sum_{\substack{n=0 \\ n\,\text{even}}}^{N} (-1)^{\frac{n}{2}} \widehat{\left(\left(u_{\mathrm{B}}\right)_j\right)}_n = 0.$$

For the symmetric configurations for a single fluid or for three-layered flows the centre of the channel is the axis of symmetry, $\tilde{y}_1 = -1$. The discretized pressure gradient condition for these cases is

$$\sum_{n=0}^{N} \widehat{\left(\left(u_{\mathrm{B}}\right)_1\right)}_n T_n(-1) = \sum_{n=0}^{N} (-1)^n \widehat{\left(\left(u_{\mathrm{B}}\right)_1\right)}_n = 1.$$

The final pressure gradient condition is that which is to be applied to the problem of planar Poiseuille flow of two fluids. Here the velocity is set to unity at the fluid-fluid interface. This gives the discretized form of the pressure gradient condition for this flow configuration

as

$$\sum_{n=0}^{N} \widehat{((u_{\mathrm{B}})_1)}_n T_n(1) = \sum_{n=0}^{N} \widehat{((u_{\mathrm{B}})_1)}_n = 1, \tag{4.13}$$

or

$$\sum_{n=0}^{N} \widehat{((u_{\mathrm{B}})_2)}_n T_n(-1) = \sum_{n=0}^{N} (-1)^n \widehat{((u_{\mathrm{B}})_2)}_n = 1. \tag{4.14}$$

4.2.2 The Solution Scheme

In Appendix C the previous discretization and the following method are employed to explicitly solve a 'toy' problem. What follows here is a general explanation of the solution scheme for the problems under consideration in this thesis.

In order to form a complete problem set the discretized base flow equations along with the relevant discretized boundary, interface and pressure gradient conditions must be incorporated into a single vector equation.

4.2.2.1 Single Fluid Problems

For the single fluid problems the vector equation is of the form

$$\begin{pmatrix} \mathbf{T}_{N-2} & \mathbf{T}_N & \mathbf{T}_N & \mathbf{T}_N & T_0 \end{pmatrix} \mathbf{f}_{\mathrm{B}}^{[1]} = 0. \tag{4.15}$$

Here

$$\mathbf{T}_{N-2} = \begin{pmatrix} T_0 & T_1 & \dots & T_{N-2} & T_0 & T_0 \end{pmatrix},$$
$$\mathbf{T}_{N} = \begin{pmatrix} T_0 & T_1 & \dots & T_{N} \end{pmatrix},$$

$$\mathbf{f}_{\mathrm{B}}^{[1]} = \begin{pmatrix} \mathbf{f}_{\mathrm{m}} \\ \mathbf{f}_{\mathrm{c1}} \\ \mathbf{f}_{\mathrm{c2}} \\ \mathbf{f}_{\mathrm{c3}} \\ f_{\mathrm{pg}} \end{pmatrix}.$$

The vectors $\mathbf{f}_{\mathrm{ci}}$ contain the terms relating to the three Giesekus or PTT constitutive equations as required. The scalar expression f_{pg} contains terms relating to the pressure gradient condition. The vector $\mathbf{f}_{\mathrm{B}}^{[1]}$ has dimension $4\,(N+1)+1$.

A number of terms relating to higher order Chebyshev polynomials have been substituted for T_0 in the first vector term. The last two components of the vector $\mathbf{f}_{\mathrm{m}}$ which relate to these substituted terms are used to implement the boundary conditions. This small truncation of the sequence of Chebyshev polynomials does not affect the accuracy of the final solutions since N is large.

4.2.2.2 Multiple Fluid Problems

A similarly structured vector equation is formed from the discretized base flow equations for the two fluid problems. This is

$$\left(\begin{array}{cccccccc} \mathbf{T}_{N-2} & \mathbf{T}_N & \mathbf{T}_N & \mathbf{T}_N & \mathbf{T}_{N-2} & \mathbf{T}_N & \mathbf{T}_N & \mathbf{T}_N & T_0 \end{array} \right) . \mathbf{f}_{\mathrm{B}}^{[2,3]} = 0, \tag{4.16}$$

where

$$\mathbf{f}_{\mathrm{B}}^{[2,3]} = \left(\begin{array}{c} (\mathbf{f}_{\mathrm{m}})_1 \\ (\mathbf{f}_{\mathrm{c1}})_1 \\ (\mathbf{f}_{\mathrm{c2}})_1 \\ (\mathbf{f}_{\mathrm{c3}})_1 \\ (\mathbf{f}_{\mathrm{m}})_2 \\ (\mathbf{f}_{\mathrm{c1}})_2 \\ (\mathbf{f}_{\mathrm{c2}})_2 \\ (\mathbf{f}_{\mathrm{c3}})_2 \\ f_{\mathrm{pg}} \end{array} \right)$$

The vector $\mathbf{f}_B^{[2,3]}$ has dimension $8\,(N+1)+1$. Here there are four rows which can be used for the boundary and interface conditions. Two rows are substituted into the last two rows of the momentum equation for fluid 1 and two into the momentum equation for fluid 2. Again, the last component of $\mathbf{f}_{\mathrm{B}}^{[2,3]}$ is used for the pressure gradient condition.

Since the Chebyshev polynomials are orthogonal it is possible to neglect the first vector

in equations (4.15) and (4.16), which leaves the final problems to be solved as

$$\mathbf{f}_{\mathrm{B}}^{[1]} = 0 \qquad \text{and} \qquad \mathbf{f}_{\mathrm{B}}^{[2,3]} = 0. \tag{4.17}$$

The components of the vectors $\mathbf{f}_{\mathrm{B}}^{[i]}$ are functions of the unknown Chebyshev coefficients. Newton's method is applied to the above equations in order to find these Chebyshev coefficients which, when known, will give a discrete solution for the base flow to an accuracy which is dependent on the value of N and the tolerance of the iterative scheme. Given a satisfactory initial guess for the values of the Chebyshev coefficients, the vector $\mathbf{f}_{\mathrm{B}}^{[i]}$ is computed and used to generate a new set of values for the Chebyshev coefficents according to Newton's equation

$$\mathbf{x}_{n+1} = \mathbf{x}_n - \frac{\mathbf{f}_{\mathrm{B}}^{[i]}(\mathbf{x}_n)}{\mathbf{f}_{\mathrm{B}}^{[i]'}(\mathbf{x}_n)}. \tag{4.18}$$

Rearranging this equation such that

$$\mathbf{f}_{\mathrm{B}}^{[i]'}(\mathbf{x}_n)\,(\mathbf{x}_{n+1} - \mathbf{x}_n) = -\,\mathbf{f}_{\mathrm{B}}^{[i]}(\mathbf{x}_n)\,,$$

$$\mathbf{f}_{\mathrm{B}}^{[i]'}(\mathbf{x}_n)\,\Delta\mathbf{x} = -\,\mathbf{f}_{\mathrm{B}}^{[i]}(\mathbf{x}_n)\,,$$

then $\Delta\mathbf{x} = \mathbf{x}_{n+1} - \mathbf{x}_n$ can easily be found by applying Gaussian reduction to the augmented matrix

$$\left(\; \mathbf{f}_{\mathrm{B}}^{[i]'}(\mathbf{x}_n) \;\middle|\; -\mathbf{f}_{\mathrm{B}}^{[i]}(\mathbf{x}_n) \;\right).$$

Here, the vector $\mathbf{f}_{\mathrm{B}}^{[i]'}$ is the Jacobian matrix of $\mathbf{f}_{\mathrm{B}}^{[i]}$ with respect to $\mathbf{x}$, which is the vector of

Chebyshev coefficients. Hence $\mathbf{f}_{\mathrm{B}}^{[i]'}$ is a square matrix with dimension equal to the dimension of the vector $\mathbf{f}_{\mathrm{B}}^{[i]}$.

The criteria which dictates whether the iterative scheme is sufficiently converged is chosen to be

$$\max\left(|\Delta x_i|\right) \leq 10^{-8},$$

i.e. that the greatest change in value of a Chebyshev coefficent, either increasing or decreasing, between sucessive iterations, does not exceed 10^{-8}.

Since the base flow of planar Poiseuille flow of an Oldroyd-B fluid is solvable analytically, this solution is generally used as an initial guess. As the Giesekus and PTT parameters, ϵ and ξ, are increased away from the Oldroyd-B fluid a continuation method is employed whereby the solutions for lower parameter values are used as initial guesses.

4.3 Calculation of the Eigenspectrum

Two methods have been used in order to calculate the eigenvalues of the fluid flow problems. The first incorporates a Chebyshev polynomial discretization, similar to that used for the base flow, with a QZ implementation to find a full eigenspectrum. The second uses a non-spectral integration method, the Runge-Kutta scheme, in conjuction with a shooting method to find individual discrete eigenvalues. The failings and benefits of each of these schemes are discussed at the end of this Chapter. Firstly, full explanations of both methods are given here.

4.3.1 The Chebyshev-QZ Scheme

$\mathbf{T}_{\text{LSE}}$	vector containing $\mathbf{T}_{N-2}$, $\mathbf{T}_{N-2}$, $\mathbf{T}_N$, $\mathbf{T}_N$, $\mathbf{T}_N$ and $\mathbf{T}_N$ in succession
$\widehat{(\bar{\mathbf{z}})}_N$	vector containing the unknown Chebyshev coefficients of truncated Chebyshev expansions of all disturbance variables in succession
$\mathbf{A}^{[i]}$ and $\mathbf{B}^{[i]}$	matrices containing numerical values relating Chebyshev polynomials and Chebyshev coefficients such that equations (4.19) and (4.20) are accurate representations of all the discretized linearized stability equations for the i-fluid problem
$\hat{\bar{h}}$	Chebyshev coefficient corresponding to the disturbed fluid-fluid interface
σ	the eigenvalue to be found
$(\mathbf{A}_{\text{eq}})_k$ and $(\mathbf{B}_{\text{eq}})_k$	matrices contained within $\mathbf{A}^{[i]}$ and $\mathbf{B}^{[i]}$ which themselves contain numerical values relating Chebyshev polynomials and Chebyshev coefficients such that $\mathbf{T}_{\text{LSE}}(\mathbf{A}_{\text{eq}})_k \widehat{(\bar{\mathbf{z}})}_N = \sigma \mathbf{T}_{\text{LSE}}(\mathbf{B}_{\text{eq}})_k \widehat{(\bar{\mathbf{z}})}_N$ is an accurate representation of the discretized form of the linearized stability equation 'eq' where eq is one of mj - the jth momentum equation cont - the continuity equation cj - the jth constitutive equation k refers to fluid 1 or fluid 2
$(\mathbf{a}_{\text{kfsc}})$ and $(\mathbf{b}_{\text{kfsc}})$	as for $(\mathbf{A}_{\text{eq}})_k$ and $(\mathbf{B}_{\text{eq}})_k$ but refering to the kinematic free surface condition and therefore $(\mathbf{a}_{\text{kfsc}})$ and $(\mathbf{b}_{\text{kfsc}})$ are vectors

Table 4.2: Table explaining the notation introduced in Section 4.3.1.

This first method is used to find the complete eigenspectrum and is frequently used in the literature, (see [9, 31, 65]).

4.3.1.1 Discretization of the Linearized Stability Equations

The linearized stability equations (3.33)-(3.41) are discretized using Chebyshev polynomials in an identical manner to that used to discretize the base flow equations. The value of the parameter N is chosen to be equal for the discretizations of both the base flow and the linearized stability equations, so as to ensure compatability of the base flow solutions with the computations of the eigenspectrum. The discretized forms of the linearized stability equations are given in full in Appendix D.

These equations give a problem in the form,

$$\mathbf{T}_{\mathrm{LSE}}.\mathbf{A}^{[1]}.\widehat{(\bar{\mathbf{z}})}_N = \sigma \mathbf{T}_{\mathrm{LSE}}.\mathbf{B}^{[1]}.\widehat{(\bar{\mathbf{z}})}_N, \tag{4.19}$$

for the single fluid problem, and in the form

$$\begin{pmatrix} \mathbf{T}_{\mathrm{LSE}} & \mathbf{T}_{\mathrm{LSE}} & T_0 \end{pmatrix}.\mathbf{A}^{[2,3]}.\begin{pmatrix} \left(\widehat{(\bar{\mathbf{z}})}_1\right)_N \\ \left(\widehat{(\bar{\mathbf{z}})}_2\right)_N \\ \widehat{\bar{h}} \end{pmatrix} = \sigma \begin{pmatrix} \mathbf{T}_{\mathrm{LSE}} & \mathbf{T}_{\mathrm{LSE}} & T_0 \end{pmatrix}.\mathbf{B}^{[2,3]}.\begin{pmatrix} \left(\widehat{(\bar{\mathbf{z}})}_1\right)_N \\ \left(\widehat{(\bar{\mathbf{z}})}_2\right)_N \\ \widehat{\bar{h}} \end{pmatrix}, \tag{4.20}$$

for the multiple fluid problems. Here

$$\mathbf{T}_{\mathrm{LSE}} = \begin{pmatrix} \mathbf{T}_{N-2} & \mathbf{T}_{N-2} & \mathbf{T}_N & \mathbf{T}_N & \mathbf{T}_N & \mathbf{T}_N \end{pmatrix},$$

$$\widehat{(\bar{\mathbf{z}})}_N = \begin{pmatrix} \widehat{(\bar{u})}_0 \\ \vdots \\ \widehat{(\bar{u})}_N \\ \widehat{(\bar{v})}_0 \\ \vdots \\ \widehat{(\bar{v})}_N \\ \widehat{(\bar{p})}_0 \\ \vdots \\ \widehat{(\bar{p})}_N \\ \widehat{(\bar{\tau}_{xx})}_0 \\ \vdots \\ \widehat{(\bar{\tau}_{yy})}_N \end{pmatrix}.$$

$$\mathbf{A}^{[1]} = \begin{pmatrix} \mathbf{A}_{\mathrm{m1}} \\ \mathbf{A}_{\mathrm{m2}} \\ \mathbf{A}_{\mathrm{cont}} \\ \mathbf{A}_{\mathrm{c1}} \\ \mathbf{A}_{\mathrm{c2}} \\ \mathbf{A}_{\mathrm{c3}} \end{pmatrix}, \qquad \mathbf{B}^{[1]} = \begin{pmatrix} \mathbf{B}_{\mathrm{m1}} \\ \mathbf{B}_{\mathrm{m2}} \\ \mathbf{B}_{\mathrm{cont}} \\ \mathbf{B}_{\mathrm{c1}} \\ \mathbf{B}_{\mathrm{c2}} \\ \mathbf{B}_{\mathrm{c3}} \end{pmatrix}$$

$$\mathbf{A}^{[2,3]} = \begin{pmatrix} (\mathbf{A}_{\mathrm{m1}})_1 \\ (\mathbf{A}_{\mathrm{m2}})_1 \\ (\mathbf{A}_{\mathrm{cont}})_1 \\ (\mathbf{A}_{\mathrm{c1}})_1 \\ (\mathbf{A}_{\mathrm{c2}})_1 \\ (\mathbf{A}_{\mathrm{c3}})_1 \\ (\mathbf{A}_{\mathrm{m1}})_2 \\ (\mathbf{A}_{\mathrm{m2}})_2 \\ (\mathbf{A}_{\mathrm{cont}})_2 \\ (\mathbf{A}_{\mathrm{c1}})_2 \\ (\mathbf{A}_{\mathrm{c2}})_2 \\ (\mathbf{A}_{\mathrm{c3}})_2 \\ (\mathbf{a}_{\mathrm{kfsc}}) \end{pmatrix}, \quad \text{and} \quad \mathbf{B}^{[2,3]} = \begin{pmatrix} (\mathbf{B}_{\mathrm{m1}})_1 \\ (\mathbf{B}_{\mathrm{m2}})_1 \\ (\mathbf{B}_{\mathrm{cont}})_1 \\ (\mathbf{B}_{\mathrm{c1}})_1 \\ (\mathbf{B}_{\mathrm{c2}})_1 \\ (\mathbf{B}_{\mathrm{c3}})_1 \\ (\mathbf{B}_{\mathrm{m1}})_2 \\ (\mathbf{B}_{\mathrm{m2}})_2 \\ (\mathbf{B}_{\mathrm{cont}})_2 \\ (\mathbf{B}_{\mathrm{c1}})_2 \\ (\mathbf{B}_{\mathrm{c2}})_2 \\ (\mathbf{B}_{\mathrm{c3}})_2 \\ (\mathbf{b}_{\mathrm{kfsc}}) \end{pmatrix}.$$

The matrices $\mathbf{A}^{[1]}$ and $\mathbf{B}^{[1]}$ are square of dimension $6(N+1)$, and the matrices $\mathbf{A}^{[2,3]}$ and $\mathbf{B}^{[2,3]}$ are square of dimension $12(N+1)+1$. Similarly to the matrix equations for the base flow, some Chebyshev polynomials have been substituted for T_0. The rows in the matrices $\mathbf{A}^{[1]}$, $\mathbf{B}^{[1]}$, $\mathbf{A}^{[2,3]}$ and $\mathbf{B}^{[2,3]}$ which correspond to these terms, contain the boundary and interface conditions. The last rows of the matrices $\mathbf{A}^{[2,3]}$ and $\mathbf{B}^{[2,3]}$ correspond to the kinematic free surface condition. In fully discretized form this is

$$\sigma\widehat{(\bar{h})}_0 + i\psi\widehat{(\bar{h})}_0 \sum_{n=0}^{N} \widehat{(u_{\mathrm{B1}})}_n = \sum_{n=0}^{N} \widehat{(\bar{v}_1)}_n \tag{4.21}$$

Again, since the Chebyshev polynomials are orthogonal, the matrix problems which are to be solved can be reduced to

$$\mathbf{A}^{[1]}.\widehat{(\bar{\mathbf{z}})}_N = \sigma \mathbf{B}^{[1]}.\widehat{(\bar{\mathbf{z}})}_N, \tag{4.22}$$

and

$$\mathbf{A}^{[2,3]}.\begin{pmatrix} \left(\widehat{(\bar{\mathbf{z}})}_1\right)_N \\ \left(\widehat{(\bar{\mathbf{z}})}_2\right)_N \\ \widehat{\bar{h}} \end{pmatrix} = \sigma \mathbf{B}^{[2,3]}.\begin{pmatrix} \left(\widehat{(\bar{\mathbf{z}})}_1\right)_N \\ \left(\widehat{(\bar{\mathbf{z}})}_2\right)_N \\ \widehat{\bar{h}} \end{pmatrix} \tag{4.23}$$

which are generalized eigenvalue problems.

4.3.1.2 Application of the Scheme

The coefficients of the matrices $\mathbf{A}^{[1]}$, $\mathbf{B}^{[1]}$, $\mathbf{A}^{[2,3]}$ and $\mathbf{B}^{[2,3]}$ are used by a *NAG* routine to compute the eigenvalues of the system using the QZ-algorithm [5]. If required the *NAG* routine can also be used to calculate the eigenvectors but these are not required for this analysis.

The computation time of the QZ-algorithm is M^3 where M is the dimension of the square matrices $\mathbf{A}^{[1]}$, $\mathbf{B}^{[1]}$, $\mathbf{A}^{[2,3]}$ and $\mathbf{B}^{[2,3]}$, hence the computational cost of the single fluid problem is equal to $C\left(6\left(N+1\right)\right)^3$ where C is an unknown proportionality constant [5]. In comparison the computational cost of the two fluid problem is equal to $C\left(12\left(N+1\right)+1\right)^3$ which is approximately 8 times greater than for the single fluid problem.

Whereas this method computes the full eigenspectrum of the generalized eigenvalue prob-

lems, (4.22) and (4.23) derived above, the second method is more suited to finding individual discrete eigenvalues and this is described in the next Section.

4.3.2 The Orthonormal Runge-Kutta Scheme

A and B	two orthonormal problems solved simultaneously to overcome the issue of unknown lower boundary values in the original problem
$\mathbf{A}_{\mathrm{lb}}$	vector containing the lower boundary values for problem A
$\mathbf{A}_{\mathrm{ub}}$	vector containing the upper boundary values for problem A
a_1 and a_2	first and second upper boundary values of problem A
$\mathbf{B}_{\mathrm{lb}}$	vector containing the lower boundary values for problem B
$\mathbf{B}_{\mathrm{ub}}$	vector containing the upper boundary values for problem B
b_1 and b_2	first and second upper boundary values of problem B
$\mathbf{v}_{\mathsf{A}}$	the vector containing the values of $\bar{v}$, $\bar{v}'$, $\bar{v}''$ and $\bar{v}'''$ at any point in problem A
$\tilde{\mathbf{v}}_{\mathsf{A}}$	the vector $\mathbf{v}_{\mathsf{A}}$ after orthonomalisation has been performed
$\mathbf{v}_{\mathsf{B}}$	the vector containing the values of $\bar{v}$, $\bar{v}'$, $\bar{v}''$ and $\bar{v}'''$ at any point in problem B
$\tilde{\mathbf{v}}_{\mathsf{B}}$	the vector $\mathbf{v}_{\mathsf{B}}$ after orthonomalisation has been performed
$\zeta = \begin{vmatrix} \mathsf{a}_1 & \mathsf{b}_1 \\ \mathsf{a}_2 & \mathsf{b}_2 \end{vmatrix} = 0$	the condition on the upper boundary values which must be satisfied by convergence of Newton's method

Table 4.3: Table explaining the notation introduced in Section 4.3.2.

This method, which will be referred to as the Orthonormal Runge-Kutta scheme (ORK) is applicable only to finding individual discrete eigenvalues and is intended to be used for a

deeper analysis of the results produced by the Chebyshev-QZ method. The method follows that described by Ho and Denn [34]. Firstly it is necessary to collate the linearized stability equations into a single fourth order ordinary differential equation for $\bar{v}$, the disturbance cross channel velocity,

$$\bar{v}^{\mathrm{IV}} = f\left(\bar{v}, \bar{v}', \bar{v}'', \bar{v}'''\right).$$

This form of the LSEs is known as the Orr-Sommerfeld equation and is not given explicitly here since it is extensive and complicated. Derivations of the full equations are given in Appendix E for Giesekus fluids and in Appendix G for PTT fluids. The base flow terms in the Orr-Sommerfeld equation are calculated using the Chebyshev-tau method described in Section 4.2 and the results converted into a nonspectral representation using the same step size as will be used by the Runge-Kutta integration. The favoured form of the Orr-Sommerfeld equation in the literature uses the disturbance stream function as the variable. This is not the chosen formulation here since this would increase the order of the Orr-Sommerfeld equation without necessarily simplifying it, thus the introduction of the stream function does not appear to introduce any advantages.

The method is shown schematically in Fig. 4.1. An initial guess is made for the eigenvalue σ, using the results from the Chebyshev-QZ scheme described in Section 4.3.1. Starting from known boundary conditions at the lower boundary fourth-order Runge-Kutta integration is performed across the channel to give upper boundary values. These upper boundary values are then compared with the required upper boundary values as described in section 3.3.1, using Newton's method, to give a new guess for σ which is used to repeat the method and

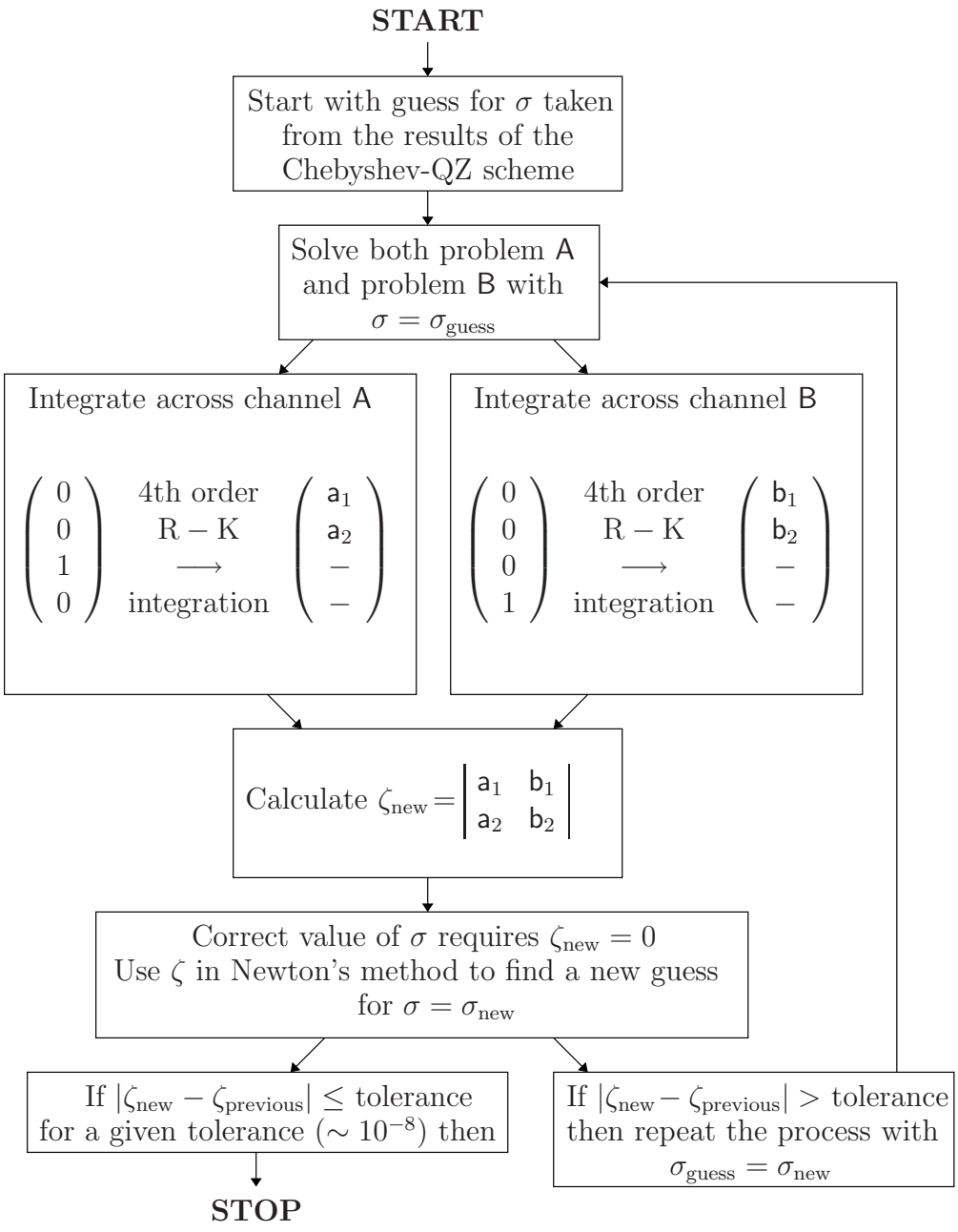

Figure 4.1: Schematic diagram showing the Orthonormal Runge-Kutta numerical scheme.

so on until convergence in the value of σ is achieved within a given tolerance.

Since the complete set of boundary values at the lower boundary is not known, two orthonormal problems, A and B, are introduced in place of the original problem so as to overcome this short-coming. The known lower boundary values are $\bar{v} = \bar{v}' = 0$ with the values for $\bar{v}''$ and $\bar{v}'''$ being unknown. The two orthonormal problems are created by introducing values for these unknown lower boundary values such that

$$\mathsf{A}_{\text{lower boundary}} = \begin{pmatrix} 0 \\ 0 \\ 1 \\ 0 \end{pmatrix}, \qquad \text{and} \qquad \mathsf{B}_{\text{lower boundary}} = \begin{pmatrix} 0 \\ 0 \\ 0 \\ 1 \end{pmatrix}.$$

thus creating two orthonormal vectors at the lower boundary,

$$\mathsf{A}_{\text{lb}}.\mathsf{B}_{\text{lb}} = 0, \qquad |\mathsf{A}_{\text{lb}}| = 1, \qquad |\mathsf{B}_{\text{lb}}| = 1.$$

The fourth-order Runge-Kutta integration is implemented on both of the two problems, A and B, for each guess of σ to give two sets of upper boundary values, $\mathsf{A}_{\text{upper boundary}}$ and $\mathsf{B}_{\text{upper boundary}}$. It is these values which are used to find a new guess for the value of σ. Since the required upper boundary values of the original problem are $\bar{v} = \bar{v}' = 0$ then the requirement for the convergence of σ is that the determinant of the matrix formed from the equivalent upper boundary values of problems A and B is zero. This determinant is

represented by ζ,

$$\zeta = \begin{vmatrix} \mathsf{a}_1 & \mathsf{b}_1 \\ \mathsf{a}_2 & \mathsf{b}_2 \end{vmatrix} = 0, \tag{4.24}$$

where,

$$\mathsf{A}_{\mathrm{ub}} = \begin{pmatrix} \mathsf{a}_1 \\ \mathsf{a}_2 \\ - \\ - \end{pmatrix}, \qquad \text{and} \qquad \mathsf{B}_{\mathrm{ub}} = \begin{pmatrix} \mathsf{b}_1 \\ \mathsf{b}_2 \\ - \\ - \end{pmatrix}.$$

Dashes (-) represent values which are not known and are not used.

4.3.2.1 Orthonormalization

In order that these two orthonormal problems give accurate results for the sought eigenvalue then their orthonomality must be preserved as the Runge-Kutta integration moves across the channel. It was noted by Ho and Denn [34] that, without intervention, this would not be the case. The same is found for these problems and the orthonormality of the problems A and B is lost after a few integration steps. Following [34] an additional step is added to the calculations whereby a chosen number of orthonormalizations are performed at regular intervals across the channel and at the final point at the upper boundary. The number of orthonormalizations will have an impact on the accuracy of the solution, as will the stepsize of the Runge-Kutta integrations. The orthonormalization is implemented thus, where tildes

($\tilde{}$) represent the orthonormalized values;

$$\tilde{\mathbf{v}}_{\mathsf{A}} = \frac{\mathbf{v}_{\mathsf{A}}}{||\mathbf{v}_{\mathsf{A}}||}, \tag{4.25}$$

$$\tilde{\mathbf{v}}_{\mathsf{B}} = \frac{\mathbf{v}_{\mathsf{B}} - (\mathbf{v}_{\mathsf{B}}, \tilde{\mathbf{v}}_{\mathsf{A}})\, \tilde{\mathbf{v}}_{\mathsf{A}}}{||\mathbf{v}_{\mathsf{B}} - (\mathbf{v}_{\mathsf{B}}, \tilde{\mathbf{v}}_{\mathsf{A}})\, \tilde{\mathbf{v}}_{\mathsf{A}}||}, \tag{4.26}$$

Here, the inner product $(\mathbf{m}, \mathbf{n})$ is defined as

$$(\mathbf{m}, \mathbf{n}) = \sum_{i=1}^{4} m_i n_i^*$$

where n_i^* is the complex conjugate of the ith term in $\mathbf{n}$, and the norm $||\mathbf{m}||$ is defined by

$$||\mathbf{m}|| = (\mathbf{m}, \mathbf{m})^{\frac{1}{2}}.$$

After each orthonormalization the Runge-Kutta integration is continued as normal, until the next orthonormalization, and so on.

The final stage of the numerical scheme uses ζ in Newton's method in the conventional manner to calculate a new guess for the eigenvalue σ. The computation is terminated when $|\zeta|$ is below a tolerated amount. That is

$$|\zeta_{\text{new}}| \leq 10^{-8}.$$

4.4 Critique of the Numerical Methods

Both spectral and nonspectral methods have been described above. Spectral methods have the advantage of lower computational costs since fewer degrees of freedom are required for a given accuracy of the final approximations. The disadvantage found in the Chebyshev-QZ method for the computation of the full eigenspectrum however is that the resolution of the continuous spectra is low. This is thought to be due to an inability of the QZ-Algorithm to handle branch cuts of the Orr-Sommerfeld equation in a well-resolved manner [9, 31]. Figs. 4.2, 4.3 and 4.4 show the eigenspectra for single Oldroyd-B, Giesekus and PTT fluids in symmetric planar Poiseuille flows. The continuous spectra are shown as 'balloons' which become narrower as the value of N, the number of Chebyshev modes used in the discretization, is increased. This ballooning is considerably less for the lower continuous spectra (known as the 'Oldroyd-B' parts, since they are only present when $\beta > 0$ [65]) than for the upper continuous spectra (known as the 'UCM' parts).

The 'Oldroyd-B' spectra show slightly more ballooning and the 'UCM' spectra show less ballooning for the Giesekus and PTT fluids compared to the spectra for an Oldroyd-B fluid. In fact the 'UCM' spectra are split into two separate continuous eigenspectra bringing the total to three when the Giesekus and PTT parameters, ϵ and ξ, are nonzero. Both these eigenspectra still show some ballooning but it is predominantly on the outer sides of the spectra with little ballooning to be seen between the spectra. It has been suggested that the changes in the level of ballooning may be due to changes in the number of singular components in the constitutive equation [31], i.e. that there has been an increase in singular

components associated with the 'Oldroyd-B' spectra and a decrease in singular components associated with each of the 'UCM' spectra.

The resolution of the Chebyshev-QZ computations of the discrete eigenvalues is good, with the exception of a few eigenvalues which are close to the continuous spectra, but the computational cost of the QZ algorithm is high and is sufficiently high so as to overcome the computational benefits of the spectral method of discretization. Thus the use of the Chebyshev-QZ method to investigate the discrete eigenvalues would be very time consuming with a level of accuracy which varied according to which eigenvalues were being calculated, hence a quicker and more accurate method has been employed for these enquiries.

The orthonormal Runge-Kutta method quickly and accurately computes individual discrete eigenvalues and is therefore ideal for mapping changes in particular eigenvalues as the fluid parameter values are adjusted, or for finding points of marginal stability. The ORK method however, does not give the full picture of the eigenspectrum which the Chebyshev-QZ method gives, and in fact the ORK method fails to calculate the continuous eigenspectra altogether. Thus, the Chebyshev-QZ method is better for obtaining an overall impression of the eigenspectra before further investigations are undertaken using the ORK method. This is the approach that is applied to the investigations of the linear stability of the flow configurations described in Chapter 3. The findings are given in Chapter 6.

Table 4.4 shows the values obtained by the Chebyshev-QZ method with increasing values of N for two particular eigenvalues. Table 4.5 shows the effect of step number and the number of orthonormalizations on the accuracy of the same eigenvalue found using the ORK method.

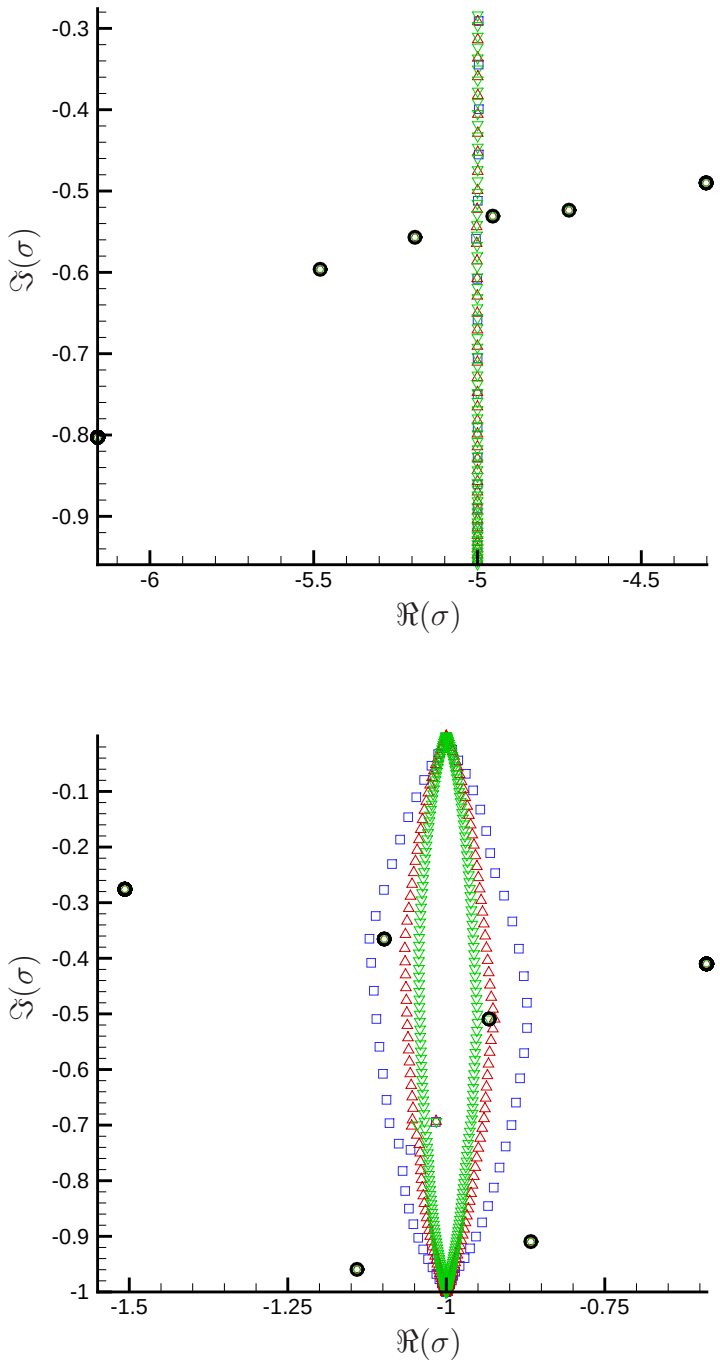

Figure 4.2: The complete eigenspectrum for an Oldroyd-B fluid, calculated numerically for $R = 0$, $W = 1$, $\beta = 0.2$, $\psi = 1$, $N = 40$ ($\square$), $N = 90$ ($\triangle$), $N = 150$ ($\triangledown$). The black circles ($\mathbf{O}$) indicate discrete eigenvalues calculated using the ORK method.

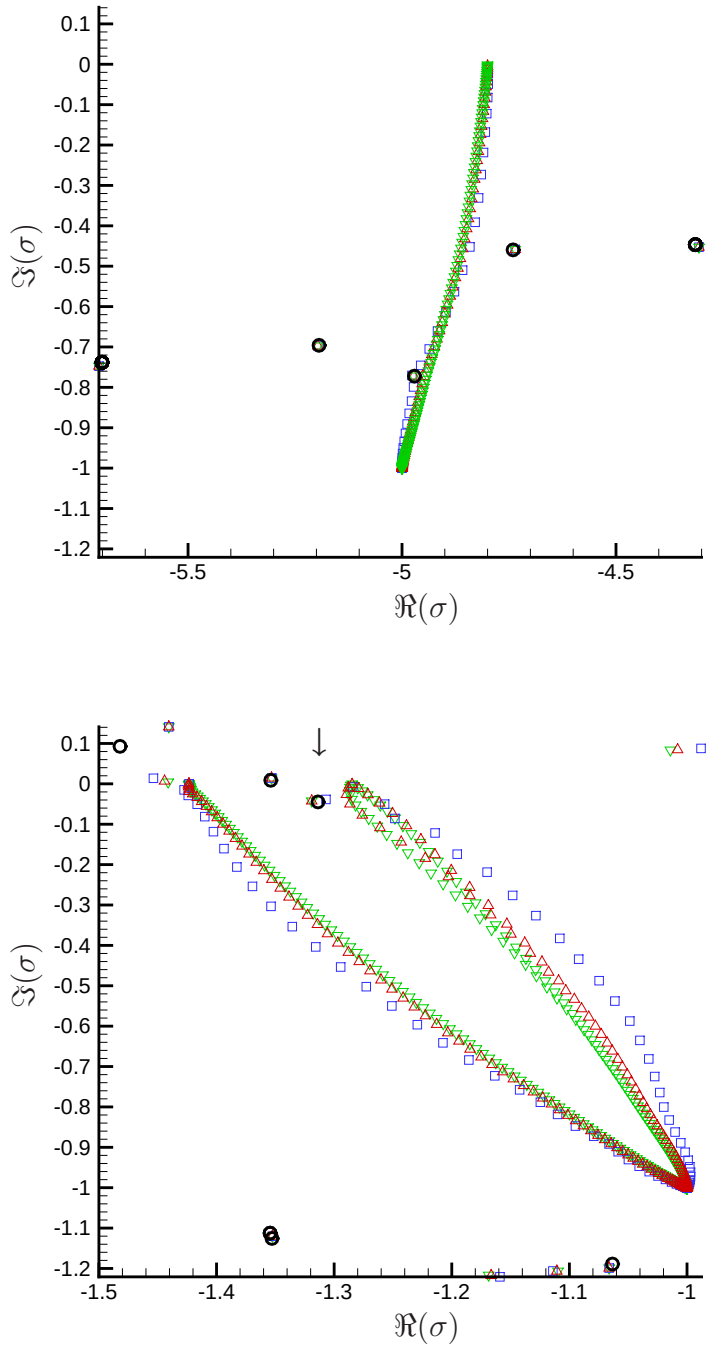

Figure 4.3: The complete eigenspectrum for a Giesekus fluid, calculated numerically for $R = 0$, $W = 1$, $\beta = 0.2$, $\epsilon = 0.1$, $\psi = 1$, $N = 40$ (□), $N = 90$ (△), $N = 150$ (▽). The black circles (O) indicate discrete eigenvalues calculated using the ORK method. The arrow indicates the eigenvalues used in Tables 4.4 and 4.5.

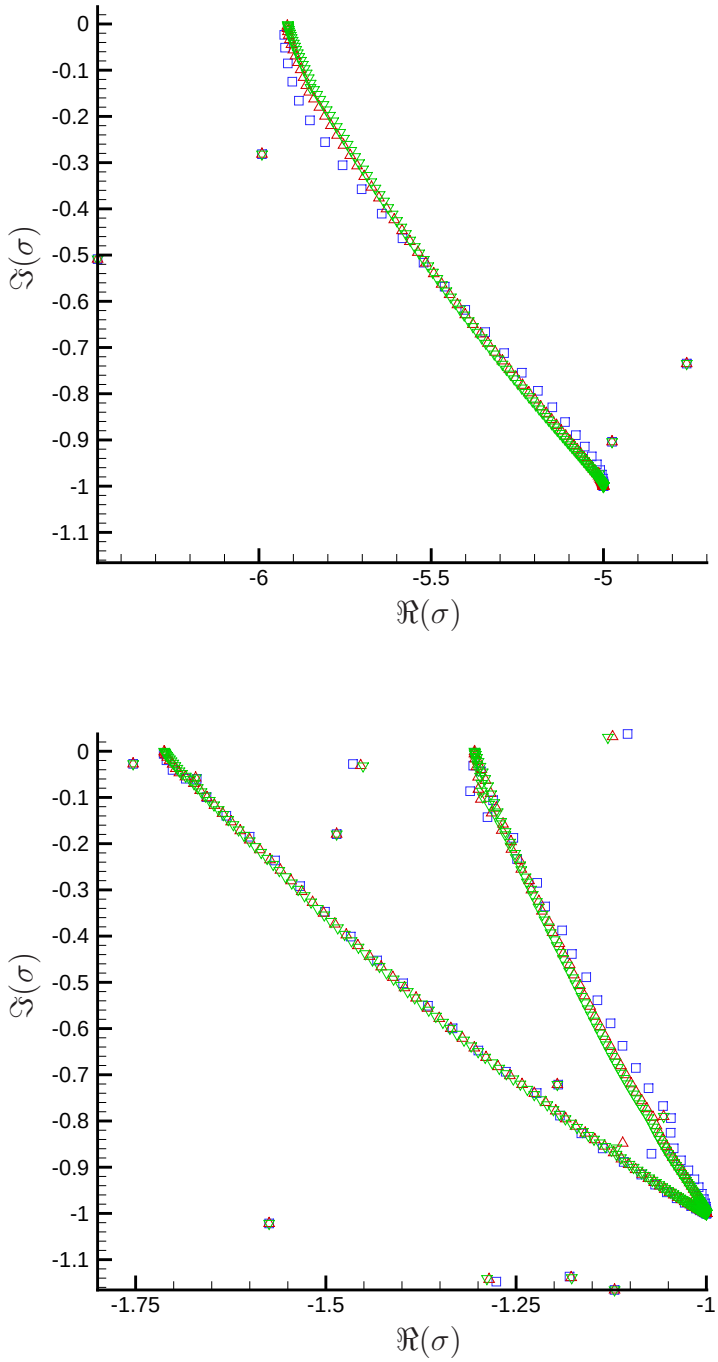

Figure 4.4: The complete eigenspectrum for a Phan-Thien Tanner fluid, calculated numerically for $R = 0$, $W = 1$, $\beta = 0.2$, $\epsilon = 0.1$, $\xi = 0.02$, $\psi = 1$, $N = 40$ ($\square$), $N = 90$ ($\triangle$), $N = 150$ ($\triangledown$).

N	the computed eigenvalue σ
40	-1.30697612877-$i\,(0.03859665701955)$
90	-1.31905022694-$i\,(0.04240425286677)$
150	-1.31904436844-$i\,(0.04241668844117)$
300	-1.31904435993-$i\,(0.04241668183488)$

Table 4.4: Table showing the effect of N, the number of Chebyshev polynomials, on the accuracy of the Chebyshev-QZ method for a particular eigenvalue.

step number	number of orthonormalizations	the computed eigenvalue σ
128	64	-1.32463284804-$i\,(0.03489133580207)$
512	256	-1.31372242756-$i\,(0.04474645605403)$
1024	512	-1.31375994918-$i\,(0.04472838716120)$
2048	1024	-1.31375474585-$i\,(0.04474069438474)$
4096	2048	-1.31375934153-$i\,(0.04473629290042)$
2048	516	-1.31375985593-$i\,(0.04473766770771)$
2048	1024	-1.31375474585-$i\,(0.04474069438474)$
2048	2048	-1.31375985593-$i\,(0.04473766770679)$
4096	128	-1.31368880343-$i\,(0.04469475668018)$
4096	256	-1.31376632540-$i\,(0.04473885508399)$
4096	512	-1.31376086184-$i\,(0.04473866281016)$
4096	1024	-1.31375245154-$i\,(0.04472761776290)$
4096	2048	-1.31375934153-$i\,(0.04473629290042)$
4096	4096	-1.31375992641-$i\,(0.04473749344840)$

Table 4.5: Table showing the effect of step size and orthonormalization on the accuracy of the ORK method for a particular eigenvalue. The initial guess for all computations was $\sigma = -1.319 - i\,(0.0424)$.

At first glance, for this eigenvalue a moderate value of 90 for N gives a satisfactory accuracy using the Chebyshev-QZ scheme. However, an accuracy of five decimal places is obtained using the ORK method for the step number of 2048 and this gives different values to those shown for the Chebyshev-QZ method. This implies that the accuracy of the Chebyshev-QZ method is very low, to only two significant figures for values of N as high as 150. For the ORK method, higher accuracies can be obtained with higher step numbers and, as the step number increases, a lower number of orthonormalizations are required for the same levels of accuracy.

The computational cost of the Chebyshev-QZ method with $N = 150$ is estimated to be of the order of 100 times the cost of the ORK method with 2048 steps. Hence the ORK method is clearly the more efficient of these two schemes for the computation of an individual eigenvalue.

Chapter 5

Base Flow Solutions

5.1 Solutions for Giesekus Fluids

5.1.1 Analytical Investigations

There are no known analytical solutions to the full base flow equations for Giesekus fluids as was discussed in Section 4.2. It is possible however to determine simple solutions for reduced cases when some of the fluid parameters are set to zero.

The Giesekus fluid model reduces to the Oldroyd-B model when $\epsilon = 0$. Since solutions for the Oldroyd-B model are elementary only a general solution is giving here. From this solution particular solutions for each geometry are easily deduced by the application of the relevant boundary, interface (where applicable) and pressure gradient conditions. This

general solution is

$$u_{\mathrm{B}} = \frac{1}{2}\frac{\partial p_{\mathrm{B}}}{\partial x}y^2 + C_1 y + C_2, \tag{5.1}$$

$$\tau_{xx\mathrm{B}} = 0, \tag{5.2}$$

$$\tau_{xy\mathrm{B}} = m\left(1-\beta\right)u'_{\mathrm{B}}, \tag{5.3}$$

$$\tau_{yy\mathrm{B}} = 2Wm\left(1-\beta\right)\left(u'_{\mathrm{B}}\right)^2, \tag{5.4}$$

where C_1 and C_2 are constants.

Further analysis of the base flows for Giesekus fluids when $\epsilon \neq 0$ must be undertaken numerically.

5.1.2 Numerical Investigations

The main aim of the numerical computation of the base flow is as a prerequisite for the numerical computation of the eigenspectra. Also of interest is the scale of the impact of each of the fluid parameters on the base flow profiles. Unusual or irregular base flow profiles can sometimes give elucidation to the presence of and the mechanisms of any instabilities. A smooth base flow is also indicative of a smaller chance of deformities and faults in any final products when applying these results to an industrial setting. In the following Sections the main features of the base flow profiles will be described.

The numerical method used is that described in Section 4.2. The value of N, the number of Chebyshev modes, is chosen to be 90 for the computation of the eigenspectra since this

gives reasonably accurate results within an appropriate computation time. The same value of N is chosen for the calculation of the base flow so as to ensure that the results are compatible with the computations for the eigenspectra.

In Section 5.1.1 analytical solutions were given for an Oldroyd-B fluid. The following results for Giesekus fluids are compared with these Oldroyd-B flows since this is the clearest way to examine the main effects of the Giesekus parts of the model, i.e. the parts $[\epsilon W/m\,(1-\beta)]\,\boldsymbol{\tau}.\boldsymbol{\tau}$ in the Giesekus constitutive equation.

Poiseuille Flow of a Single Giesekus Fluid

The velocity and stress profiles for an Oldroyd-B fluid and a Giesekus fluid with a high level of shear thinning are shown in Fig. 5.1. There is clearly an element of flattening of the velocity profile for non-zero ϵ and this is a common phenomenom for many non-Newtonian fluids [33]. The second normal stress also shows a flattening of its parabolic profile. The shear stress shows a considerable change in character from a straight line profile to a profile with a high degree of curvature. The greatest change is seen in the first normal stress profile however, which is no longer zero with the introduction of shear thinning.

The numerical computations of the base flow become more difficult as certain parameters are altered. In these cases, as ϵ is increased the convergence of the base flow is slower and more iterations are needed before the accuracy of the solution is within the chosen tolerance. Also, a smaller incremental step size for ϵ is necessary for convergence. Consequently there are limits to the parameter values which can be investigated. For symmetric Poiseuille flow of a Giesekus fluid the limit on shear thinning is in the region of $\epsilon = 0.5$. After this point

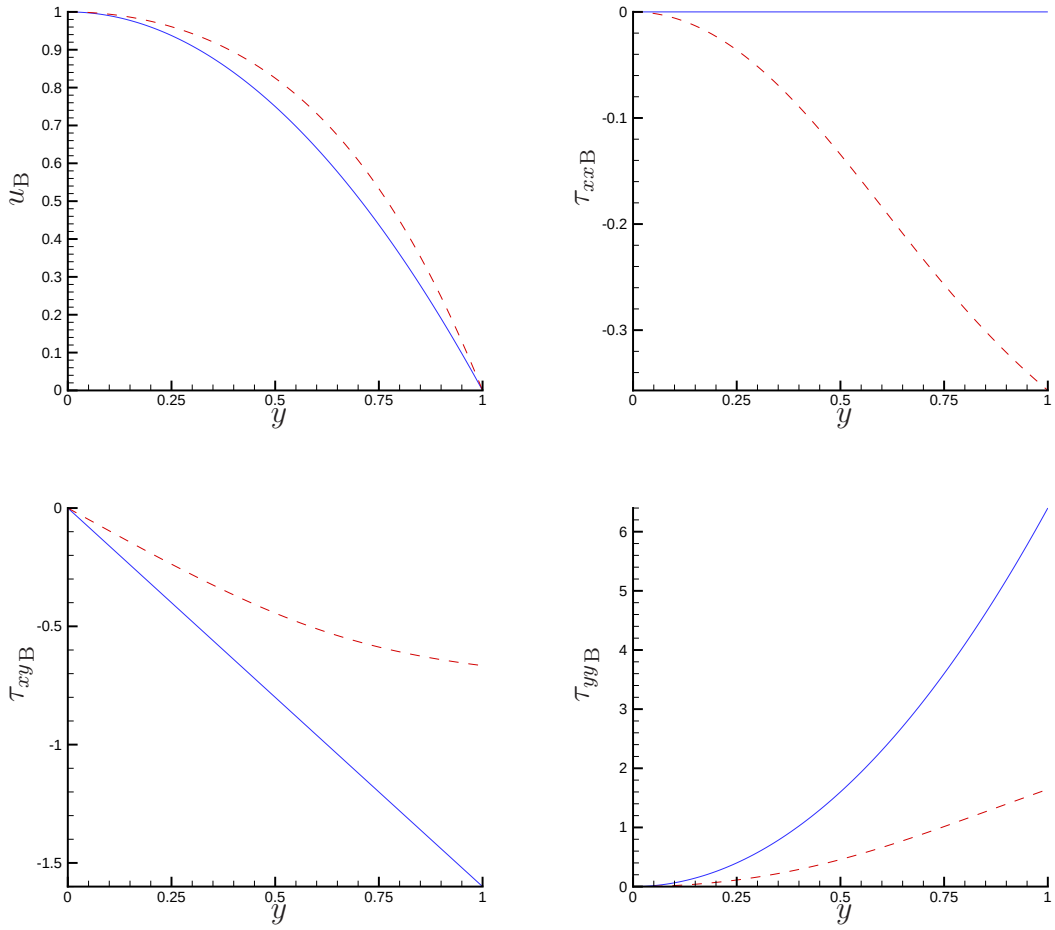

Figure 5.1: Base flow velocity and stress profiles for the symmetric Poiseuille flow of a single Giesekus fluid. The fluid parameters are: $W = 1$, $\beta = 0.2$, $\epsilon = 0$ (Solid lines) and $\epsilon = 0.5$ (Dashed lines).

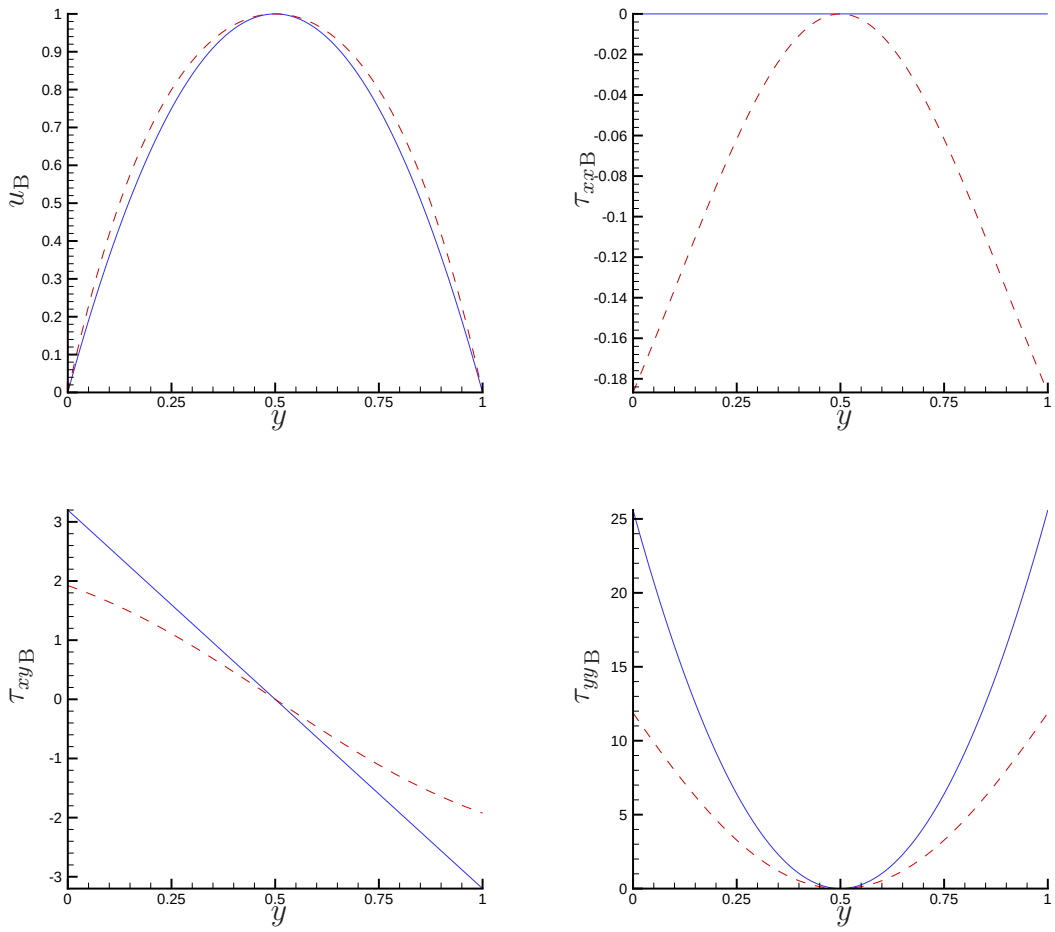

Figure 5.2: Base flow velocity and stress profiles for non-symmetric Poiseuille flow of a single Giesekus fluid. The fluid parameters are: $W = 1$, $\beta = 0.2$, $\epsilon = 0$ (Solid lines) and $\epsilon = 0.04$ (Dashed lines).

computations become cumbersome and time-consuming. It is this value of ϵ that has been chosen for the plots in Fig. 5.1 so as to show the maximum effect possible.

Fig. 5.2 shows the base flow profiles for the non-symmetric Poiseuille flow of a single Giesekus fluid. The limiting value of ϵ for this case is significantly lower than for the symmetric flow, at 0.04, than for the symmetric case. This is still sufficient however to show that the characteristics of the base flow profiles discussed for the symmetric case still hold here. There is less flaring of the first normal stress profile at the channel walls than can be seen for the symmetric case, but this is most likely due to the enforced use of a much lower value of shear thinning.

Poiseuille Flow of Two Giesekus Fluids

The computational difficulties experienced for the non-symmetric Poiseuille flow of a single Giesekus fluid are also experienced to the same extent for the two fluid configuration, the base flow profiles for which are shown in Fig. 5.3. Again, the computational difficulties give a limit to the value of the shear thinning parameter which can be investigated. Here the limit is similar to that for the non-symmetric single fluid case and the value of ϵ used is again chosen to be 0.04. These computational restrictions on the value of ϵ for these two non-symmetric flow configurations would imply that the lack of symmetry in the problem formulation can lead to more computational challenges than for, say, an equivalent symmetric problem. This may be because of the nature of the formulations of the non-symmetric problems (see Chapter 3). For the symmetric problems the velocity at the centre of the channels is set to unity and this point is also defined as the maximum velocity by the pressure

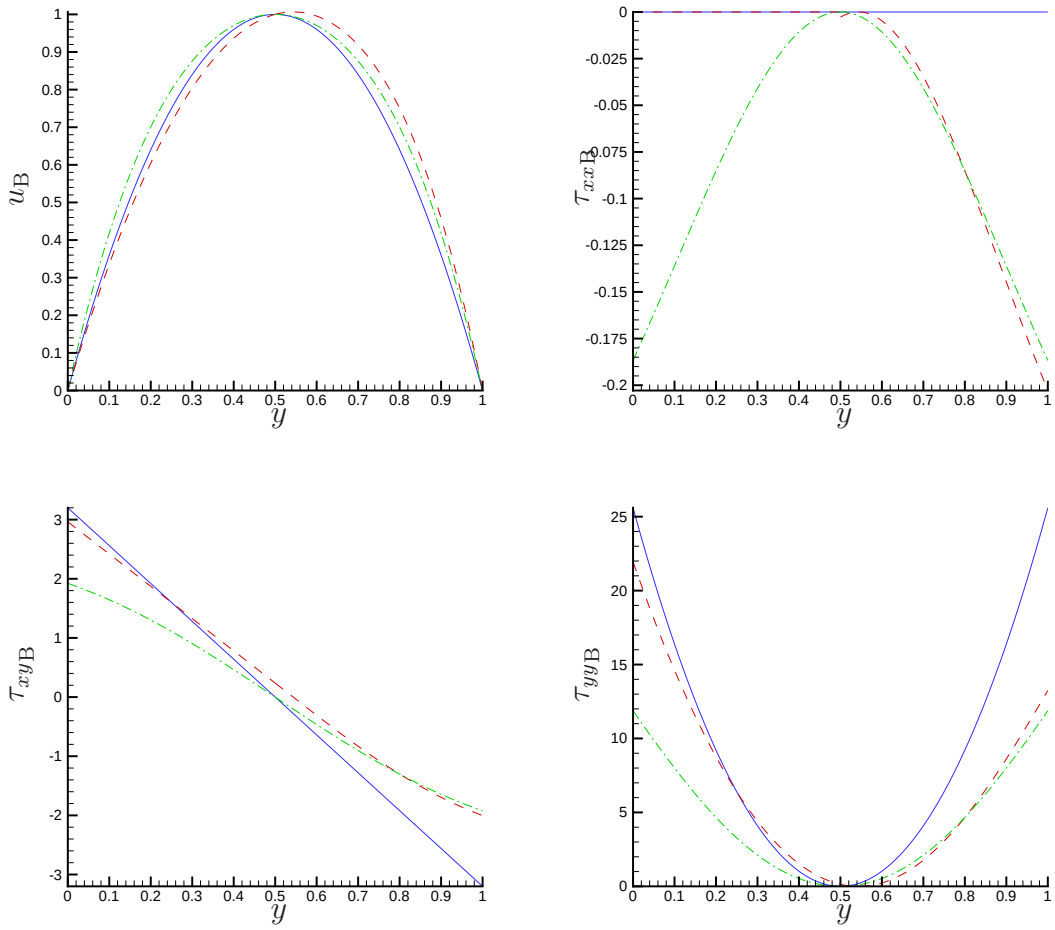

Figure 5.3: Base flow velocity and stress profiles for non-symmetric Poiseuille flow of two Giesekus fluids. The fluid parameters are: $m = 1$, $l = 0.5$; for fluid 1: $W_1 = 1$ and $\beta_1 = 0.2$; and for fluid 2: $W_2 = 1$ and $\beta_2 = 0.2$; with $\epsilon_1 = 0$ and $\epsilon_2 = 0$ (Solid lines), $\epsilon_1 = 0$ and $\epsilon_2 = 0.04$ (Dashed lines) and $\epsilon_1 = 0.04$ and $\epsilon_2 = 0.04$ (Dash-Dotted lines).

gradient condition on the derivative of the velocity. For the non-symmetric problems however there are three boundary and pressure gradient conditions set at three different point across the channel, as opposed to two being set at the same point for the symmetric problems. This may provide a weak point in the formulation of the non-symmetric problems, hence causing the computational difficulties seen here.

The base flow profiles in Fig. 5.3 show similar behaviour to that shown for the single fluid flows. When the parameters in the two fluids are equal then the profiles are identical to those for the single non-symmetric problem, as would be expected. The differing values across the channel give non-symmetric profiles where the characteristics of the non-zero shear thinning are shown in the relevant fluid (fluid 2), and also have some impact, via the fluid-fluid interface, on the Oldroyd-B fluid (fluid 1), and vice versa. This is particularly clear for the velocity profile where the maximum value has shifted away from the interface at $l = 0.5$, into fluid 2 which has a non-zero shear thinning parameter.

The first normal stress is higher in fluid 2 for the case of unequal shear thinning parameters than for equal non-zero shear thinning parameters. The curve is shifted upwards in fluid 2, towards the zero value which holds across fluid 1. The shear stress profile also shows an overlap of characteristics for the case of unequal shear thinning parameters. The curvature caused by non-zero ϵ is seen, but this is reduced in fluid 1, where $\epsilon = 0$ and the curve becomes straighter, but does not match the line for the case of two Oldroyd-B fluids. The second normal stress also shows similar characteristics whereby the parabola is non-symmetric and is closest to the curve of two Oldroyd-B fluids for fluid 1, and closest to the curve for two

Giesekus fluids for fluid 2.

In general then, when the parameters match across the two fluids, this problem is identical to the single non-symmetric configuration, as would be expected. When the parameters do not match for the two fluids, characteristics for each set of parameters can be seen in the relevant fluid, but an effect is also had on the other fluid.

It is not necessary to consider the case of an Oldroyd-B fluid overlying a Giesekus fluid here since this is equivalent to the reflected case of a Giesekus fluid overlying an Oldroyd-B fluid (Dashed lines). Gravity has been neglected in the formulations for all flow configurations and so fluids 1 and 2 are interchangeable in this configuration without loss of generality.

Three-Layered Poiseuille Flow of Two Giesekus Fluids

The velocity and stress base flow profiles for two Gieskus fluids in a three-layered configuration are shown in Fig.5.4 for several combinations of zero and non-zero values of the shear thinning parameters. Since in this configuration fluid 1 is contained within fluid 2 it is necessary to consider the profiles for an Oldroyd-B fluid contained within a Giesekus fluid (Dashed lines) as well as the case of a Gieskus fluid contained with an Oldroyd-B fluid (Dash-Dotted lines). Fluids 1 and 2 are not interchangeable in this configuration as was the case for the two-layered flows in the previous Section.

The base flow velocity profiles show similar characteristics to those seen for the other flow configurations. An exception is the case of a $\epsilon_1 = 0.5$ and $\epsilon_2 = 0$ (Dash-Dotted lines) where the profile is lower than those shown for equal shear thinning across the channel. Similarly for the first normal stress, as opposed to the fluid 1 part of the profile being increased towards

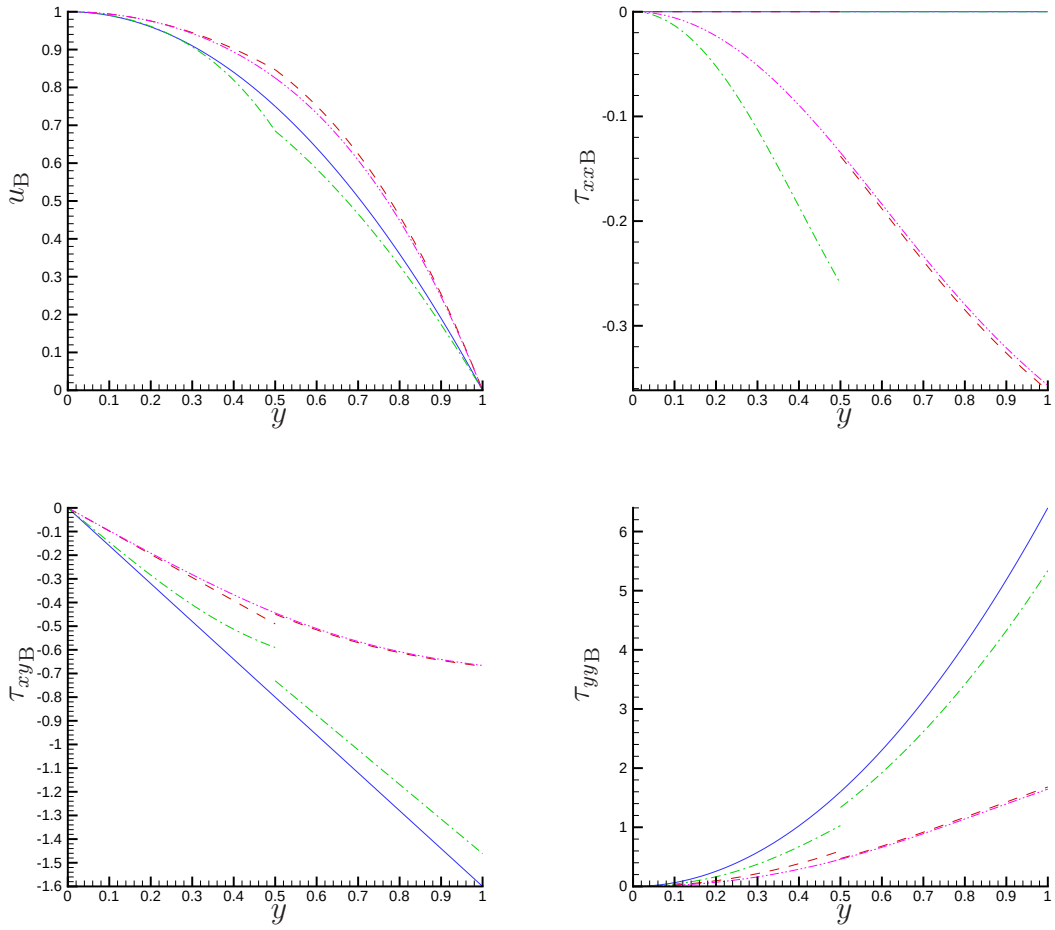

Figure 5.4: Base flow velocity and stress profiles for Poiseuille flow of two Giesekus fluids in a symmetric three-layered configuration. The fluid parameters are: $m = 1$, $l = 0.5$ and; for fluid 1: $W_1 = 1$ and $\beta_1 = 0.2$; and for fluid 2: $W_2 = 1$ and $\beta_2 = 0.2$ with; $\epsilon_1 = 0$ and $\epsilon_2 = 0$ (Solid lines), $\epsilon_1 = 0$ and $\epsilon_2 = 0.5$ (Dashed lines), $\epsilon_1 = 0.5$ and $\epsilon_2 = 0$ (Dash-Dotted lines) and $\epsilon_1 = 0.5$ and $\epsilon_2 = 0.5$ (Dash-Dot-Dotted lines).

zero by the surrounding Oldroyd-B fluid, the first normal stress is reduced beyond that shown for two matched Giesekus fluids (Dash-Dot-Dotted lines). Similar qualities are shown in the profiles for the shear stress and the second normal stress. It would appear therefore that the by containing a Giesekus fluid within an Oldroyd-B fluid, far from dampening any Giesekus characteristics, amplifies them in the central Giesekus fluid.

An additional feature worth noting is the jump in first normal stress when the shear thinning parameter is not matched across the fluids (Dashed lines and Dash-Dotted lines). As was discussed in Chapter 1 Su and Khomami [62] showed that elastic interfacial instabilities were caused by jumps in the first normal stress difference. Although the first normal stress difference is not the same as just the first normal stress they are obviously related and consideration will be made of this later in Chapter 6, when examining the eigenspectra.

In Chapter 6 these base flow results are employed into the relevant numerical methods to produce complete eigenspectra for the same range of parameters. Meanwhile, the base flow velocity and stress profiles for Phan-Thien Tanner fluids are discussed in the next Section.

5.2 Solutions for Phan-Thien Tanner Fluids

5.2.1 Analytical Investigations

There are no simple analytical solutions for Phan-Thien Tanner fluids, although complex solutions of limited application have been given by Alves *et. al.* [6] and Cruz *et. al.* [13]. These were discussed earlier in Section 4.2. When both the shear thinning parameter ϵ and

the strand stretching parameter ξ are set to zero however, the Phan-Thien Tanner model reduces to an Oldroyd-B model. Setting only the shear thinning parameter to zero and leaving $\xi \neq 0$ also gives a set of equations which are solvable. Since the main characteristic of the Phan-Thien Tanner constitutive equation is defined by the linear function ϵf (see Section 2.4.4) then this model ceases to be a PTT model with $\epsilon = 0$. This set of equations therefore represents the base flow for an Oldroyd-B fluid with a more general Johnson-Segalman derivative in place of the upper convected derivative. The equations to be solved are

$$0 = -\frac{\partial p_{\mathrm{B}}}{\partial x} + \frac{\mathrm{d}\tau_{xy_{\mathrm{B}}}}{\mathrm{d}y} + m\beta\frac{\mathrm{d}^2 u_{\mathrm{B}}}{\partial y^2}, \tag{5.5}$$

$$-W\xi\tau_{xy_{\mathrm{B}}}\frac{\mathrm{d}u_{\mathrm{B}}}{\mathrm{d}y} + \tau_{xx\mathrm{B}} = 0, \tag{5.6}$$

$$-W\left(1-\frac{\xi}{2}\right)\tau_{xx\mathrm{B}}\frac{\mathrm{d}u_{\mathrm{B}}}{\mathrm{d}y} + \frac{W\xi}{2}\tau_{yy_{\mathrm{B}}}\frac{\mathrm{d}u_{\mathrm{B}}}{\mathrm{d}y} + \tau_{xy_{\mathrm{B}}} = m\left(1-\beta\right)\frac{\mathrm{d}u_{\mathrm{B}}}{\mathrm{d}y}, \tag{5.7}$$

$$W\left(\xi-2\right)\tau_{xy_{\mathrm{B}}}\frac{\mathrm{d}u_{\mathrm{B}}}{\mathrm{d}y} + \tau_{yy_{\mathrm{B}}} = 0. \tag{5.8}$$

The general solution is

$$u_{\mathrm{B}} = \frac{1}{2}\frac{\partial p_{\mathrm{B}}}{\partial x}y^2 + C_1 y + C_2, \tag{5.9}$$

$$\tau_{xx\mathrm{B}} = W\xi m\left(1-\beta\right)\left(u'_{\mathrm{B}}\right)^2, \tag{5.10}$$

$$\tau_{xy_{\mathrm{B}}} = m\left(1-\beta\right)u'_{\mathrm{B}}, \tag{5.11}$$

$$\tau_{yy_{\mathrm{B}}} = W\left(2-\xi\right)m\left(1-\beta\right)\left(u'_{\mathrm{B}}\right)^2. \tag{5.12}$$

Clearly the introduction of the Johnson-Segalman derivative does not change the velocity

profile or the shear stress, but does play a part in the solutions for the normal stresses. The main result is that the first normal stress $\tau_{xx\mathrm{B}}$ is non-zero with a parabolic profile similar to the second normal stress. Further investigations of the effects of individual parameters on the base flow are undertaken numerically in the next Section.

5.2.2 Numerical Investigations

Poiseuille Flow of a Single Phan-Thien Tanner Fluid

The velocity and stress base flow profiles for symmetric Poiseuille flow of a single Phan-Thien Tanner liquid are shown in Fig. 5.5. For all the profiles there is a direct competition between the effects of varying the shear thinning parameter and the effects of varying the extensional parameter.

The introduction of a non-zero extensional parameter ξ gives a steeper velocity profile and this effect is maintained despite the introduction of non-zero shear thinning (Dash-Dot-Dotted lines) which gives a flatter velocity profile when introduced alone (Dash-Dotted lines). The first normal stress performs inversely for the extensional parameter here than was seen for the Giesekus fluid. Here, a non-zero value for ξ gives a parabolic profile above the y axis as opposed to the profile being entirely below the axis for a Giesekus fluid. An increase in shear thinning still maintains a reducing effect however and the profile remains identically zero when $\xi = 0$. The reason for this difference in behaviour of the first normal stress can be traced back to the differences between the term $\boldsymbol{\tau}.\boldsymbol{\tau}$ in the Giesekus constitutive equation and the term $\mathrm{tr}(\boldsymbol{\tau})\boldsymbol{\tau}$ in the PTT constitutive equation.

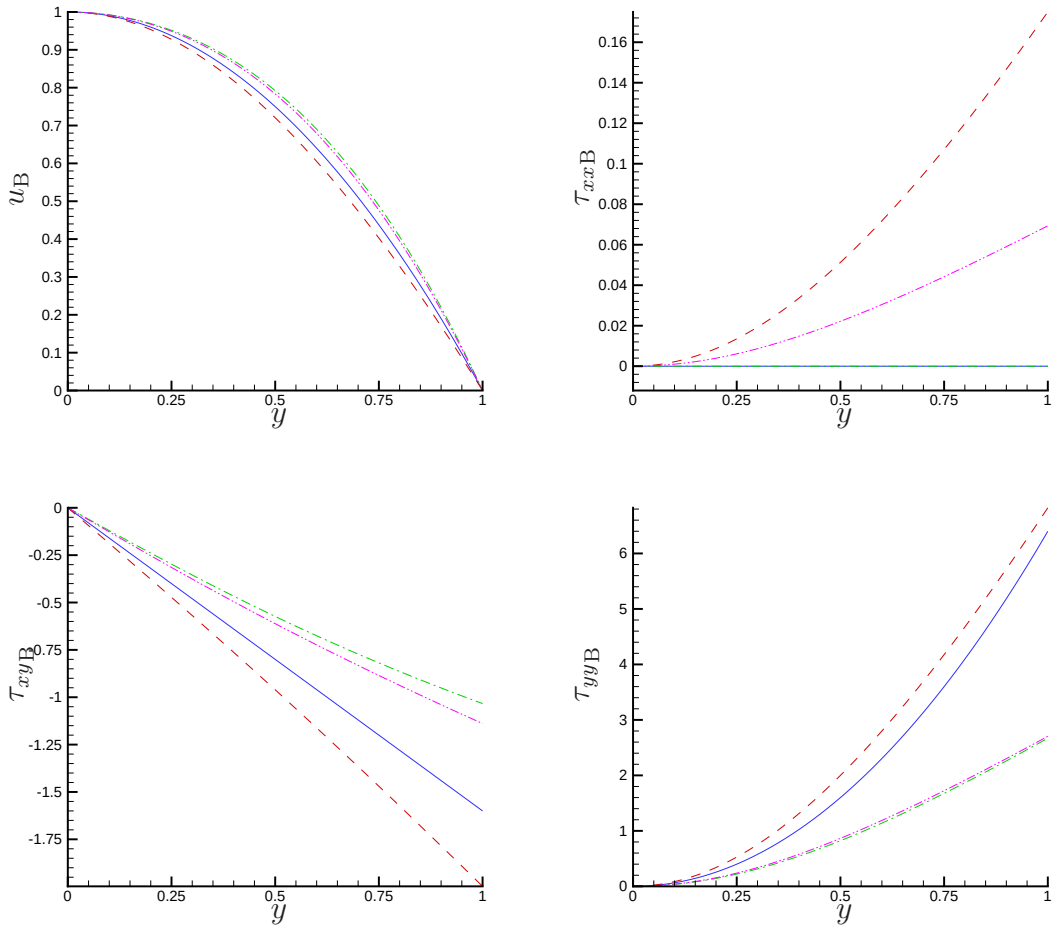

Figure 5.5: Base flow velocity and stress profiles for the symmetric Poiseuille flow of a single Phan-Thien Tanner fluid. The fluid parameters are: $W = 1$ and $\beta = 0.2$ with; $\epsilon = 0$ and $\xi = 0$ (Solid lines); $\epsilon = 0$ and $\xi = 0.05$ (Dashed lines); $\epsilon = 0.25$ and $\xi = 0$ (Dash-Dotted lines); and $\epsilon = 0.25$ and $\xi = 0.05$ (Dash-Dot-Dotted lines).

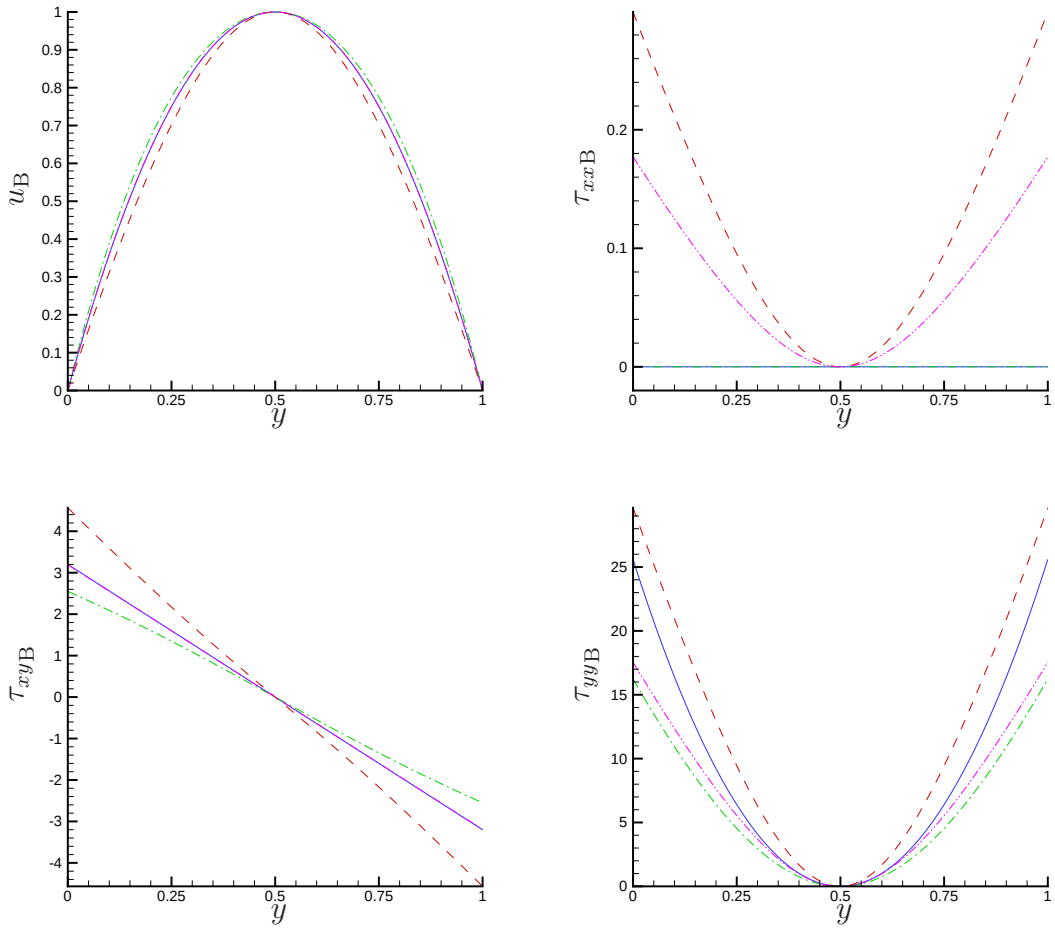

Figure 5.6: Base flow velocity and stress profiles for the non-symmetric Poiseuille flow of a single Phan-Thien Tanner fluid. The fluid parameters are: $W = 1$ and $\beta = 0.2$ with; $\epsilon = 0$ and $\xi = 0$ (Solid lines); $\epsilon = 0$ and $\xi = 0.02$ (Dashed lines); $\epsilon = 0.02$ and $\xi = 0$ (Dash-Dotted lines); and $\epsilon = 0.02$ and $\xi = 0.02$ (Dash-Dot-Dotted lines).

The shear stress profile becomes steeper as ξ is raised above zero. There is no additional curvature added to the profile however, and the curvature that is seen when $\epsilon \neq 0$ is dampened when both parameters are non-zero. The profile for the second normal stress also shows similar reactions whereby the parabolic profile steepens for non-zero ξ and the flattening of the profile that non-zero shear thinning provides is reduced, albeit slightly, by the reintroduction of $\xi \neq 0$.

The profiles for the non-symmetric base flow of a PTT fluid, shown in Fig. 5.6, show similar properties to those seen for the symmetric configuration. Computational difficulties, not unlike those experienced for the Giesekus fluids, again restrict the values of the parameters which can be investigated since smaller consecutive steps in the value of the continuation parameter are required to obtain convergence. Again, these difficulties are stronger for the non-symmetric cases, hence the parameter values shown here are significantly less than those computed for the symmetric equivalent. The effects on the base flow velocity and stress profiles as the shear thinning and extensional parameters are adjusted are therefore less dramatic for the non-symmetric case than was shown previously.

Poiseuille Flow of Two Phan-Thien Tanner Fluids

Figs. 5.7 and 5.8 show the base flow velocity and stress profiles for Poiseuille flow of two PTT fluids. In Fig. 5.7 the shear thinning and extensional parameters are kept at zero for fluid 1, and in Fig. 5.8 these parameters are both non-zero. The behaviours exhibited here are similar to those seen for the non-symmetric single fluid configuration. The velocity profile becomes steeper as ξ is increased, and then flatter as ϵ is increased. The velocity profiles for

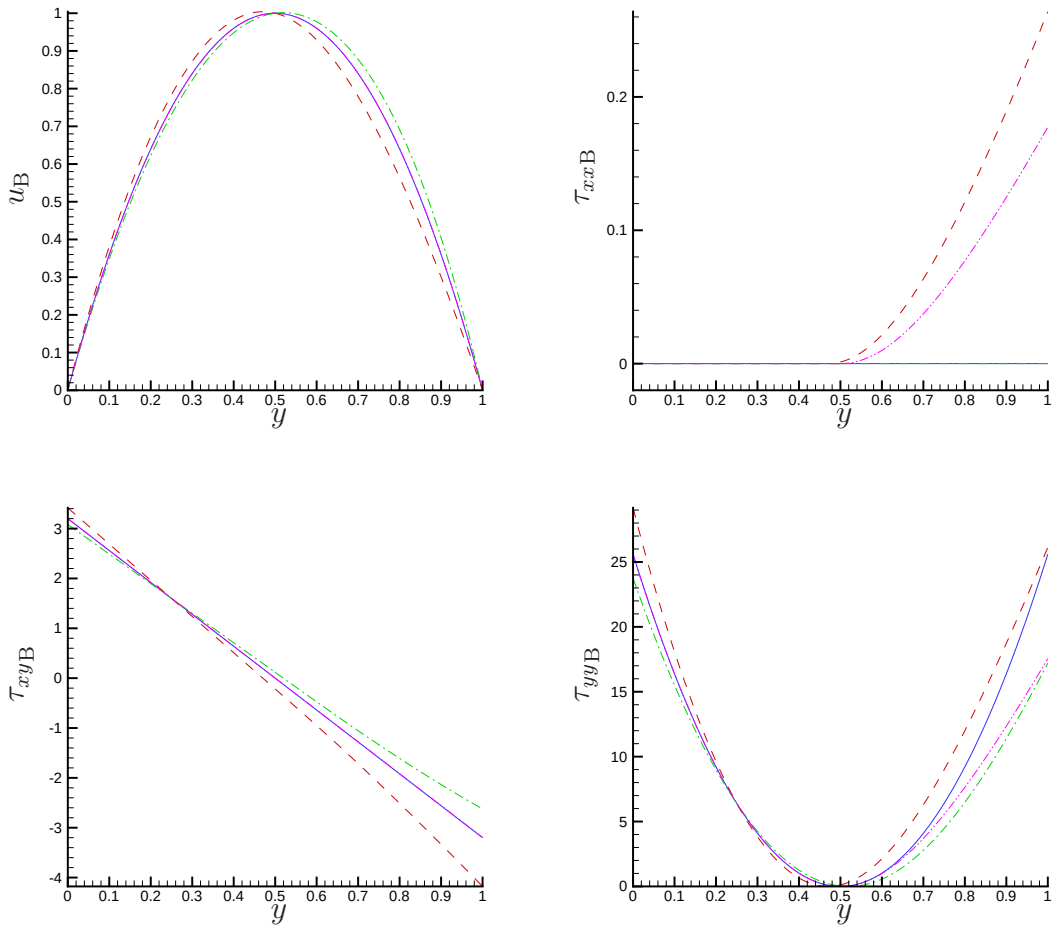

Figure 5.7: Base flow velocity and stress profiles for non-symmetric Poiseuille flow of two Phan-Thien Tanner fluids. The fluid parameters are: $m = 1$, $l = 0.5$; for fluid 1: $W_1 = 1$, $\beta_1 = 0.2$, $\boldsymbol{\epsilon_1 = 0}$ **and** $\boldsymbol{\xi_1 = 0}$; and for fluid 2: $W_2 = 1$ and $\beta_2 = 0.2$, $\epsilon_2 = 0$ and $\xi_2 = 0$ (Solid lines), $\epsilon_2 = 0$ and $\xi = 0.02$ (Dashed lines), $\epsilon_2 = 0.02$ and $\xi_2 = 0$ (Dash-Dotted lines) and $\epsilon_2 = 0.02$ and $\xi_2 = 0.02$ (Dash-Dot-Dotted).

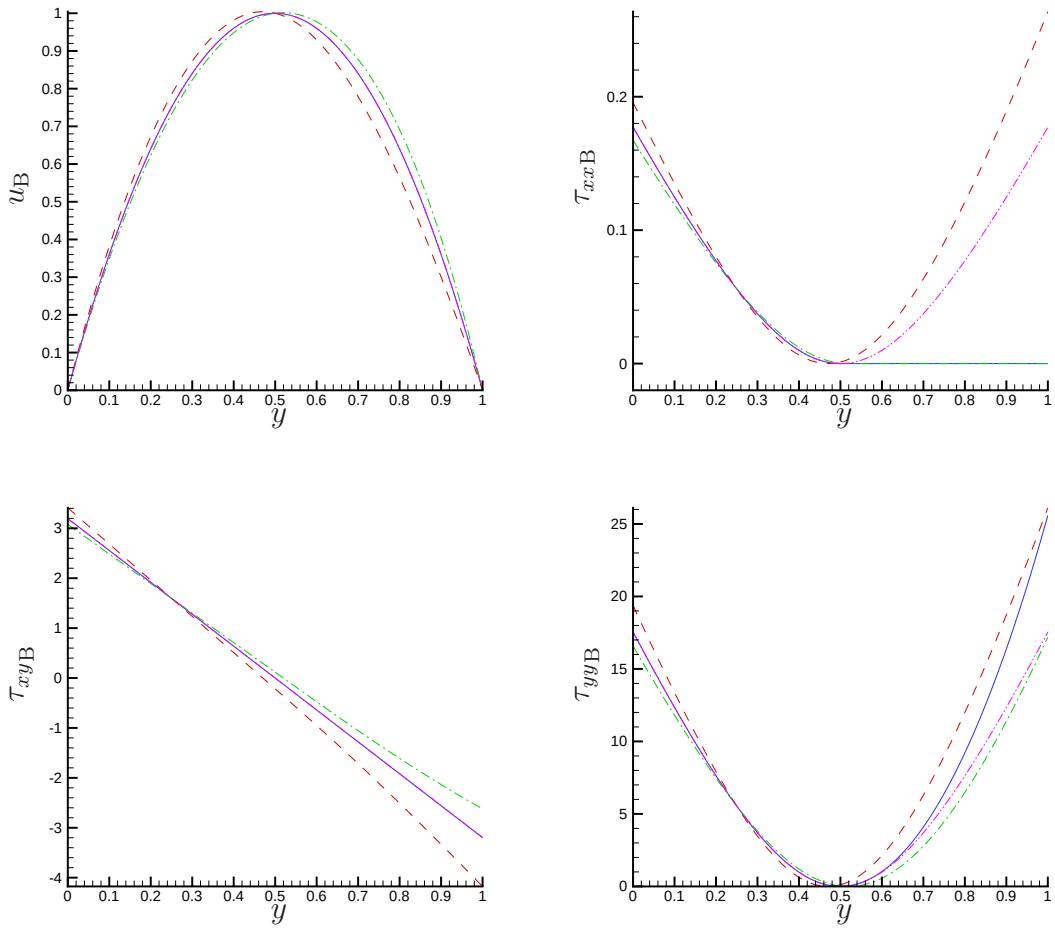

Figure 5.8: Base flow velocity and stress profiles for non-symmetric Poiseuille flow of two Phan-Thien Tanner fluids. The fluid parameters are: $m = 1$, $l = 0.5$; for fluid 1: $W_1 = 1$, $\beta_1 = 0.2$, $\boldsymbol{\epsilon_1 = 0.02}$ **and** $\boldsymbol{\xi_1 = 0.02}$; and for fluid 2: $W_2 = 1$ and $\beta_2 = 0.2$, $\epsilon_2 = 0$ and $\xi_2 = 0$ (Solid lines), $\epsilon_2 = 0$ and $\xi = 0.02$ (Dashed lines), $\epsilon_2 = 0.02$ and $\xi_2 = 0$ (Dash-Dotted lines) and $\epsilon_2 = 0.02$ and $\xi_2 = 0.02$ (Dash-Dot-Dotted lines).

the two cases shown in Figs. 5.7 and 5.8 appear identical at first glance, however whereas the symmetry across the interface is broken for all but the first set of values in Fig. 5.7 (Solid lines), it is maintained for only the last set of values in Fig. 5.8 (Dash-Dot-Dotted lines). The other profiles show a break in the symmetry of the velocity profiles with the parabola being larger in the fluid with the lower value of ξ and/or the higher value of ϵ. The other base flow profiles for the stress show similar symmetry breaking behaviour.

Three-Layered Poiseuille Flow of Two Phan-Thien Tanner Fluids

Figs. 5.9, 5.10, 5.11 and 5.12 show velocity and stress profiles for the base flow of Poisueille flow of two PTT liquids in a symmetric three-layered configuration for a range of parameter values. As was noted earlier, it is necessary to consider parameter values for both fluids since they are not transposable as is the case for the previously considered two-layered flow configuration. The main features of these profiles are similar to those described for the symmetric single case, but with the inclusion of discontinuities at the fluid-fluid interface. Of particular interest is the jump in first normal stress shown for all four variable sets. As was discussed earlier, this may have some effect on the existence of interfacial, elastic instabilities.

In the next Chapter the complete eigenspectra are discussed for a similar range of parameters for each flow configuration.

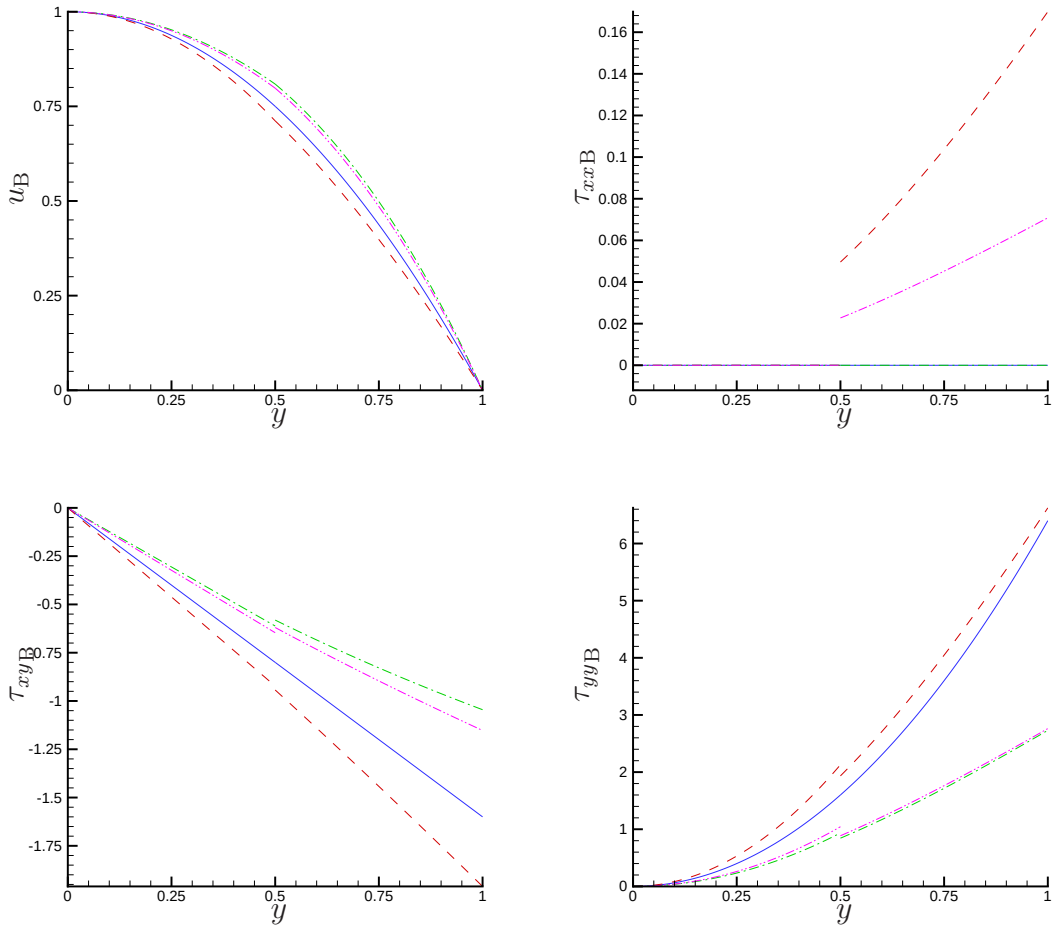

Figure 5.9: Base flow velocity and stress profiles for Poiseuille flow of two Phan-Thien Tanner fluids in a symmetric three-layered configuration. The fluid parameters are: $m = 1$, $l = 0.5$; for fluid 1: $W_1 = 1$, $\beta_1 = 0.2$, $\boldsymbol{\epsilon_1 = 0}$ **and** $\boldsymbol{\xi_1 = 0}$; and for fluid 2: $W_2 = 1$ and $\beta_2 = 0.2$, $\epsilon_2 = 0$ and $\xi_2 = 0$ (Solid lines), $\epsilon_2 = 0$ and $\xi_2 = 0.05$ (Dashed lines), $\epsilon_2 = 0.25$ and $\xi_2 = 0$ (Dash-Dotted lines) and $\epsilon_2 = 0.25$ and $\xi_2 = 0.05$ (Dash-Dot-Dotted).

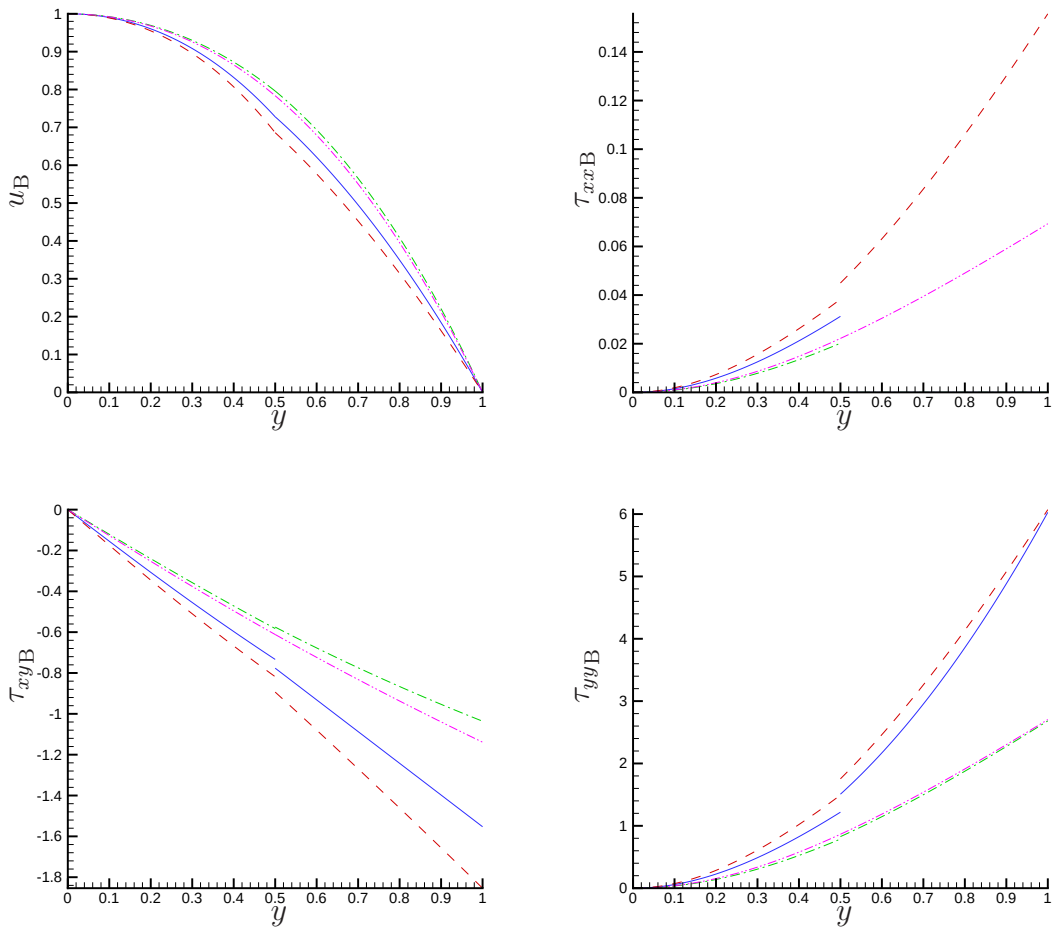

Figure 5.10: Base flow velocity and stress profiles for Poiseuille flow of two Phan-Thien Tanner fluids in a symmetric three-layered configuration. The fluid parameters are: $m = 1$, $l = 0.5$; for fluid 1: $W_1 = 1$, $\beta_1 = 0.2$, $\boldsymbol{\epsilon_1 = 0.25}$ **and** $\boldsymbol{\xi_1 = 0.05}$; and for fluid 2: $W_2 = 1$ and $\beta_2 = 0.2$, $\epsilon_2 = 0$ and $\xi_2 = 0$ (Solid lines), $\epsilon_2 = 0$ and $\xi_2 = 0.05$ (Dashed lines), $\epsilon_2 = 0.25$ and $\xi_2 = 0$ (Dash-Dotted lines) and $\epsilon_2 = 0.25$ and $\xi_2 = 0.05$ (Dash-Dot-Dotted lines).

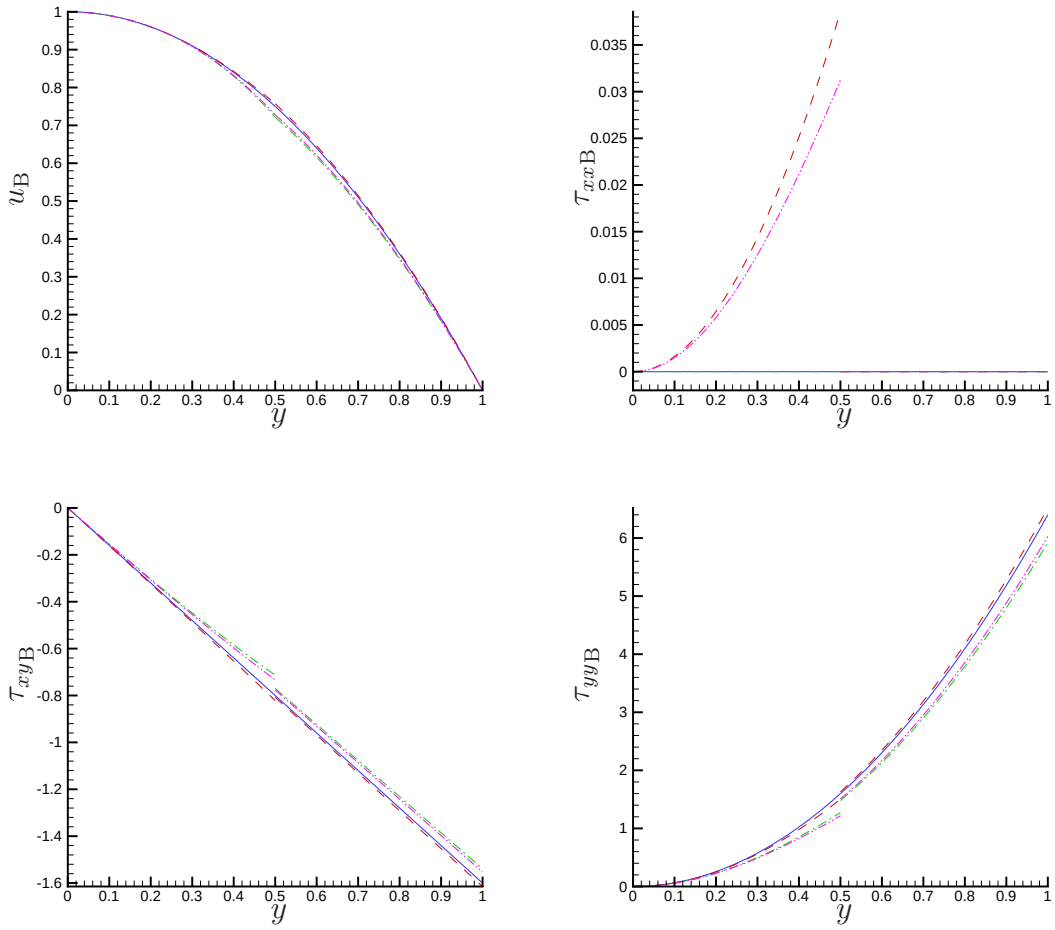

Figure 5.11: Base flow velocity and stress profiles for Poiseuille flow of two Phan-Thien Tanner fluids in a symmetric three-layered configuration. The fluid parameters are: $m = 1$, $l = 0.5$; for fluid 1: $W_1 = 1$ and $\beta_1 = 0.2$, $\epsilon_1 = 0$ and $\xi_1 = 0$ (Solid lines), $\epsilon_1 = 0$ and $\xi_1 = 0.05$ (Dashed lines), $\epsilon_1 = 0.25$ and $\xi_1 = 0$ (Dash-Dotted lines) and $\epsilon_1 = 0.25$ and $\xi_1 = 0.05$ (Dash-Dot-Dotted lines); and for fluid 2: $W_2 = 1$, $\beta_2 = 0.2$, $\boldsymbol{\epsilon_2 = 0}$ **and** $\boldsymbol{\xi_2 = 0}$.

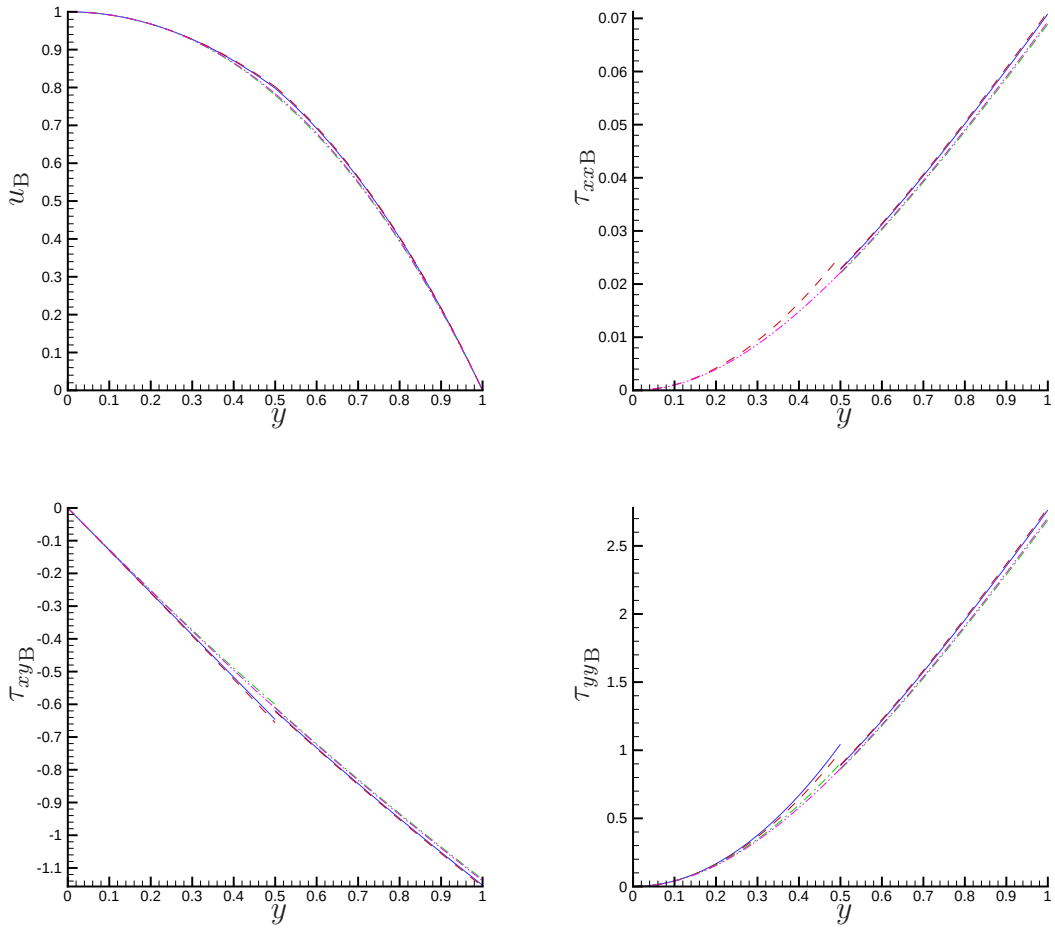

Figure 5.12: Base flow velocity and stress profiles for Poiseuille flow of two Phan-Thien Tanner fluids in a symmetric three-layered configuration. The fluid parameters are: $m = 1$, $l = 0.5$; for fluid 1: $W_1 = 1$ and $\beta_1 = 0.2$, $\epsilon_1 = 0$ and $\xi_1 = 0$ (Solid lines), $\epsilon_1 = 0$ and $\xi_1 = 0.05$ (Dashed lines), $\epsilon_1 = 0.25$ and $\xi_1 = 0$ (Dash-Dotted lines) and $\epsilon_1 = 0.25$ and $\xi_1 = 0.05$ (Dash-Dot-Dotted lines); and for fluid 2: $W_2 = 1$, $\beta_2 = 0.2$, $\boldsymbol{\epsilon_2 = 0.25}$ **and** $\boldsymbol{\xi_2 = 0.05}$.

Chapter 6

Structure of the Eigenspectra

6.1 Eigenspectra for Giesekus Fluids

6.1.1 Analytical Investigations: Continuous Parts of the Eigenspectra

It has been possible to find semi-analytical solutions for continuous parts of the eigenspectra for Giesekus fluids. Here, semi-analytical is used to express the fact that a full analytical solution has been determined for the Orr-Somerfeld equation, but that this solution is dependent on a solution for the base flow, which has only been determined numerically. Full details of the method and the solutions are given in Appendix F. Firstly it is necessary to derive the full Orr-Sommerfeld equations, i.e. to reduce the set of linearised stability equations for Giesekus fluids, equations (3.33)-(3.38), to a single equation for one of the disturbed variables, in this case the disturbed cross channel velocity $\bar{v}$. The details of this reduction

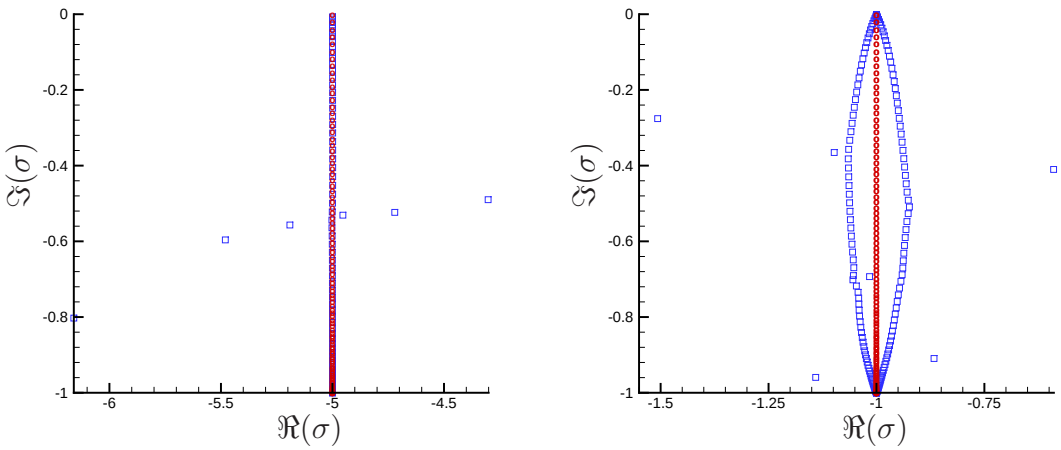

Figure 6.1: The complete eigenspectrum for the symmetric Poiseuille flow of a single Oldroyd-B fluid. The numerical results (□) are compared with the semi-analytical results (○).

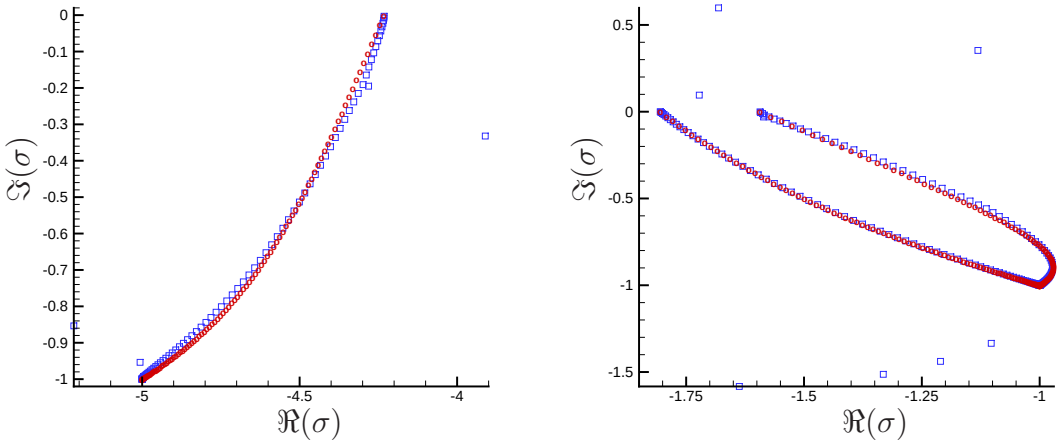

Figure 6.2: The complete eigenspectrum for symmetric Poiseuille flow of a single Giesekus fluid. The numerical results (□) are compared with the semi-analytical results (○).

are given in Appendix E. In order to derive continuous parts of the eigenspectra the branch cuts of the Orr-Sommerfeld equation must be sought. These are the points at which the Orr-Sommerfeld equation becomes singular. At all other points the Orr-Sommerfeld equation is a function of y and the eigenvalue σ. The points at which the Orr-Sommerfeld equation becomes singular are the points for which the denominator is zero. These are also the points at which the coefficient of the highest derivative of $\hat{v}$ vanishes to zero. As shown in Appendix F this is a cubic equation in σ which is then solved using the cubic formula. This solution is not given explictly due to its complexity, however it has been calculated numerically by including numerical solutions for the base flow, for which analytical solutions do not exist. Some of these semi-analytical solutions are shown in Figs. 6.1 and 6.2 and it can be clearly seen that they are very accurate. Comparisons of these solutions can also reveal the extent of the ballooning of the numerical eigenspectra when computed using the Chebyshev-QZ scheme.

6.1.2 Numerical Investigations

Poiseuille Flow of a Single Giesekus Fluid

The complete eigenspectra for symmetric Poiseuille flows of a single Oldroyd-B fluid and a single Giesekus fluid are shown in Fig. 6.3. The two parts of each of the eigenspectra are clearly distinguishable as balloons around the continuous parts of the eigenspectra at $\Re(\sigma) \approx -1$ and -5. The 'UCM' parts of the eigenspectra, at $\Re(\sigma) \approx -1$ are split into two separate spectra when $\epsilon \neq 0$. This has been confirmed by the semi-analytical solutions,

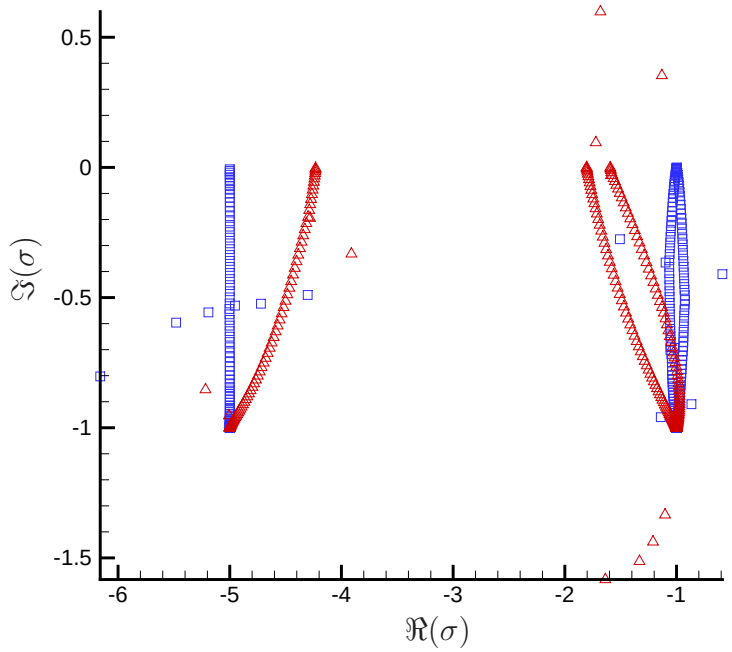

Figure 6.3: The complete eigenspectra for the symmetric Poiseuille flows of a single Giesekus fluid. The fluid parameters are: $R = 0$, $\psi = 1$, $W = 1$, $\beta = 0.2$, $\epsilon = 0$ (□) and $\epsilon = 0.5$ (△).

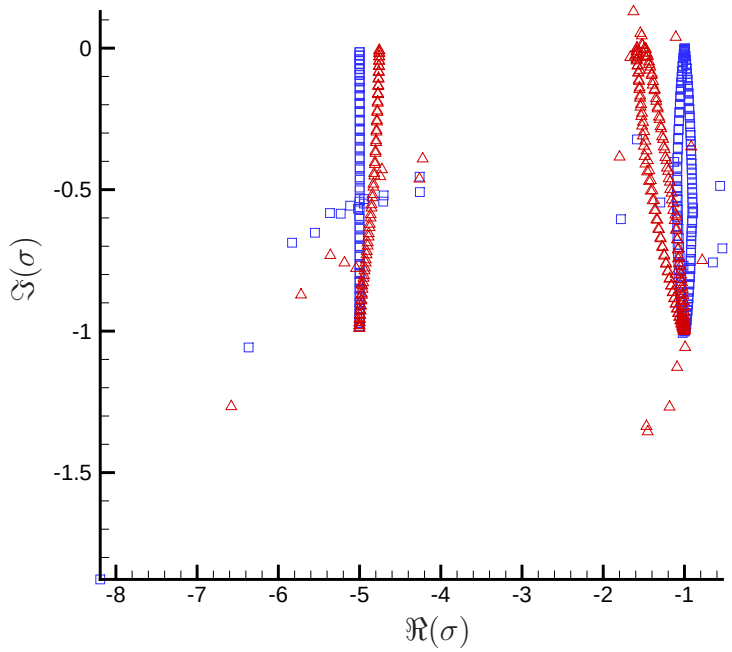

Figure 6.4: The complete eigenspectra for non-symmetric Poiseuille flows of a single Giesekus fluid. The fluid parameters are: $R = 0$, $\psi = 1$, $W = 1$, $\beta = 0.2$, $\epsilon = 0$ (□) and $\epsilon = 0.04$ (△).

as shown in Fig. 6.2 and is also consistent with the findings of Grillet *et al.* [31]. These UCM parts of the spectrum show a strong tilt away from the positive real parts, whereas the 'Oldroyd-B' part of the eigenspectrum shows a strong tilt towards the positive real parts. The discrete eigenvalues which surround the UCM continuous spectra are all shifted to the more negative side of the continuous spectra as shear thinning is introduced. Since the UCM parts of the spectra are most likely to play a part in any instabilities which may arise it can be tentatively suggested that the introduction of shear thinning in this case has a stabilising effect.

Similar results are seen for a single Oldroyd-B fluid and a single Giesekus fluid in non-symmetric Poiseuille flows as shown in Fig. 6.4. The tilting of the continuous spectra is less pronounced here and this is most likely due to the lower values of ϵ for which result have been obtained. There are more discrete eigenvalues for this non-symmetric configuration than for the symmetric equivalent. Some of these eigenvalues are most probably spurious numerical artifacts arising from the weaknesses in the formulation discussed in Section 5.1.2.

Poiseuille Flow of Two Giesekus Fluids

Fig. 6.5 shows the eigenspectra for two Oldroyd-B, one Oldroyd-B and one Giesekus, and two Giesekus fluids in two-layered Poiseuille flow. Each fluid shows its own continuous eigenspectrum such that in the case of unmatched fluids ($\triangle$) there are five separate continuous spectra; two for the Oldroyd-B fluid, and three for the Giesekus fluid. In the two cases of matched fluids the continuous spectra for fluid 1 overlies an identical continuous spectra for fluid 2, so as to give results which match the single fluid cases above.

The discrete eigenvalues appear to differ very slightly from those of the equivalent single fluid flows. The exception to this is that, due to the presence of the fluid-fluid interface there is an additional eigenvalue for this multiple fluid flow. This is the interfacial eigenvalue and is neutrally stable at $\sigma = -i$.

Three-Layered Poiseuille Flow of Two Giesekus Fluids

The complete eigenspectra for three-layered flows of Giesekus and Oldroyd-B fluids are shown in Fig. 6.6. The cases of matched fluids ($\square$ and $\diamond$) are shown separately from the cases

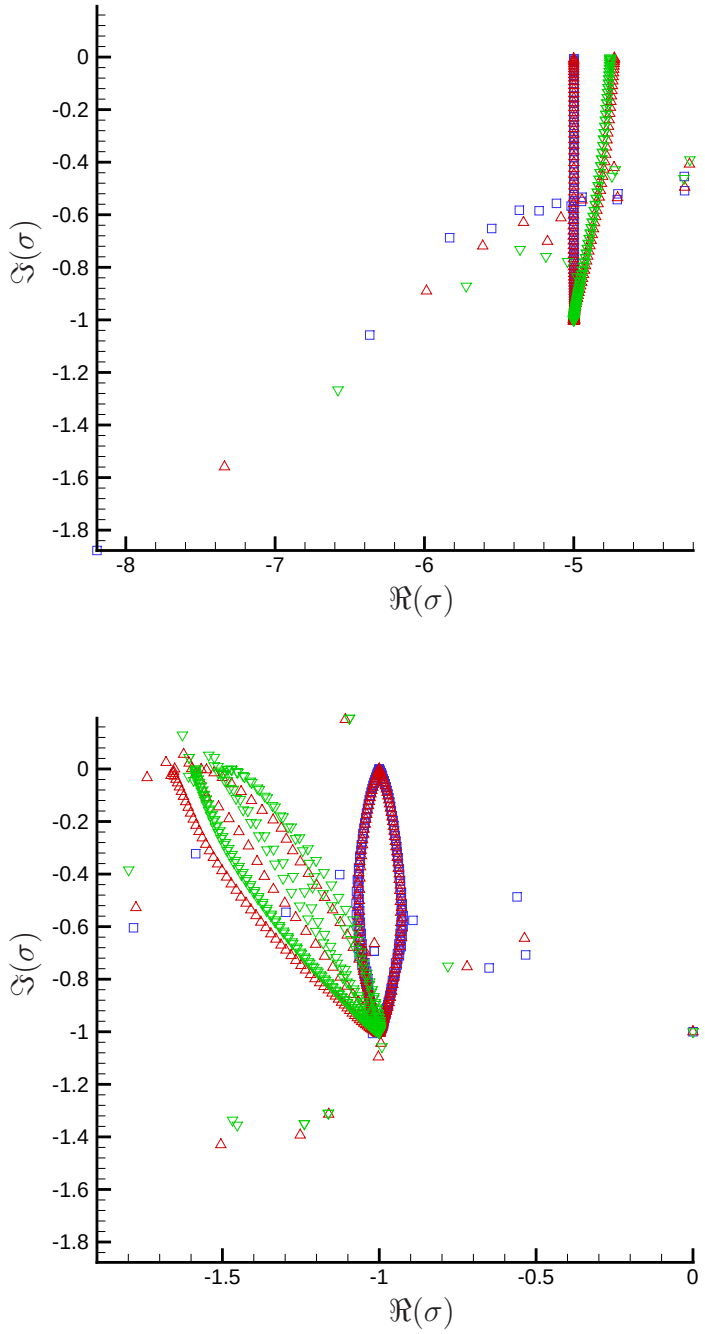

Figure 6.5: The complete eigenspectra for non-symmetric Poiseuille flows of two Giesekus fluids. The fluid parameters are: $\psi = 1$, $m = 1$, $l = 0.5$; for fluid 1: $R_1 = 0$, $W_1 = 1$ and $\beta_1 = 0.2$; and for fluid 2: $R_2 = 0$, $W_2 = 1$ and $\beta_2 = 0.2$; with $\epsilon_1 = 0$ and $\epsilon_2 = 0$ ($\square$), $\epsilon_1 = 0$ and $\epsilon_2 = 0.04$ ($\triangle$) and $\epsilon_1 = 0.04$ and $\epsilon_2 = 0.04$ ($\triangledown$).

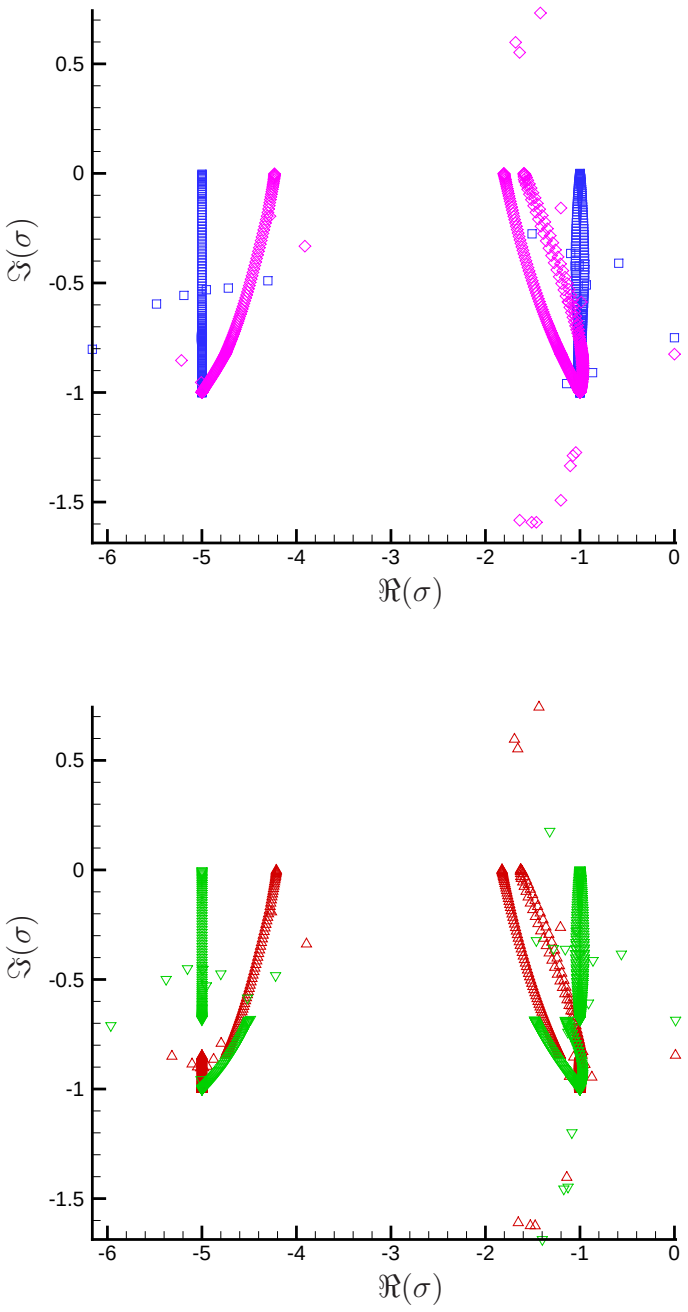

Figure 6.6: The complete eigenspectra for Poiseuille flows of two Giesekus fluids in a symmetric three-layered configuration. The fluid parameters are: $\psi = 1$, $m = 1$, $l = 0.5$ and; for fluid 1: $R_1 = 0$, $W_1 = 1$ and $\beta_1 = 0.2$; and for fluid 2: $R_2 = 0$, $W_2 = 1$ and $\beta_2 = 0.2$ with; $\epsilon_1 = 0$ and $\epsilon_2 = 0$ ($\square$), $\epsilon_1 = 0$ and $\epsilon_2 = 0.5$ ($\triangle$), $\epsilon_1 = 0.5$ and $\epsilon_2 = 0$ ($\triangledown$) and $\epsilon_1 = 0.5$ and $\epsilon_2 = 0.5$ ($\diamond$).

of different fluids ($\triangle$ and $\triangledown$). For the matched fluids the continuous eigenspectra correspond with those found for the symmetric single fluid flows. For the unmatched fluids, parts of the Oldroyd-B continuous spectra are displayed alongside parts of the Giesekus continuous spectra. Denoting the point where the continuous spectra split as $\Re(\sigma) - ai$, there exists an interfacial eigenvalue at $\sigma = -ai$. The value of a is different for each different set of fluid parameters.

In a similar manner to the base flow, the case of a Giesekus fluid contained with an Oldroyd-B fluid ($\triangledown$) shows an increased shear thinning effect than for a single, or for two matched, shear thinning fluids. This is indicated by the increased tilting of the lower parts of the continuous spectra for this case in comparison to the tilt shown for matched fluids with non-zero shear thinning ($\triangle$).

6.1.3 An Instability

An instability has been found for the symmetric Poiseuille flow of a single Giesekus fluid. The complete eigenspectrum, including the unstable eigenvalue, is shown in Fig. 6.7 with the semi-analytical solutions for the continuous eigenspectra. This eigenvalue has been determined more accurately using the ORK numerical method as $\sigma = 0.030000 - i\,(0.801886)$. For the Weissenberg number 6.02, the computational difficulties are high. As the Weissenberg number is increased there is slower convergence and a smaller step size for W is required in a similar manner as the difficulties experienced for computations of the base flow in Chapter 5 for high values of ϵ or ξ.

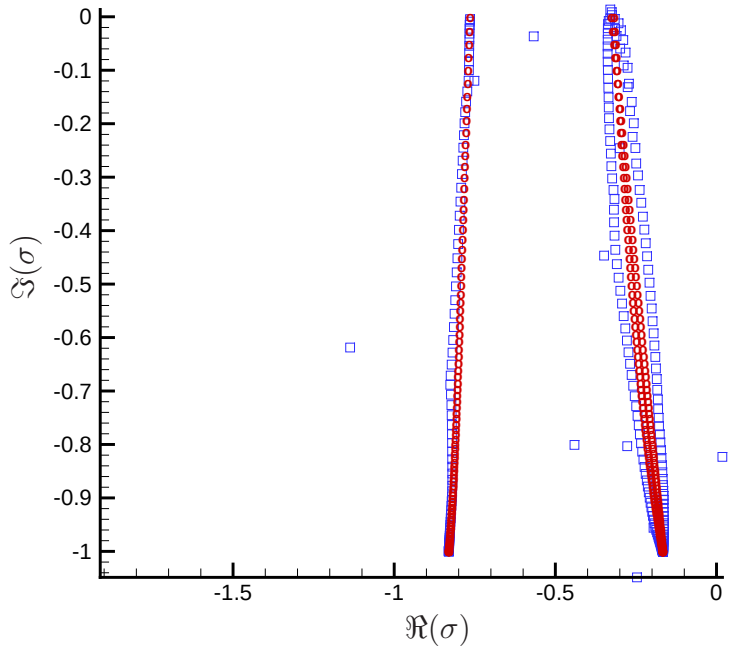

Figure 6.7: The complete eigenspectra for symmetric Poiseuille flow of a single Giesekus fluid, including an unstable eigenvalue. The fluid parameters are: $R = 0$, $\psi = 1$, $W = 6.02$, $\beta = 0.2$ and $\epsilon = 0.01$ (□). The semi-analytical solutions for the continuous spectra (○) are also shown.

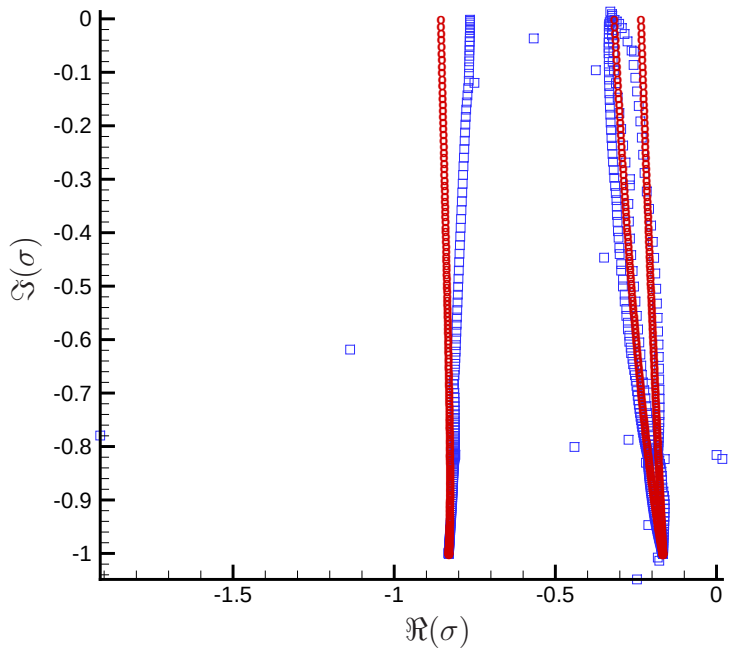

Figure 6.8: The complete eigenspectra for Poiseuille flow of two Giesekus fluids in a symmetric three-layered configuration, including an unstable eigenvalue. The fluid parameters are: $R = 0$, $\psi = 1$, $W_1 = W_2 = 6.02$, $\beta_1 = \beta_2 = 0.2$ and $\epsilon_1 = \epsilon_2 = 0.01$ (□). The semi-analytical solutions for the continuous spectra (○) are also shown.

Despite these difficulties the same unstable eigenvalue has been found for the symmetric three-layered flow configuration with the same fluid parameters and for matched fluids. The complete eigenspectrum is shown in Fig. 6.8, again with the semi-analytical solutions for the continuous eigenspectra. It can be seen here, and in Fig. 6.7, that although the unstable eigenvalue is close to the interfacial eigenvalue, it is a different eigenvalue and it comes from the UCM part of the eigenspectrum.

A preliminary investigation of this eigenvalue is undertaken using the ORK method to calculate the eigenvalue individually. Fig. 6.9 shows the path of the eigenvalue towards insta-

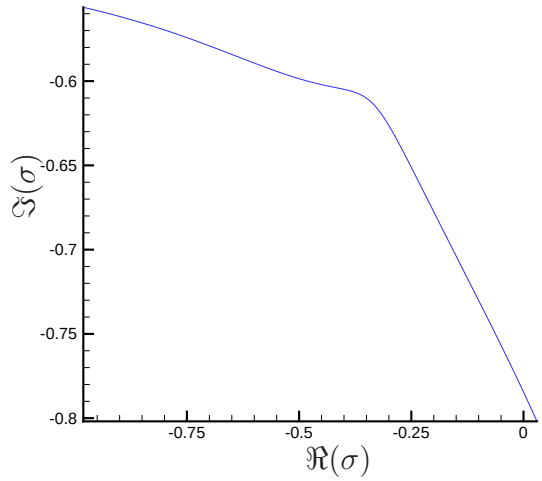

Figure 6.9: The path of the unstable eigenvalue for $W \in [1, 6.02]$.

bility as the Weissenberg number is increased. Marginal stability curves have been computed using Newton's method to ensure convergence of the results from the ORK computations to the point of neutral stability where $\Re(\sigma) = 0$. Three of these curves are shown in Fig. 6.10 where the neutral values of the shear thinning parameter ϵ, the solvent to total viscosity ratio β, and the disturbance wavelength ψ have been determined for a range of Weissenberg numbers W.

The range of W over which successful calculations have been achieved is limited since at the lower boundaries of each of these ranges the computations fail. In other words, no matter how small the incremental step for W, no further convergence can be obtained. This would imply that there is a change in the character of the system. Investigations of a nonlinear nature are required to elucidate further information and this is beyond the scope of this thesis. Investigations of the instability for symmetric three-layered flows have not been

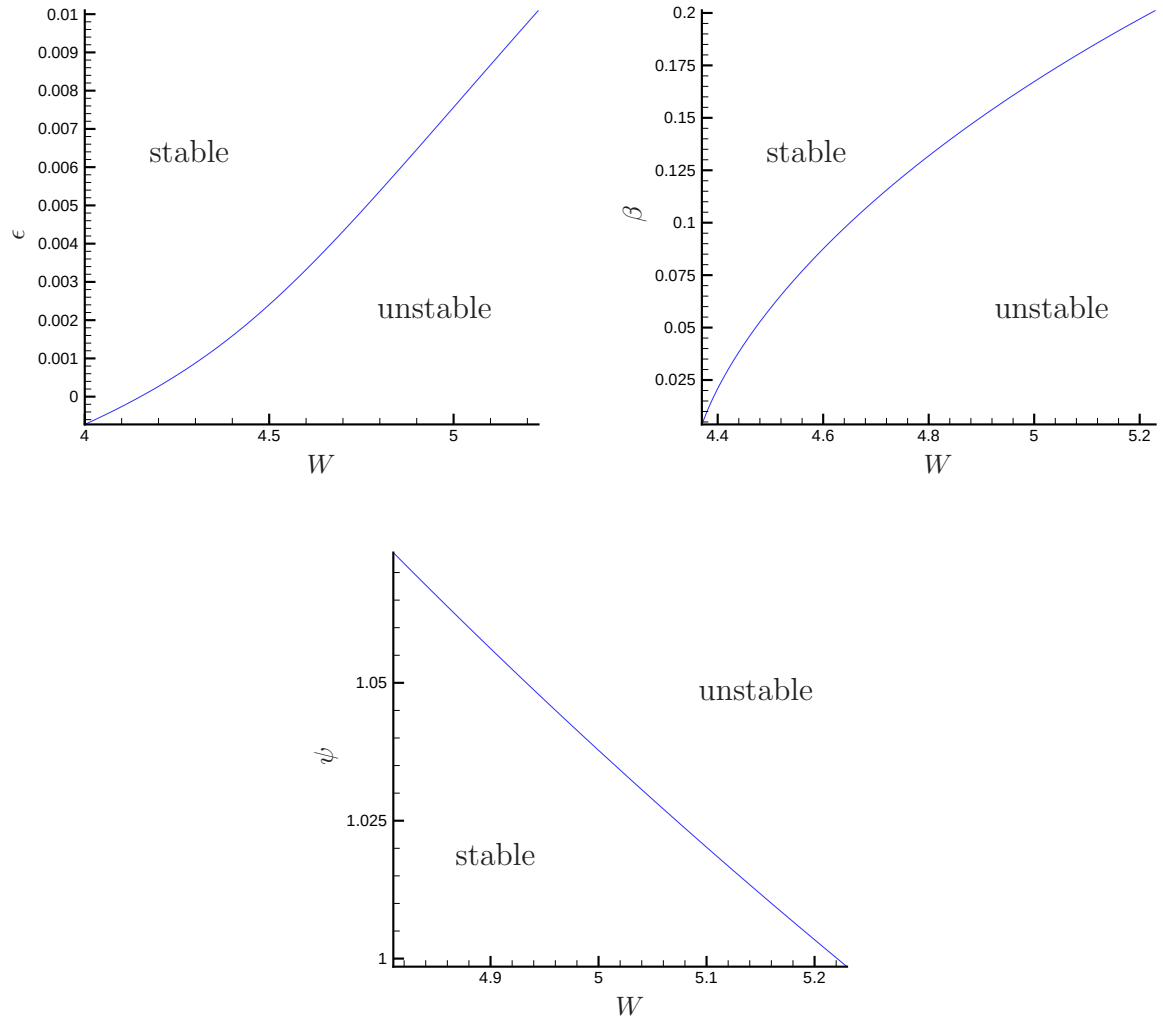

Figure 6.10: Marginal stability curves for the symmetric Poiseuille flow of a single Giesekus fluid.

undertaken since the increased complexity of the system has prevented any convergence of the ORK method.

6.2 Eigenspectra for Phan-Thien Tanner Fluids

6.2.1 Analytical Investigations: Continuous Parts of the Eigenspectra

An identical technique to that used to determine semi-analytic solutions for the continuous parts of the eigenspectra for Giesekus fluids has been attempted for PTT fluids. The method to determine the full Orr-Sommerfeld equation for PTT fluids is shown in Appendix G. In Appendix H the coefficient of the highest derivative of $\bar{v}$ in the Orr-Sommerfeld equation is determined. This gives a sixth order polynomial equation for the eigenvalue σ, equation (H.1), for which no solutions have yet been found.

6.2.2 Numerical Investigations

Figs. 6.11 and 6.12; 6.13 and 6.14; and 6.15, 6.16, 6.17 and 6.18 show the complete eigenspectra for planar Poiseuille flows of a range of PTT fluids in single-, two- and three-layered configurations respectively. The parameter values chosen for the shear thinning parameter ϵ and the extensional parameter ξ match those used for the corresponding base flows.

For non-zero ϵ or ξ the UCM parts of the continuous spectra split, similarly to the

behaviour seen for Giesekus fluids. The inclusion of shear thinning causes these parts of the eigenspectra to slope away from the positive reals and similarly for the Oldroyd-B parts of the eigenspectra. For the Gieskus fluids, the introduction of a non-zero shear thinning parameter caused the Oldroyd-B parts of the eigenspectra to slope towards the positive reals. This contrasting behaviour between the two fluids reflects the contrasting behaviour for the first normal stress of the base flow. It is therefore proposed that the effect of the shear thinning parameter on the Oldroyd-B part of the continuous eigenspectra is directly linked to the term $\boldsymbol{\tau}.\boldsymbol{\tau}$ in the Giesekus constitutive equations, or to the $\mathrm{tr}\,(\boldsymbol{\tau})\,\boldsymbol{\tau}$ term in the PTT constitutive equations.

The introduction of a non-zero extension, $\xi \neq 0$, also causes the Oldroyd-B part of the eigenspectra to slope away from the positive reals. The effect on the UCM part, however, is to cause a sloping towards the positive reals, implying that a non-zero extensional parameter has an destabilizing effect on the base flow. Although no instabilities have been discovered for Poiseuille flow of linear PTT fluids, a good place to begin a search may be by increasing the extensional parameter. The ability to do this here has been limited by the computational constraints discussed in Chapter 5.

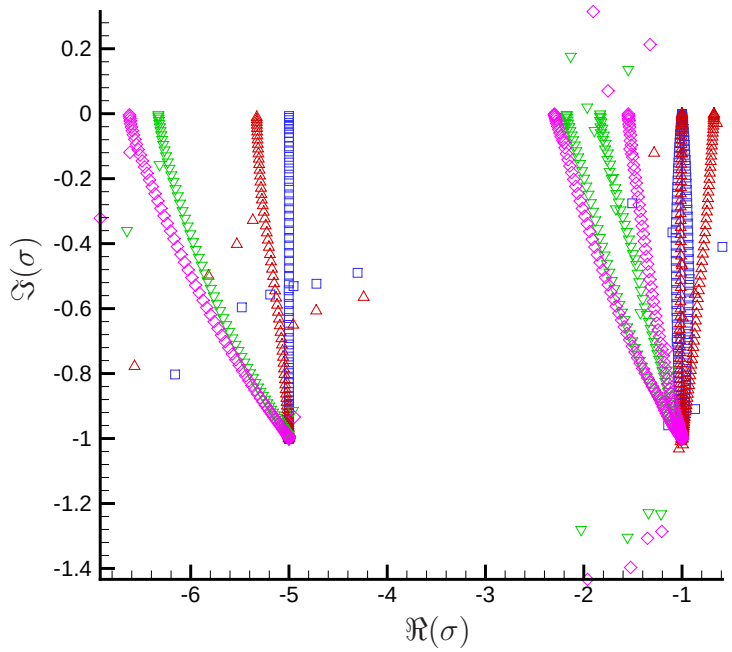

Figure 6.11: The complete eigenspectra for symmetric Poiseuille flows of a single Phan-Thien Tanner fluid. The fluid parameters are: $R = 0$, $\psi = 1$, $W = 1$ and $\beta = 0.2$ with; $\epsilon = 0$ and $\xi = 0$ ($\square$); $\epsilon = 0$ and $\xi = 0.05$ ($\triangle$); $\epsilon = 0.25$ and $\xi = 0$ ($\triangledown$); and $\epsilon = 0.25$ and $\xi = 0.05$ ($\diamond$).

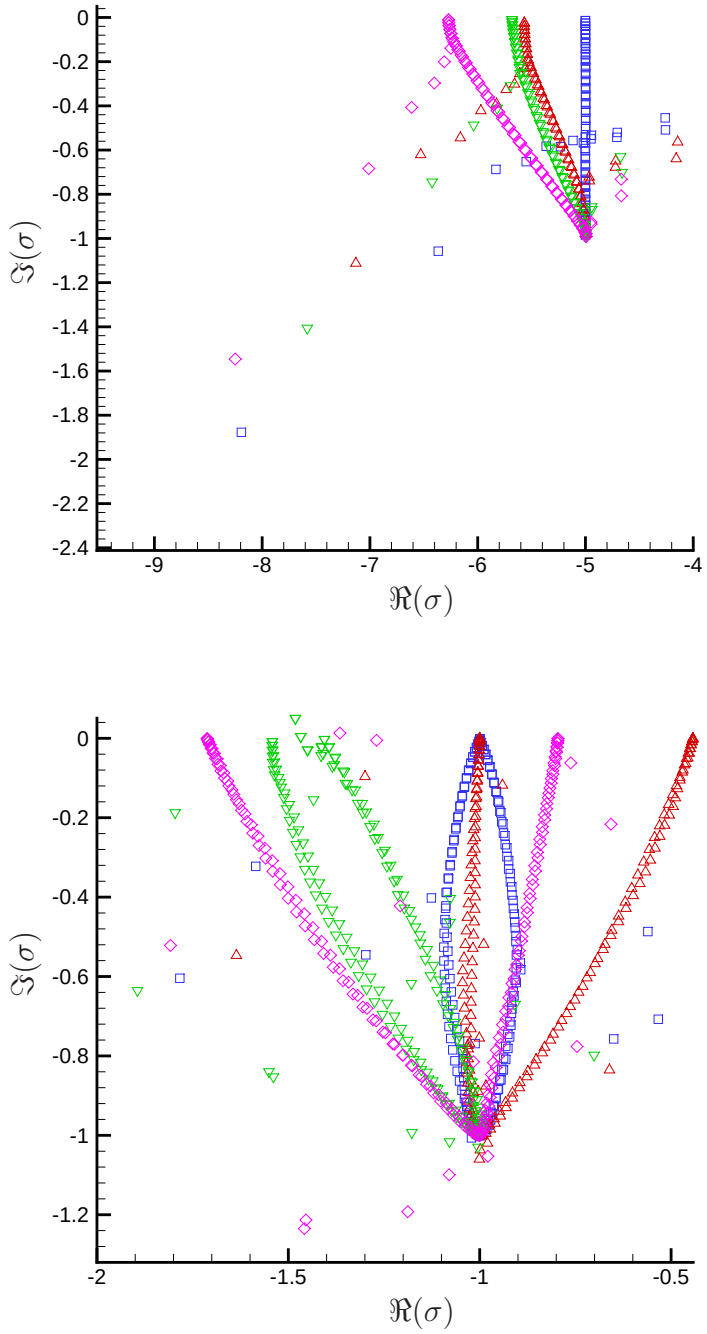

Figure 6.12: The complete eigenspectra for non-symmetric Poiseuille flows of a single Phan-Thien Tanner fluid. The fluid parameters are: $R = 0$, $\psi = 0$, $W = 1$ and $\beta = 0.2$ with; $\epsilon = 0$ and $\xi = 0$ (□); $\epsilon = 0$ and $\xi = 0.02$ (△); $\epsilon = 0.02$ and $\xi = 0$ (△); and $\epsilon = 0.02$ and $\xi = 0.02$ (◇).

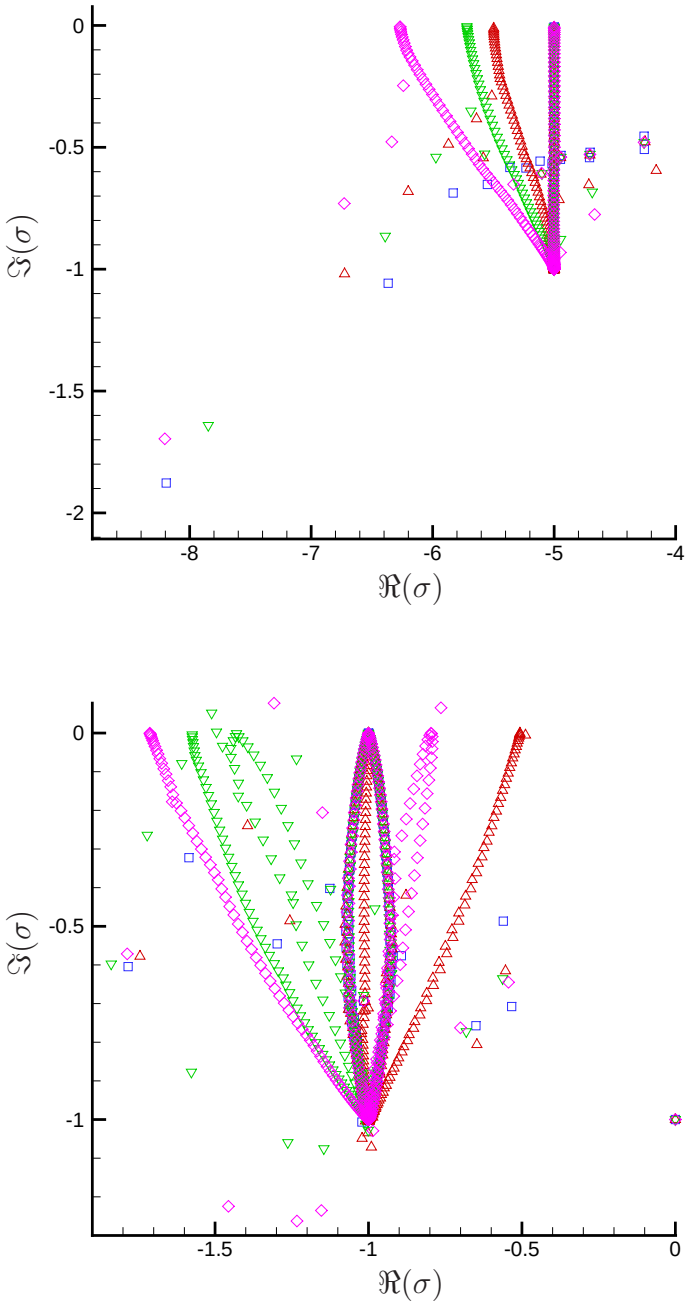

Figure 6.13: The complete eigenspectra for non-symmetric Poiseuille flows of two Phan-Thien Tanner fluids. The fluid parameters are: $\psi = 1$, $m = 1$, $l = 0.5$; for fluid 1: $R_1 = 0$, $W_1 = 1$, $\beta_1 = 0.2$, $\boldsymbol{\epsilon_1 = 0}$ **and** $\boldsymbol{\xi_1 = 0}$; and for fluid 2: $R_2 = 0$, $W_2 = 1$ and $\beta_2 = 0.2$, $\epsilon_2 = 0$ and $\xi_2 = 0$ (□), $\epsilon_2 = 0$ and $\xi = 0.02$ (△), $\epsilon_2 = 0.02$ and $\xi_2 = 0$ (△) and $\epsilon_2 = 0.02$ and $\xi_2 = 0.02$ (◇).

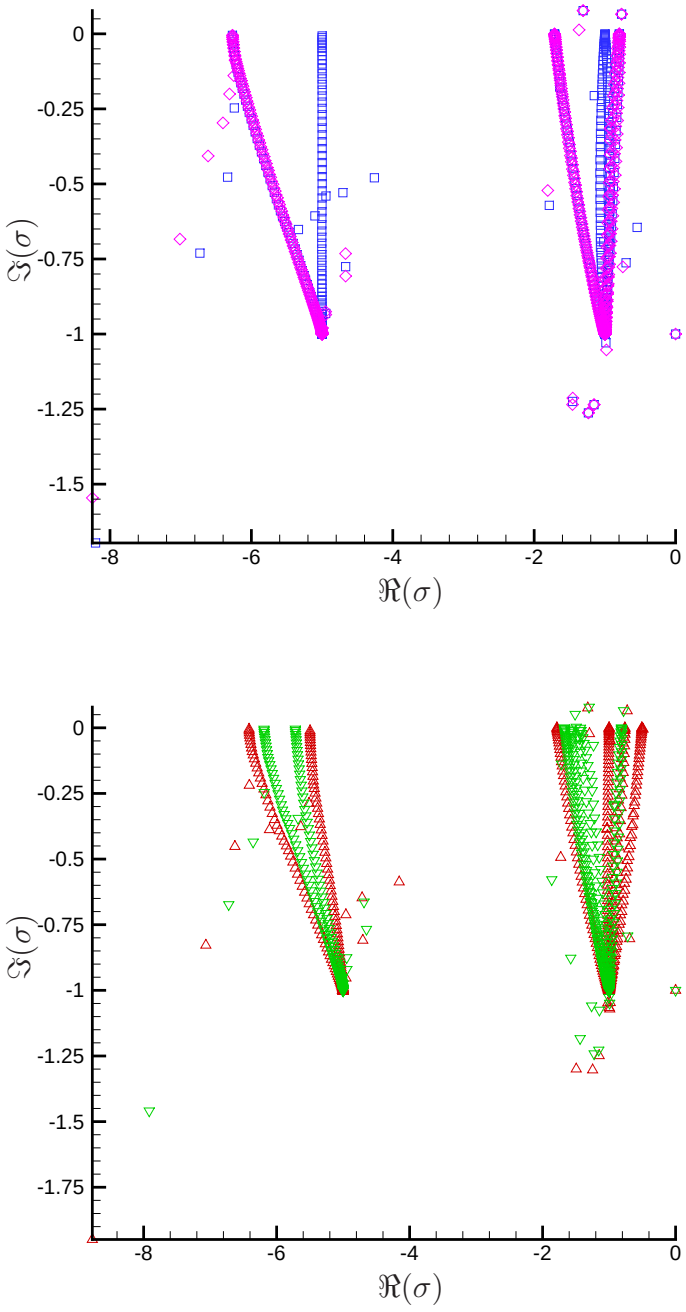

Figure 6.14: The complete eigenspectra for non-symmetric Poiseuille flows of two Phan-Thien Tanner fluids. The fluid parameters are: $\psi = 1$, $m = 1$, $l = 0.5$; for fluid 1: $R_1 = 0$, $W_1 = 1$, $\beta_1 = 0.2$, $\boldsymbol{\epsilon_1 = 0.02}$ **and** $\boldsymbol{\xi_1 = 0.02}$; and for fluid 2: $R_2 = 0$, $W_2 = 1$ and $\beta_2 = 0.2$, $\epsilon_2 = 0$ and $\xi_2 = 0$ ($\square$), $\epsilon_2 = 0$ and $\xi = 0.02$ ($\triangle$), $\epsilon_2 = 0.02$ and $\xi_2 = 0$ ($\triangledown$) and $\epsilon_2 = 0.02$ and $\xi_2 = 0.02$ ($\diamond$).

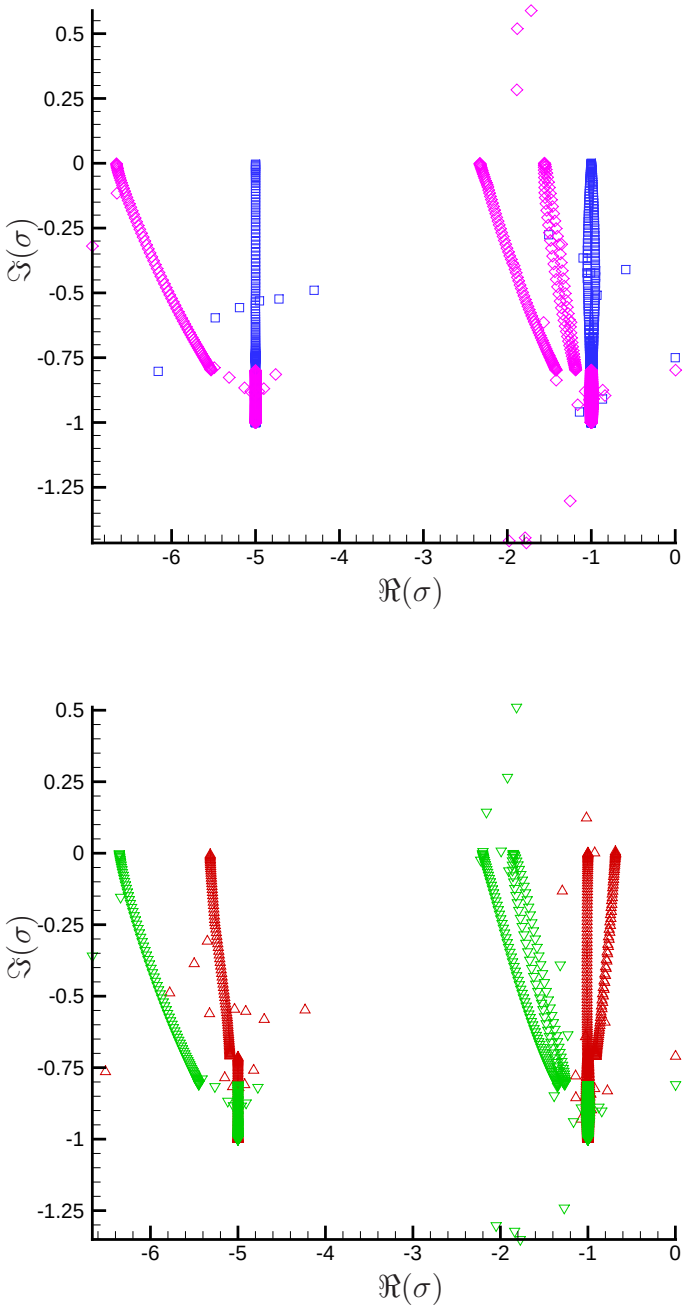

Figure 6.15: The complete eigenspectra for Poiseuille flows of two Phan-Thien Tanner fluids in a symmetric three-layered configuration. The fluid parameters are: $\psi = 1$, $m = 1$, $l = 0.5$; for fluid 1: $R_1 = 0$, $W_1 = 1$, $\beta_1 = 0.2$, $\boldsymbol{\epsilon_1 = 0}$ **and** $\boldsymbol{\xi_1 = 0}$; and for fluid 2: $R_2 = 0$, $W_2 = 1$ and $\beta_2 = 0.2$, $\epsilon_2 = 0$ and $\xi_2 = 0$ (□), $\epsilon_2 = 0$ and $\xi_2 = 0.05$ (△), $\epsilon_2 = 0.25$ and $\xi_2 = 0$ (△) and $\epsilon_2 = 0.25$ and $\xi_2 = 0.05$ (◇).

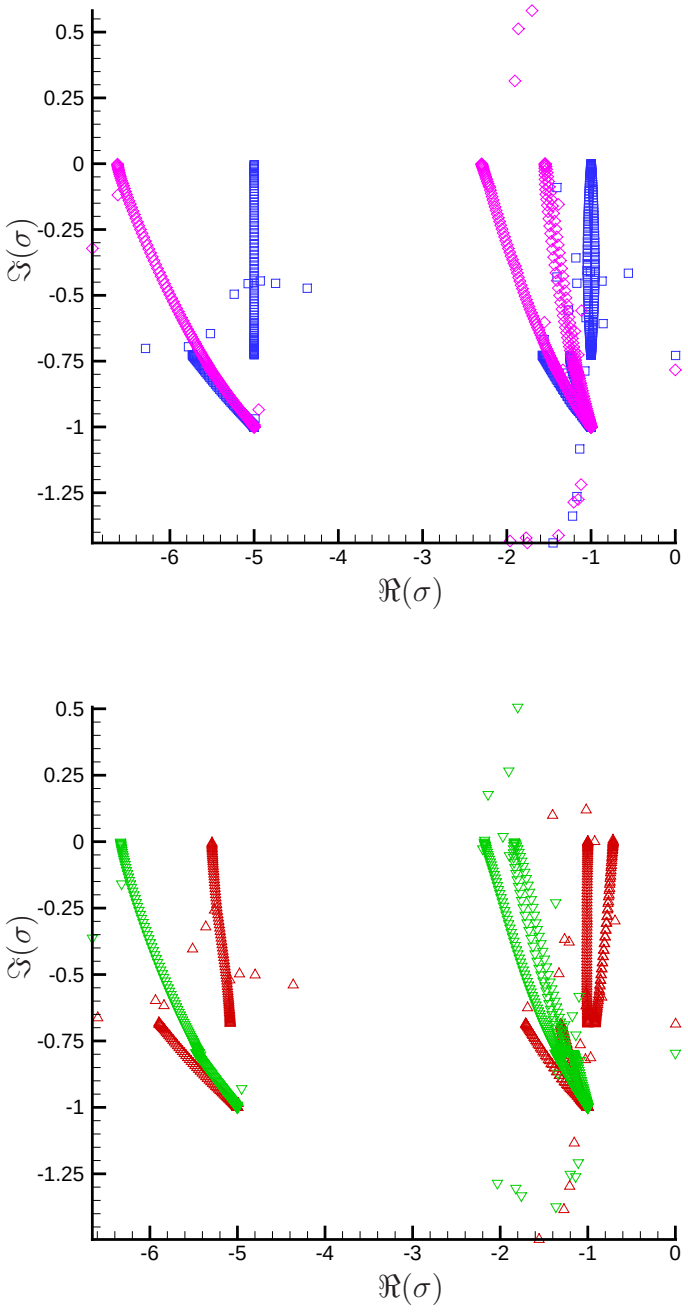

Figure 6.16: The complete eigenspectra for Poiseuille flows of two Phan-Thien Tanner fluids in a symmetric three-layered configuration. The fluid parameters are: $\psi = 1$, $m = 1$, $l = 0.5$; for fluid 1: $R_1 = 0$, $W_1 = 1$, $\beta_1 = 0.2$, $\boldsymbol{\epsilon_1 = 0.25}$ **and** $\boldsymbol{\xi_1 = 0.05}$; and for fluid 2: $R_2 = 0$, $W_2 = 1$ and $\beta_2 = 0.2$, $\epsilon_2 = 0$ and $\xi_2 = 0$ ($\square$), $\epsilon_2 = 0$ and $\xi_2 = 0.05$ ($\triangle$), $\epsilon_2 = 0.25$ and $\xi_2 = 0$ ($\triangledown$) and $\epsilon_2 = 0.25$ and $\xi_2 = 0.05$ ($\diamond$).

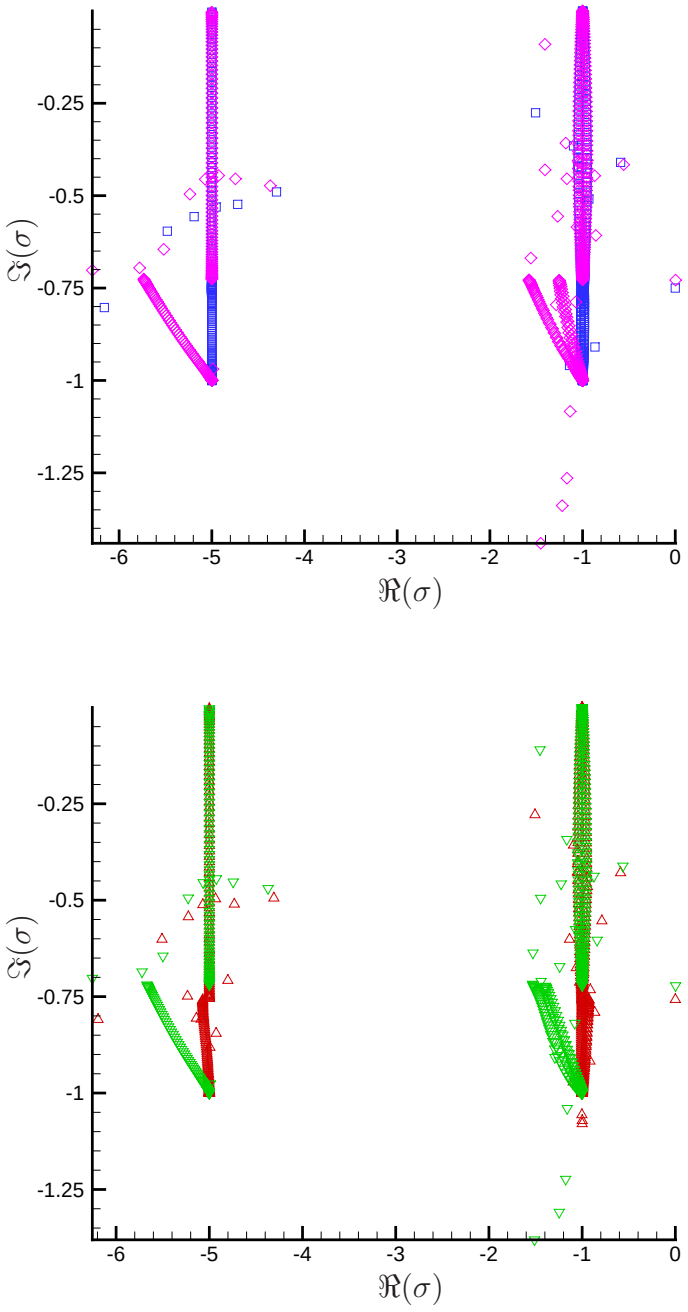

Figure 6.17: The complete eigenspectra for Poiseuille flows of two Phan-Thien Tanner fluids in a symmetric three-layered configuration. The fluid parameters are: $\psi = 1$, $m = 1$, $l = 0.5$; for fluid 1: $R_1 = 0$ $W_1 = 1$ and $\beta_1 = 0.2$, $\epsilon_1 = 0$ and $\xi_1 = 0$ ($\square$), $\epsilon_1 = 0$ and $\xi_1 = 0.05$ ($\triangle$), $\epsilon_1 = 0.25$ and $\xi_1 = 0$ ($\triangledown$) and $\epsilon_1 = 0.25$ and $\xi_1 = 0.05$ ($\diamond$); and for fluid 2: $R_2 = 0$, $W_2 = 1$, $\beta_2 = 0.2$, $\boldsymbol{\epsilon_2 = 0}$ **and** $\boldsymbol{\xi_2 = 0}$.

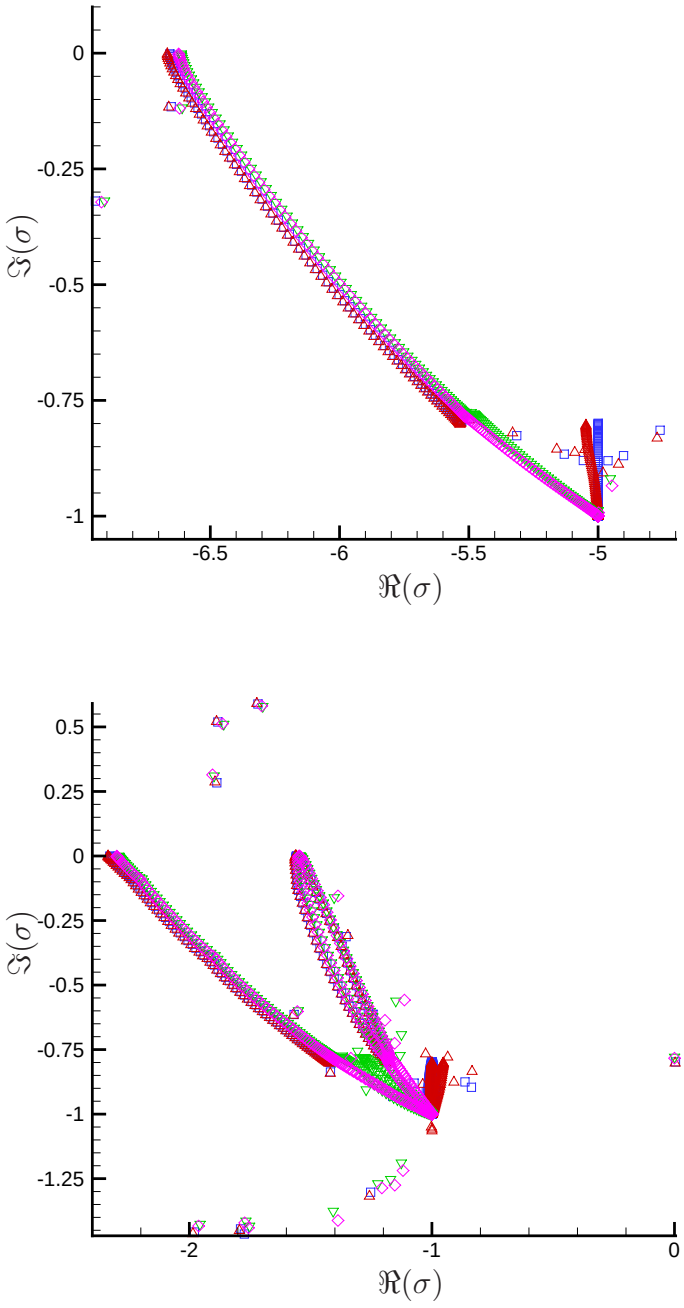

Figure 6.18: The complete eigenspectra for Poiseuille flows of two Phan-Thien Tanner fluids in a symmetric three-layered configuration. The fluid parameters are: $\psi = 1$, $m = 1$, $l = 0.5$; for fluid 1: $R_1 = 0$, $W_1 = 1$ and $\beta_1 = 0.2$, $\epsilon_1 = 0$ and $\xi_1 = 0$ ($\square$), $\epsilon_1 = 0$ and $\xi_1 = 0.05$ ($\triangle$), $\epsilon_1 = 0.25$ and $\xi_1 = 0$ ($\triangledown$) and $\epsilon_1 = 0.25$ and $\xi_1 = 0.05$ ($\diamond$); and for fluid 2: $R_2 = 0$, $W_2 = 1$, $\beta_2 = 0.2$, $\boldsymbol{\epsilon_2 = 0.25}$ **and** $\boldsymbol{\xi_2 = 0.05}$.

6.3 Inertial Effects

The complete eigenspectra for a number of single symmetric Poiseuille flows of an Oldroyd-B fluid is shown in Fig. 6.19 for different values of the Reynolds number, R. The Reynolds number does not appear in the base flow equations and so inertial effects are only shown through the eigenspectrum. It can be speculated that a large number of discrete eigenvalues come in from ∞, towards the continuous parts of the eigenspectra, as the Reynolds number is increased. Clearly, many of these eigenvalues are unstable. Therefore, planar Poiseuille flow of an Oldroyd-B fluid is unstable for all nonzero values of the Reynolds number. These instabilities have proved difficult to investigate numerically however, since it is the limit of the Reynolds number tending to zero from above. Asymptotic methods would be a recommended technique for these investigations but this is beyond the scope of this thesis.

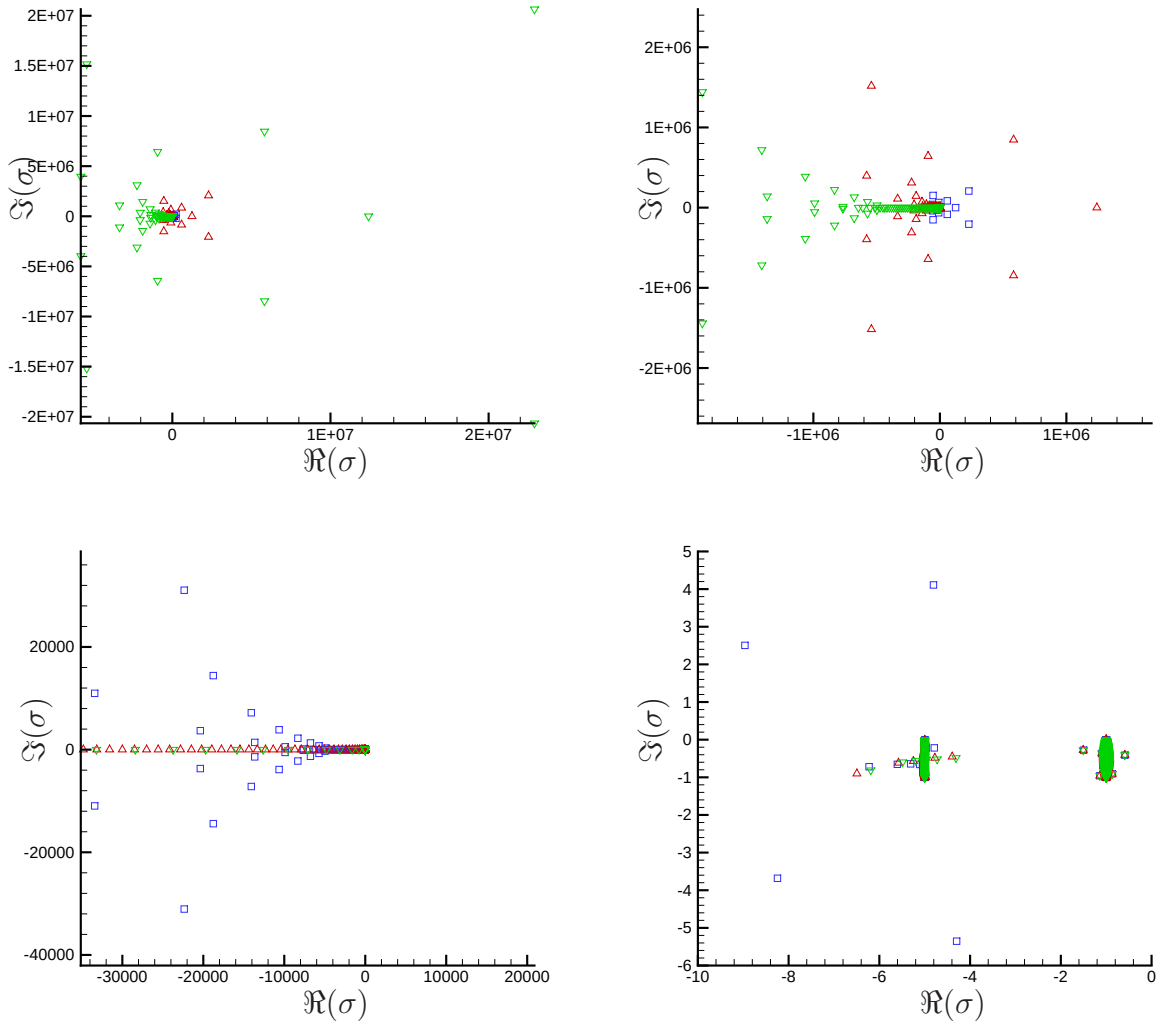

Figure 6.19: The complete eigenspectra for symmetric Poiseuille flows of a single Oldroyd-B fluid. The fluid parameters are: $\psi = 0$, $W = 1$ and $\beta = 0.2$, $\epsilon = 0.01$, $R = 1$ ($\square$), $R = 0.1$ ($\triangle$), and $R = 0.01$ ($\triangledown$).

Chapter 7

Conclusions

The base flow and complete eigenspectra for several channel flows have been investigated. No anlaytical solutions for the base flow for either the full Giesekus model or the full PTT model were obtained, but a comprehensive numerical survey has been undertaken using Chebyshev discretization. For both the Giesekus and the PTT fluid models it was found that there are computational limits on the values of the fluid parameters and these limits were approached in order to show the greatest effects of each of the parameters.

In general, an increase in shear thinning causes a flattening of the velocity base flow profile and an increase in extension causes a steepening of the velocity profile. The relationship between the stresses and the fluid parameters is more complex and opposing behaviours are seen for the Giesekus and PTT fluids, particularly in the case of the first normal stresses.

For the multilayered flow configurations the base flow profiles showed predictable behaviour and some interaction is seen between fluid layers whereby one layer reacts to changing parameter values in the other layer. The base flow equations do not contain the Reynolds

number and therefore the base flow is unresponsive to inertial effects.

Semi-analytical solutions for the continuous parts of the eigenspectra for Giesekus fluids have been obtained and are shown to be accurate. Although some attempts have been made to predict the continuous spectra by Grillet *et al.* [31] these results have limited accuracy. The results given in this thesis have been derived from well-defined eigenproblem theory and similar method applied to the Oldroyd-B fluid has been well received [65]. Hence the semi-analytical results given here are considered to be new, and are an improvement on the results of Grillet *et al.*

The numerical computation of the complete eigenspectra, for identical parameter values as for the base flow, has been completed successfully using a Chebyshev-QZ scheme. The results for the Oldroyd-B fluids match those given in [65], and the new results for the Giesekus and linear PTT models show reasonable and predictive behaviour. The results for single and two-layer flow of PTT fluids have already been successfully published [47, 48].

An instability has been determined for symmetric Poiseuille flow of a single Giesekus fluid. Preliminary investigations, in the form of marginal stability curves calculated using an orthonormal Runge-Kutta scheme, have led to implications of bifurcations near to $W = 4.4$.

The effects of inertia on the eigenspectra have been preliminarily investigated and a number of large discrete eigenvalues, many unstable have been determined.

Further investigations following the work in this thesis have a wide scope. An asymptotic analysis of the inertial behaviour of the eigenspectra would provide more information on the phenomena described in Section 6.3. A nonlinear stability analysis would be useful in the

investigation of the possibility of bifurcations in the Poiseuille flow of Giesekus fluids. Further numerical investigations for higher values of the extensional parameter may also identify an instability for the PTT fluids.

Appendix A

Detailed Derivation of a Linearized Stability Equation

What follows here is a detailed derivation of the linearized stability equation (3.34).

The velocity, pressure and stresses are defined as the sum of the base flow variables and an additional disturbance variable such that

$$\mathbf{u}_j = (\mathbf{u}_\mathrm{B})_j + \tilde{\mathbf{u}}_j, \tag{A.1}$$

$$p_j = (p_\mathrm{B})_j + \tilde{p}_j, \tag{A.2}$$

$$\boldsymbol{\tau}_j = (\boldsymbol{\tau}_\mathrm{B})_j + \tilde{\boldsymbol{\tau}}_j. \tag{A.3}$$

Substituting these variables into the governing equation (3.6) gives

$$R_j\left(\frac{\partial\left(v_{\mathrm{B}}\right)_j}{\partial t}+\frac{\partial\tilde{v}_j}{\partial t}+\left(\left(u_{\mathrm{B}}\right)_j+\tilde{u}_j\right)\left(\frac{\partial\left(v_{\mathrm{B}}\right)_j}{\partial x}+\frac{\partial\tilde{v}_j}{\partial x}\right)+\left(\left(v_{\mathrm{B}}\right)_j+\tilde{v}_j\right)\left(\frac{\partial\left(v_{\mathrm{B}}\right)_j}{\partial y}+\frac{\partial\tilde{v}_j}{\partial y}\right)\right)= -\left(\frac{\partial\left(p_{\mathrm{B}}\right)_j}{\partial y}+\frac{\partial\tilde{p}_j}{\partial y}\right)+\frac{\partial\left(\tau_{xy\mathrm{B}}\right)_j}{\partial x}+\frac{\partial\tilde{\tau}_{xy_j}}{\partial x}+\frac{\partial\left(\tau_{yy\mathrm{B}}\right)_j}{\partial y}+\frac{\partial\tilde{\tau}_{yy_j}}{\partial y} +m_j\beta_j\left(\frac{\partial^2\left(v_{\mathrm{B}}\right)_j}{\partial x^2}+\frac{\partial^2\tilde{v}_j}{\partial x^2}+\frac{\partial^2\left(v_{\mathrm{B}}\right)_j}{\partial y^2}+\frac{\partial^2\tilde{v}_j}{\partial y^2}\right). \quad \text{(A.4)}$$

By including a number of assumptions on the base flow; that the flow is steady, that the cross channel velocity is zero, and that all velocities and stresses are independent of x, then a number of the base flow terms can be cancelled as follows

$$R_j\left(\cancel{\frac{\partial\left(v_{\mathrm{B}}\right)_j}{\partial t}}+\frac{\partial\tilde{v}_j}{\partial t}+\left(\left(u_{\mathrm{B}}\right)_j+\tilde{u}_j\right)\left(\cancel{\frac{\partial\left(v_{\mathrm{B}}\right)_j}{\partial x}}+\frac{\partial\tilde{v}_j}{\partial x}\right)+\left(\cancel{\left(v_{\mathrm{B}}\right)_j}+\tilde{v}_j\right)\left(\cancel{\frac{\partial\left(v_{\mathrm{B}}\right)_j}{\partial y}}+\frac{\partial\tilde{v}_j}{\partial y}\right)\right)= -\left(\frac{\partial\left(p_{\mathrm{B}}\right)_j}{\partial y}+\frac{\partial\tilde{p}_j}{\partial y}\right)+\cancel{\frac{\partial\left(\tau_{xy\mathrm{B}}\right)_j}{\partial x}}+\frac{\partial\tilde{\tau}_{xy_j}}{\partial x}+\frac{\partial\left(\tau_{yy\mathrm{B}}\right)_j}{\partial y}+\frac{\partial\tilde{\tau}_{yy_j}}{\partial y} +m_j\beta_j\left(\cancel{\frac{\partial^2\left(v_{\mathrm{B}}\right)_j}{\partial x^2}}+\frac{\partial^2\tilde{v}_j}{\partial x^2}+\cancel{\frac{\partial^2\left(v_{\mathrm{B}}\right)_j}{\partial y^2}}+\frac{\partial^2\tilde{v}_j}{\partial y^2}\right). \quad \text{(A.5)}$$

The remaining linear base flow terms

$$0=-\frac{\partial\left(p_{\mathrm{B}}\right)_j}{\partial y}+\frac{\mathrm{d}\left(\tau_{yy\mathrm{B}}\right)_j}{\mathrm{d}y},$$

are satisfied by the base flow equation (3.15) and hence can be neglected from equation

(A.5). The following terms remain;

$$R_j\left(\frac{\partial\tilde{v}_j}{\partial t}+\left(\left(u_\mathrm{B}\right)_j+\tilde{u}_j\right)\frac{\partial\tilde{v}_j}{\partial x}+\tilde{v}_j\frac{\partial\tilde{v}_j}{\partial y}\right)=-\frac{\partial\tilde{p}_j}{\partial y}+\frac{\partial\tilde{\tau}_{xyj}}{\partial x}+\frac{\partial\tilde{\tau}_{yyj}}{\partial y}+m_j\beta_j\left(\frac{\partial^2\tilde{v}_j}{\partial x^2}+\frac{\partial^2\tilde{v}_j}{\partial y^2}\right). \tag{A.6}$$

As stated in Section 3.3 the disturbance variables are of the form

$$\tilde{\mathbf{u}}_j=\bar{\mathbf{u}}_j(y)e^{i\psi x+\sigma t},\qquad \tilde{p}_j=\bar{p}_j(y)e^{i\psi x+\sigma t},\qquad \tilde{\boldsymbol{\tau}}_j=\bar{\boldsymbol{\tau}}_j(y)e^{i\psi x+\sigma t}, \tag{A.7}$$

where the functions $\bar{\mathbf{u}}_j(y)$, $\bar{p}_j(y)$ and $\bar{\boldsymbol{\tau}}_j(y)$ are of infinitesimal magnitude such that quadratric and higher terms can be neglected. This leads to the cancellation of the terms $\tilde{u}_j\left(\partial\tilde{v}_j/\partial x\right)$ and $\tilde{v}_j\left(\partial\tilde{v}_j/\partial y\right)$ in equation (A.6) which now becomes

$$R_j\left(\frac{\partial\tilde{v}_j}{\partial t}+\left(u_\mathrm{B}\right)_j\frac{\partial\tilde{v}_j}{\partial x}\right)=-\frac{\partial\tilde{p}_j}{\partial y}+\frac{\partial\tilde{\tau}_{xyj}}{\partial x}+\frac{\partial\tilde{\tau}_{yyj}}{\partial y}+m_j\beta_j\left(\frac{\partial^2\tilde{v}_j}{\partial x^2}+\frac{\partial^2\tilde{v}_j}{\partial y^2}\right). \tag{A.8}$$

Differentiating the variables in (A.7) with respect to x, y and t leads to the following expressions

$$\begin{aligned}
\frac{\partial\tilde{\mathbf{u}}_j}{\partial x}&=i\psi\bar{\mathbf{u}}_je^{i\psi x+\sigma t}, & \frac{\partial\tilde{\mathbf{u}}_j}{\partial y}&=\frac{\mathrm{d}\bar{\mathbf{u}}_j}{\mathrm{d}y}e^{i\psi x+\sigma t}, & \frac{\partial\tilde{\mathbf{u}}_j}{\partial t}&=\sigma\bar{\mathbf{u}}_je^{i\psi x+\sigma t},\\
\frac{\partial\tilde{p}_j}{\partial x}&=i\psi\bar{p}_je^{i\psi x+\sigma t}, & \frac{\partial\tilde{p}_j}{\partial y}&=\frac{\mathrm{d}\bar{p}_j}{\mathrm{d}y}e^{i\psi x+\sigma t}, & \frac{\partial\tilde{p}_j}{\partial t}&=\sigma\bar{p}_je^{i\psi x+\sigma t},\\
\frac{\partial\tilde{\boldsymbol{\tau}}_j}{\partial x}&=i\psi\bar{\boldsymbol{\tau}}_je^{i\psi x+\sigma t}, & \frac{\partial\tilde{\boldsymbol{\tau}}_j}{\partial y}&=\frac{\mathrm{d}\bar{\boldsymbol{\tau}}_j}{\mathrm{d}y}e^{i\psi x+\sigma t}, & \frac{\partial\tilde{\boldsymbol{\tau}}_j}{\partial t}&=\sigma\bar{\boldsymbol{\tau}}_je^{i\psi x+\sigma t},
\end{aligned}$$

which are then substituted into equation (A.8) to give

$$R_j\left(\sigma\bar{v}_j e^{i\psi x+\sigma t}+(u_{\mathrm{B}})_j\, i\psi\bar{v}_j e^{i\psi x+\sigma t}\right)=-\bar{p}'_j e^{i\psi x+\sigma t}+i\psi\bar{\tau}_{xy_j}e^{i\psi x+\sigma t}+\bar{\tau}'_{yy_j}e^{i\psi x+\sigma t}$$
$$+m_j\beta_j\left(-\psi^2\bar{v}_j e^{i\psi x+\sigma t}+\bar{v}''_j e^{i\psi x+\sigma t}\right). \quad \text{(A.9)}$$

Here primes have been introduced to express full differentiation with respect to y. The exponential expressions can be cancelled since they occur in every term. Hence

$$R_j\left(\sigma\bar{v}_j+(u_{\mathrm{B}})_j\, i\psi\bar{v}_j\right)=-\bar{p}'_j+i\psi\bar{\tau}_{xy_j}+\bar{\tau}'_{yy_j}+m_j\beta_j\left(-\psi^2\bar{v}_j+\bar{v}''_j\right) \quad \text{(A.10)}$$

is the final form of the linearized stability equation and this corresponds to equation (3.34).

Appendix B

Discretized Forms of the Base Flow Equations

The discretized forms of the base flow equations are as follows:

Conservation of momentum, equation (4.6)

$$0 = -\widehat{\left(\frac{\partial p_{\mathrm{B}}}{\partial x}\right)}_0 + \frac{2}{L}\sum_{n=0}^{N}\frac{2}{c_n}\sum_{\substack{p=n+1\\ p+n\,\mathrm{odd}}}^{N} p\widehat{(\tau_{xy\mathrm{B}})}_p T_n + m\beta\frac{4}{L^2}\sum_{n=0}^{N}\frac{1}{c_n}\sum_{\substack{p=n+2\\ p+n\,\mathrm{even}}}^{N} p(p^2-n^2)\widehat{(u_{\mathrm{B}})}_p T_n, \quad \text{(B.1)}$$

the Giesekus constitutive equation

$$\sum_{n=0}^{N}\widehat{(\tau_{xx\mathrm{B}})}_n T_n + \frac{\epsilon W}{m\,(1-\beta)}\sum_{n=0}^{N}\sum_{p=0}^{N}\widehat{(\tau_{xx\mathrm{B}})}_n\widehat{(\tau_{xx\mathrm{B}})}_p\frac{\left(T_{n+p}+T_{|n-p|}\right)}{2} + \frac{\epsilon W}{m\,(1-\beta)}\sum_{n=0}^{N}\sum_{p=0}^{N}\widehat{(\tau_{xy\mathrm{B}})}_n\widehat{(\tau_{xy\mathrm{B}})}_p\frac{\left(T_{n+p}+T_{|n-p|}\right)}{2} = 0, \quad \text{(B.2)}$$

$$
\begin{aligned}
&- W\frac{2}{L}\sum_{n=0}^{N}\sum_{p=0}^{N}\frac{2}{c_p}\sum_{\substack{q=p+1\\ p+q\,\text{odd}}}^{N}\widehat{(\tau_{xx\mathrm{B}})}_n\widehat{q(u_{\mathrm{B}})}_q\frac{\left(T_{n+p}+T_{|n-p|}\right)}{2}+\sum_{n=0}^{N}\widehat{(\tau_{xy_{\mathrm{B}}})}_n T_n\\
&\qquad+\frac{\epsilon W}{m\,(1-\beta)}\sum_{n=0}^{N}\sum_{p=0}^{N}\widehat{(\tau_{xx\mathrm{B}})}_n\widehat{(\tau_{xy_{\mathrm{B}}})}_p\frac{\left(T_{n+p}+T_{|n-p|}\right)}{2}\\
&\qquad+\frac{\epsilon W}{m\,(1-\beta)}\sum_{n=0}^{N}\sum_{p=0}^{N}\widehat{(\tau_{xy_{\mathrm{B}}})}_n\widehat{(\tau_{yy_{\mathrm{B}}})}_p\frac{\left(T_{n+p}+T_{|n-p|}\right)}{2}\\
&\qquad\qquad=m\,(1-\beta)\,\frac{2}{L}\sum_{n=0}^{N}\frac{2}{c_n}\sum_{\substack{p=n+1\\ p+n\,\text{odd}}}^{N}\widehat{p(u_{\mathrm{B}})}_p T_n, \quad \text{(B.3)}
\end{aligned}
$$

$$
\begin{aligned}
&- 2W\frac{2}{L}\sum_{n=0}^{N}\sum_{p=0}^{N}\frac{2}{c_p}\sum_{\substack{q=p+1\\ p+q\,\text{odd}}}^{N}\widehat{(\tau_{xy_{\mathrm{B}}})}_n\widehat{q(u_{\mathrm{B}})}_q\frac{\left(T_{n+p}+T_{|n-p|}\right)}{2}+\sum_{n=0}^{N}\widehat{(\tau_{yy_{\mathrm{B}}})}_n T_n\\
&\qquad+\frac{\epsilon W}{m\,(1-\beta)}\sum_{n=0}^{N}\sum_{p=0}^{N}\widehat{(\tau_{xy_{\mathrm{B}}})}_n\widehat{(\tau_{xy_{\mathrm{B}}})}_p\frac{\left(T_{n+p}+T_{|n-p|}\right)}{2}\\
&\qquad\qquad+\frac{\epsilon W}{m\,(1-\beta)}\sum_{n=0}^{N}\sum_{p=0}^{N}\widehat{(\tau_{yy_{\mathrm{B}}})}_n\widehat{(\tau_{yy_{\mathrm{B}}})}_p\frac{\left(T_{n+p}+T_{|n-p|}\right)}{2}=0, \quad \text{(B.4)}
\end{aligned}
$$

and the Phan-Thien Tanner constitutive equation

$$
\begin{aligned}
&- W\xi\frac{2}{L}\sum_{n=0}^{N}\sum_{p=0}^{N}\frac{2}{c_p}\sum_{\substack{q=p+1\\ p+q\,\text{odd}}}^{N}\widehat{(\tau_{xy_{\mathrm{B}}})}_n\widehat{q(u_{\mathrm{B}})}_q\frac{\left(T_{n+p}+T_{|n-p|}\right)}{2}+\sum_{n=0}^{N}\widehat{(\tau_{xx\mathrm{B}})}_n T_n\\
&\qquad+\frac{\epsilon W}{m\,(1-\beta)}\sum_{n=0}^{N}\sum_{p=0}^{N}\widehat{(\tau_{xx\mathrm{B}})}_n\widehat{(\tau_{xx\mathrm{B}})}_p\frac{\left(T_{n+p}+T_{|n-p|}\right)}{2}\\
&\qquad\qquad+\frac{\epsilon W}{m\,(1-\beta)}\sum_{n=0}^{N}\sum_{p=0}^{N}\widehat{(\tau_{xx\mathrm{B}})}_n\widehat{(\tau_{yy_{\mathrm{B}}})}_p\frac{\left(T_{n+p}+T_{|n-p|}\right)}{2}=0, \quad \text{(B.5)}
\end{aligned}
$$

$$W\left(\frac{\xi}{2}-1\right)\frac{2}{L}\sum_{n=0}^{N}\sum_{p=0}^{N}\frac{2}{c_p}\sum_{\substack{q=p+1\\ p+q\,\mathrm{odd}}}^{N}\widehat{(\tau_{xx\mathrm{B}})}_n\widehat{q(u_{\mathrm{B}})}_q\frac{\left(T_{n+p}+T_{|n-p|}\right)}{2}$$
$$+W\frac{\xi}{2}\frac{2}{L}\sum_{n=0}^{N}\sum_{p=0}^{N}\frac{2}{c_p}\sum_{\substack{q=p+1\\ p+q\,\mathrm{odd}}}^{N}\widehat{(\tau_{yy\mathrm{B}})}_n\widehat{q(u_{\mathrm{B}})}_q\frac{\left(T_{n+p}+T_{|n-p|}\right)}{2}+\sum_{n=0}^{N}\widehat{(\tau_{xy\mathrm{B}})}_nT_n$$
$$+\frac{\epsilon W}{m\left(1-\beta\right)}\sum_{n=0}^{N}\sum_{p=0}^{N}\widehat{(\tau_{xx\mathrm{B}})}_n\widehat{(\tau_{xy\mathrm{B}})}_p\frac{\left(T_{n+p}+T_{|n-p|}\right)}{2}$$
$$+\frac{\epsilon W}{m\left(1-\beta\right)}\sum_{n=0}^{N}\sum_{p=0}^{N}\widehat{(\tau_{xy\mathrm{B}})}_n\widehat{(\tau_{yy\mathrm{B}})}_p\frac{\left(T_{n+p}+T_{|n-p|}\right)}{2}$$
$$=m\left(1-\beta\right)\frac{2}{L}\sum_{n=0}^{N}\frac{2}{c_p}\sum_{\substack{p=n+1\\ p+n\,\mathrm{odd}}}^{N}\widehat{(u_{\mathrm{B}})}_pT_n, \quad \text{(B.6)}$$

$$-W\left(2-\xi\right)\frac{2}{L}\sum_{n=0}^{N}\sum_{p=0}^{N}\frac{2}{c_p}\sum_{\substack{q=p+1\\ p+q\,\mathrm{odd}}}^{N}\widehat{(\tau_{xy\mathrm{B}})}_n\widehat{q(u_{\mathrm{B}})}_q\frac{\left(T_{n+p}+T_{|n-p|}\right)}{2}+\sum_{n=0}^{N}\widehat{(\tau_{yy\mathrm{B}})}_nT_n$$
$$+\frac{\epsilon W}{m\left(1-\beta\right)}\sum_{n=0}^{N}\sum_{p=0}^{N}\widehat{(\tau_{xx\mathrm{B}})}_n\widehat{(\tau_{yy\mathrm{B}})}_p\frac{\left(T_{n+p}+T_{|n-p|}\right)}{2}$$
$$+\frac{\epsilon W}{m\left(1-\beta\right)}\sum_{n=0}^{N}\sum_{p=0}^{N}\widehat{(\tau_{yy\mathrm{B}})}_n\widehat{(\tau_{yy\mathrm{B}})}_p\frac{\left(T_{n+p}+T_{|n-p|}\right)}{2}=0. \quad \text{(B.7)}$$

Appendix C

The Solution Method For a 'Toy' Problem

In this Appendix the solution method described in Section 4.2.2 is demonstrated for a simple 'toy' problem. The problem under consideration is

$$f(y) = yy'' + 1 = 0. \tag{C.1}$$

Here y is a function of the single independent variable x and primes denote differentiation with respect to this variable. The dependent variable y is discretized in an identical manner to the discretization shown in Section 4.2.1. So (from 4.2)

$$y_N = \sum_{n=0}^{N} \hat{y}_n T_n(x) \tag{C.2}$$

for some suitably high value of N. For simplicity in this illustration N is chosen to be four, so

$$y_4 = \hat{y}_0 T_0 + \hat{y}_1 T_1 + \hat{y}_2 T_2 + \hat{y}_3 T_3 + \hat{y}_4 T_4. \tag{C.3}$$

Employing the relation (4.4), the second derivative of y can be expressed as

$$y_4'' = \sum_{n=0}^{4} y_n^{(2)} T_n, \qquad y_n^{(2)} = \frac{1}{c_n} \sum_{\substack{q=n+2 \\ q+n \text{ even}}}^{4} q(q^2 - n^2)\hat{y}_q, \tag{C.4}$$

where

$$c_n = \begin{cases} 2 & \text{if } n = 0 \\ 1 & \text{if } n \geq 1. \end{cases}$$

Expanding this expression for y'' gives

$$y'' = \frac{1}{c_0}\left(2\left(4-0\right)\hat{y}_2 + 4\left(16-0\right)\hat{y}_4\right) T_0 + \frac{1}{c_1}\left(3\left(9-1\right)\hat{y}_3\right) T_1 + \frac{1}{c_2}\left(4\left(16-4\right)\hat{y}_4\right) T_2 \tag{C.5}$$

$$= \left(4\hat{y}_2 + 32\hat{y}_4\right) T_0 + 24\hat{y}_3 T_1 + 48\hat{y}_4 T_2. \tag{C.6}$$

Substituting the above into equation (C.1) gives the discretized form of the toy problem as

$$\left[\hat{y}_0 T_0 + \hat{y}_1 T_1 + \hat{y}_2 T_2 + \hat{y}_3 T_3 + \hat{y}_4 T_4\right]\left[\left(4\hat{y}_2 + 32\hat{y}_4\right) T_0 + 24\hat{y}_3 T_1 + 48\hat{y}_4 T_2\right] + T_0 = 0. \tag{C.7}$$

Expanding this equation and using the identity 4.5 to express the nonlinear terms involving

Chebyshev polynomials in a linear manner gives the following

$$\begin{aligned}0 =&\hat{y}_0\left(4\hat{y}_2+32\hat{y}_4\right)T_0+24\hat{y}_0\hat{y}_3T_1+48\hat{y}_0\hat{y}_4T_2+\hat{y}_1\left(4\hat{y}_2+32\hat{y}_4\right)T_1+24\hat{y}_1\hat{y}_3\left(\frac{T_2+T_0}{2}\right)\\&+48\hat{y}_1\hat{y}_4\left(\frac{T_3+T_1}{2}\right)+\hat{y}_2\left(4\hat{y}_2+32\hat{y}_4\right)T_2+24\hat{y}_2\hat{y}_3\left(\frac{T_3+T_1}{2}\right)+48\hat{y}_2\hat{y}_4\left(\frac{T_4+T_0}{2}\right)\\&+\hat{y}_3\left(4\hat{y}_2+32\hat{y}_4\right)T_3+24\hat{y}_3\hat{y}_3\left(\frac{T_4+T_2}{2}\right)+48\hat{y}_3\hat{y}_4\left(\frac{\cancel{T_5}+T_1}{2}\right)+\hat{y}_4\left(4\hat{y}_2+32\hat{y}_4\right)T_4\\&+24\hat{y}_4\hat{y}_3\left(\frac{\cancel{T_5}+T_3}{2}\right)+48\hat{y}_4\hat{y}_4\left(\frac{\cancel{T_6}+T_2}{2}\right)+T_0.\end{aligned} \tag{C.8}$$

Note that Chebyshev polynomials ranked higher than four are neglected. Collating terms according to their Chebyshev polynomial components gives the same equation but in a clearer form

$$\begin{aligned}0 =&T_0\left[\hat{y}_0\left(4\hat{y}_2+32\hat{y}_4\right)+12\hat{y}_1\hat{y}_3+24\hat{y}_2\hat{y}_4+1\right]\\&+T_1\left[24\hat{y}_0\hat{y}_3+\hat{y}_1\left(4\hat{y}_2+32\hat{y}_4\right)+24\hat{y}_1\hat{y}_4+12\hat{y}_2\hat{y}_3+24\hat{y}_3\hat{y}_4\right]\\&+T_2\left[48\hat{y}_0\hat{y}_4+12\hat{y}_1\hat{y}_3+\hat{y}_2\left(4\hat{y}_2+32\hat{y}_4\right)+12\hat{y}_3^2+24\hat{y}_4^2\right]\\&+T_3\left[24\hat{y}_1\hat{y}_4+12\hat{y}_2\hat{y}_3+\hat{y}_3\left(4\hat{y}_2+32\hat{y}_4\right)+12\hat{y}_3\hat{y}_4\right]\\&+T_4\left[12\hat{y}_2\hat{y}_4+12\hat{y}_3^2+\hat{y}_4\left(4\hat{y}_2+32\hat{y}_4\right)\right]\end{aligned} \tag{C.9}$$

in which form it can easily be seen that the Chebyshev polynomial terms may be extracted

as a separate vector to give the vector equation

$$\begin{pmatrix} T_0 & T_1 & T_2 & T_3 & T_4 \end{pmatrix} \cdot \begin{pmatrix} \hat{y}_0\left(4\hat{y}_2+32\hat{y}_4\right)+12\hat{y}_1\hat{y}_3+24\hat{y}_2\hat{y}_4+1 \\ 24\hat{y}_0\hat{y}_3+\hat{y}_1\left(4\hat{y}_2+32\hat{y}_4\right)+24\hat{y}_1\hat{y}_4+12\hat{y}_2\hat{y}_3+24\hat{y}_3\hat{y}_4 \\ 48\hat{y}_0\hat{y}_4+12\hat{y}_1\hat{y}_3+\hat{y}_2\left(4\hat{y}_2+32\hat{y}_4\right)+12\hat{y}_3^2+24\hat{y}_4^2 \\ 24\hat{y}_1\hat{y}_4+12\hat{y}_2\hat{y}_3+\hat{y}_3\left(4\hat{y}_2+32\hat{y}_4\right)+12\hat{y}_3\hat{y}_4 \\ 12\hat{y}_2\hat{y}_4+12\hat{y}_3^2+\hat{y}_4\left(4\hat{y}_2+32\hat{y}_4\right) \end{pmatrix} = 0 \tag{C.10}$$

which is of identical form to equations (4.15) and (4.16). Hence, due to the orthogonality of the Chebyshev polynomials it remains to solve the set of nonlinear simultaneous equations given by

$$\hat{y}_0\left(4\hat{y}_2+32\hat{y}_4\right)+12\hat{y}_1\hat{y}_3+24\hat{y}_2\hat{y}_4+1=0, \tag{C.11}$$

$$24\hat{y}_0\hat{y}_3+\hat{y}_1\left(4\hat{y}_2+32\hat{y}_4\right)+24\hat{y}_1\hat{y}_4+12\hat{y}_2\hat{y}_3+24\hat{y}_3\hat{y}_4=0, \tag{C.12}$$

$$48\hat{y}_0\hat{y}_4+12\hat{y}_1\hat{y}_3+\hat{y}_2\left(4\hat{y}_2+32\hat{y}_4\right)+12\hat{y}_3^2+24\hat{y}_4^2=0, \tag{C.13}$$

$$24\hat{y}_1\hat{y}_4+12\hat{y}_2\hat{y}_3+\hat{y}_3\left(4\hat{y}_2+32\hat{y}_4\right)+12\hat{y}_3\hat{y}_4=0, \tag{C.14}$$

$$12\hat{y}_2\hat{y}_4+12\hat{y}_3^2+\hat{y}_4\left(4\hat{y}_2+32\hat{y}_4\right)=0, \tag{C.15}$$

or in a vector form identical to expressions (4.17)

$$\mathbf{f}_{\text{toy}}=0. \tag{C.16}$$

In order to find a final solution to this toy problem, that is to find values for the coefficients $\hat{y}_0$, $\hat{y}_1$, $\hat{y}_2$, $\hat{y}_3$ and $\hat{y}_4$, an initial guess can be made for these coefficients, $\mathbf{y}_i$ say. This guess is used in equation (C.16) or in the set of simultaneous equations (C.11)-(C.15) to determine the vector $(\mathbf{f}_{\text{toy}})_i$. Applying Newton's method according to the equation

$$\mathbf{y}_{i+1} = \mathbf{y}_i - \frac{(\mathbf{f}_{\text{toy}})_i}{(\mathbf{f}_{\text{toy}})'_i}, \tag{C.17}$$

which is is identical to equation (4.18), gives a set of values for a 'next guess' for the values of the Chebyshev coefficients, $\mathbf{y}_{i+1}$. The derivative term $(\mathbf{f}_{\text{toy}})'_i$ is the Jacobean matrix of $(\mathbf{f}_{\text{toy}})_i$. Convergence is achieved when the 'next guess' is within a small specified distance of the previous guess.

Appendix D

Discretized Forms of the Linearized Stability Equations

The discretized forms of the linearized stability equations are as follows:

Continuity of momentum

$$
\begin{aligned}
R\left(i\psi\sum_{n=0}^{N}\sum_{p=0}^{N}\widehat{(u_{\mathrm{B}})}_n\widehat{(\bar{u})}_p\frac{T_{n+p}+T_{|n-p|}}{2}+\sigma\sum_{n=0}^{N}\widehat{(\bar{u})}_nT_n\right)&\\
-m\beta\left(\frac{4}{L^2}\sum_{n=0}^{N}\frac{1}{c_n}\sum_{\substack{p=n+2\\ p+n\,\text{even}}}^{N}p(p^2-n^2)\widehat{(\bar{u})}_pT_n-\psi^2\sum_{n=0}^{N}\widehat{(\bar{u})}_nT_n\right)&\\
+R\frac{2}{L}\sum_{n=0}^{N}\sum_{p=0}^{N}\frac{1}{c_p}\sum_{\substack{q=p+1\\ q+p\,\text{odd}}}^{N}q\widehat{(\bar{v})}_n\widehat{(u_{\mathrm{B}})}_q\left(T_{n+p}+T_{|n-p|}\right)&\\
=i\psi\left(\sum_{n=0}^{N}\widehat{(\bar{\tau}_{xx})}_nT_n-\sum_{n=0}^{N}\widehat{(\bar{p})}_nT_n\right)+\frac{2}{L}\sum_{n=0}^{N}\frac{2}{c_n}\sum_{\substack{p=n+1\\ p+n\,\text{odd}}}^{N}p\widehat{(\bar{\tau}_{xy})}_pT_n,&\quad\text{(D.1)}
\end{aligned}
$$

$$R\left(i\psi\sum_{n=0}^{N}\sum_{p=0}^{N}\widehat{(u_{\mathrm{B}})}_n\widehat{(\bar{v})}_p\frac{T_{n+p}+T_{|n-p|}}{2}+\sigma\sum_{n=0}^{N}\widehat{(\bar{v})}_nT_n\right)$$
$$-m\beta\left(\frac{4}{L^2}\sum_{n=0}^{N}\frac{1}{c_n}\sum_{\substack{p=n+2\\ p+n\,\mathrm{even}}}^{N}p(p^2-n^2)\widehat{(\bar{v})}_pT_n-\psi^2\sum_{n=0}^{N}\widehat{(\bar{v})}_nT_n\right)$$
$$=i\psi\sum_{n=0}^{N}\widehat{(\bar{\tau}_{xy})}_nT_n+\frac{2}{L}\sum_{n=0}^{N}\frac{2}{c_n}\sum_{\substack{p=n+1\\ p+n\,\mathrm{odd}}}^{N}p\widehat{(\bar{\tau}_{yy})}_pT_n-\frac{2}{L}\sum_{n=0}^{N}\frac{2}{c_n}\sum_{\substack{p=n+1\\ p+n\,\mathrm{odd}}}^{N}p\widehat{(\bar{p})}_pT_n, \quad \text{(D.2)}$$

and continuity of mass

$$i\psi\sum_{n=0}^{N}\widehat{(\bar{u})}_nT_n+\frac{2}{L}\sum_{n=0}^{N}\frac{2}{c_n}\sum_{\substack{p=n+1\\ p+n\,\mathrm{odd}}}^{N}p\widehat{(\bar{v})}_pT_n=0. \quad \text{(D.3)}$$

The Giesekus constitutive equation

$$W\left(i\psi\sum_{n=0}^{N}\sum_{p=0}^{N}\widehat{(u_{\mathrm{B}})}_n\widehat{(\bar{\tau}_{xx})}_p\frac{T_{n+p}+T_{|n-p|}}{2}+\sigma\sum_{n=0}^{N}\widehat{(\bar{\tau}_{xx})}_nT_n\right)$$
$$+W\frac{2}{L}\sum_{n=0}^{N}\sum_{p=0}^{N}\frac{1}{c_p}\sum_{\substack{q=p+1\\ q+p\,\mathrm{odd}}}^{N}q\widehat{(\bar{v})}_n\widehat{(\tau_{xx\mathrm{B}})}_q\left(T_{n+p}+T_{|n-p|}\right)$$
$$-2i\psi W\left(\sum_{n=0}^{N}\sum_{p=0}^{N}\widehat{(\tau_{xx\mathrm{B}})}_n\widehat{(\bar{u})}_p\frac{T_{n+p}+T_{|n-p|}}{2}+\sum_{n=0}^{N}\sum_{p=0}^{N}\widehat{(\tau_{xy\mathrm{B}})}_n\widehat{(\bar{v})}_p\frac{T_{n+p}+T_{|n-p|}}{2}\right)$$
$$+\frac{\epsilon W}{m\left(1-\beta\right)}\left(\sum_{n=0}^{N}\sum_{p=0}^{N}\widehat{(\tau_{xx\mathrm{B}})}_n\widehat{(\bar{\tau}_{xx})}_p\left(T_{n+p}+T_{|n-p|}\right)+\sum_{n=0}^{N}\sum_{p=0}^{N}\widehat{(\tau_{xy\mathrm{B}})}_n\widehat{(\bar{\tau}_{xy})}_p\left(T_{n+p}+T_{|n-p|}\right)\right)$$
$$+\sum_{n=0}^{N}\widehat{(\bar{\tau}_{xx})}_nT_n=2i\psi m\left(1-\beta\right)\sum_{n=0}^{N}\widehat{(\bar{u})}_nT_n, \quad \text{(D.4)}$$

$$
\begin{aligned}
W\left(i\psi\sum_{n=0}^{N}\sum_{p=0}^{N}\widehat{(u_{\mathrm{B}})}_n\widehat{(\bar{\tau}_{xy})}_p\frac{T_{n+p}+T_{|n-p|}}{2}+\sigma\sum_{n=0}^{N}\widehat{(\bar{\tau}_{xy})}_nT_n\right)\\
+W\frac{2}{L}\sum_{n=0}^{N}\sum_{p=0}^{N}\frac{1}{c_p}\sum_{\substack{q=p+1\\ q+p\,\mathrm{odd}}}^{N}q\widehat{(\bar{v})}_n\widehat{\left(\tau_{xy_{\mathrm{B}}}\right)}_q\left(T_{n+p}+T_{|n-p|}\right)\\
-W\frac{2}{L}\sum_{n=0}^{N}\sum_{p=0}^{N}\frac{1}{c_p}\sum_{\substack{q=p+1\\ q+p\,\mathrm{odd}}}^{N}q\widehat{(\tau_{xx_{\mathrm{B}}})}_n\widehat{(\bar{u})}_q\left(T_{n+p}+T_{|n-p|}\right)\\
-W\frac{2}{L}\sum_{n=0}^{N}\sum_{p=0}^{N}\frac{1}{c_p}\sum_{\substack{q=p+1\\ q+p\,\mathrm{odd}}}^{N}q\widehat{(\bar{\tau}_{xx})}_n\widehat{(u_{\mathrm{B}})}_q\left(T_{n+p}+T_{|n-p|}\right)\\
-i\psi W\sum_{n=0}^{N}\sum_{p=0}^{N}\widehat{\left(\tau_{yy_{\mathrm{B}}}\right)}_n\widehat{(\bar{v})}_p\frac{T_{n+p}+T_{|n+p|}}{2}+\sum_{n=0}^{N}\widehat{(\bar{\tau}_{xy})}_nT_n\\
+\frac{\epsilon W}{m\left(1-\beta\right)}\left(\sum_{n=0}^{N}\sum_{p=0}^{N}\widehat{(\tau_{xx_{\mathrm{B}}})}_n\widehat{(\bar{\tau}_{xy})}_p\frac{T_{n+p}+T_{|n-p|}}{2}+\sum_{n=0}^{N}\sum_{p=0}^{N}\widehat{\left(\tau_{xy_{\mathrm{B}}}\right)}_n\widehat{(\bar{\tau}_{xx})}_p\frac{T_{n+p}+T_{|n-p|}}{2}\right)\\
+\frac{\epsilon W}{m\left(1-\beta\right)}\left(\sum_{n=0}^{N}\sum_{p=0}^{N}\widehat{\left(\tau_{xy_{\mathrm{B}}}\right)}_n\widehat{(\bar{\tau}_{yy})}_p\frac{T_{n+p}+T_{|n-p|}}{2}+\sum_{n=0}^{N}\sum_{p=0}^{N}\widehat{\left(\tau_{yy_{\mathrm{B}}}\right)}_n\widehat{(\bar{\tau}_{xy})}_p\frac{T_{n+p}+T_{|n-p|}}{2}\right)\\
=m\left(1-\beta\right)\left(\frac{2}{L}\sum_{n=0}^{N}\frac{2}{c_n}\sum_{\substack{p=n+1\\ p+n\,\mathrm{odd}}}^{N}p\widehat{(\bar{u})}_pT_n+i\psi\sum_{n=0}^{N}\widehat{(\bar{v})}_nT_n,\right)
\end{aligned}
\tag{D.5}
$$

$$
\begin{aligned}
W\left(i\psi\sum_{n=0}^{N}\sum_{p=0}^{N}\widehat{(u_{\mathrm{B}})_n}\widehat{(\bar{\tau}_{yy})_p}\frac{T_{n+p}+T_{|n-p|}}{2}+\sigma\sum_{n=0}^{N}\widehat{(\bar{\tau}_{yy})_n}T_n\right)\\
+W\frac{2}{L}\sum_{n=0}^{N}\sum_{p=0}^{N}\frac{1}{c_p}\sum_{\substack{q=p+1\\ q+p\,\mathrm{odd}}}^{N}q\widehat{(\bar{v})_n}\widehat{\left(\tau_{yy_{\mathrm{B}}}\right)_q}\left(T_{n+p}+T_{|n-p|}\right)\\
-2W\frac{2}{L}\sum_{n=0}^{N}\sum_{p=0}^{N}\frac{1}{c_p}\sum_{\substack{q=p+q\\ q+p\,\mathrm{odd}}}^{N}q\widehat{\left(\tau_{yy_{\mathrm{B}}}\right)_n}\widehat{(\bar{v})_q}\left(T_{n+p}+T_{|n-p|}\right)\\
-2W\frac{2}{L}\sum_{n=0}^{N}\sum_{p=0}^{N}\frac{1}{c_p}\sum_{\substack{q=p+1\\ q+p\,\mathrm{odd}}}^{N}q\widehat{(\bar{\tau}_{xy})_n}\widehat{(u_{\mathrm{B}})_q}\left(T_{n+p}+T_{|n-p|}\right)\\
-2W\frac{2}{L}\sum_{n=0}^{N}\sum_{p=0}^{N}\frac{1}{c_p}\sum_{\substack{q=p+q\\ q+p\,\mathrm{odd}}}^{N}q\widehat{(\bar{u})_n}\widehat{\left(\tau_{xy_{\mathrm{B}}}\right)_q}\left(T_{n+p}+T_{|n-p|}\right)+\sum_{n=0}^{N}\widehat{(\bar{\tau}_{xy})_n}T_n\\
+\frac{\epsilon W}{m\left(1-\beta\right)}\left(\sum_{n=0}^{N}\sum_{p=0}^{N}\widehat{\left(\tau_{xy_{\mathrm{B}}}\right)_n}\widehat{(\bar{\tau}_{xy})_p}\left(T_{n+p}+T_{|n-p|}\right)+\sum_{n=0}^{N}\sum_{p=0}^{N}\widehat{\left(\tau_{yy_{\mathrm{B}}}\right)_n}\widehat{(\bar{\tau}_{yy})_p}\left(T_{n+p}+T_{|n-p|}\right)\right)\\
=2m\left(1-\beta\right)\frac{2}{L}\sum_{n=0}^{N}\frac{2}{c_n}\sum_{\substack{p=n+1\\ n+p\,\mathrm{odd}}}^{N}p\widehat{(\bar{u})_p}T_n. \quad \text{(D.6)}
\end{aligned}
$$

The Phan-Thien Tanner constitutive equation

$$
\begin{aligned}
W\left(i\psi\sum_{n=0}^{N}\sum_{p=0}^{N}\widehat{(u_{\mathrm{B}})_n}\widehat{(\bar{\tau}_{xx})_p}\frac{T_{n+p}+T_{|n-p|}}{2}+\sigma\sum_{n=0}^{N}\widehat{(\bar{\tau}_{xx})_n}T_n\right)\\
+W\frac{2}{L}\sum_{n=0}^{N}\sum_{p=0}^{N}\frac{1}{c_n}\sum_{\substack{q=p+1\\ p+q\,\mathrm{odd}}}^{N}q\widehat{(\bar{v})_n}\widehat{(\tau_{xx\mathrm{B}})_q}\left(T_{n+p}+T_{|n-p|}\right)\\
-W\left(1-\xi\right)i\psi\sum_{n=0}^{N}\sum_{p=0}^{N}\widehat{(\tau_{xx\mathrm{B}})_n}\widehat{(\bar{u})_p}\left(T_{n+p}+T_{|n-p|}\right)\\
-W\left(2-\xi\right)i\psi\sum_{n=0}^{N}\sum_{p=0}^{N}\widehat{\left(\tau_{xy\mathrm{B}}\right)_n}\widehat{(\bar{v})_p}\frac{T_{n+p}+T_{|n-p|}}{2}\\
+W\xi\frac{2}{L}\sum_{n=0}^{N}\sum_{p=0}^{N}\frac{1}{c_n}\sum_{\substack{q=p+1\\ p+q\,\mathrm{odd}}}^{N}q\widehat{\left(\tau_{xy\mathrm{B}}\right)_n}\widehat{(\bar{u})_q}\left(T_{n+p}+T_{|n-p|}\right)\\
+W\xi\frac{2}{L}\sum_{n=0}^{N}\sum_{p=0}^{N}\frac{1}{c_n}\sum_{\substack{q=p+1\\ p+q\,\mathrm{odd}}}^{N}q\widehat{(\bar{\tau}_{xy})_n}\widehat{(u_{\mathrm{B}})_q}\left(T_{n+p}+T_{|n-p|}\right)\\
+\sum_{n=0}^{N}\widehat{(\bar{\tau}_{xx})_n}T_n+\frac{\epsilon W}{m\left(1-\beta\right)}\sum_{n=0}^{N}\sum_{p=0}^{N}\widehat{(\tau_{xx\mathrm{B}})_n}\widehat{(\bar{\tau}_{xx})_p}\left(T_{n+p}+T_{|n-p|}\right)\\
+\frac{\epsilon W}{m\left(1-\beta\right)}\left(\sum_{n=0}^{N}\sum_{p=0}^{N}\widehat{\left(\tau_{yy\mathrm{B}}\right)_n}\widehat{(\bar{\tau}_{xx})_p}\frac{T_{n+p}+T_{|n-p|}}{2}+\sum_{n=0}^{N}\sum_{p=0}^{N}\widehat{\left(\tau_{yy\mathrm{B}}\right)_n}\widehat{(\bar{\tau}_{yy})_p}\frac{T_{n+p}+T_{|n-p|}}{2}\right)\\
=2m\left(1-\beta\right)i\psi\sum_{n=0}^{N}\widehat{(\bar{u})_n}T_n,
\end{aligned}
\tag{D.7}
$$

$$
\begin{aligned}
W\left(i\psi\sum_{n=0}^{N}\sum_{p=0}^{N}\widehat{(u_{\mathrm{B}})}_n\widehat{(\bar{\tau}_{xy})}_p\frac{T_{n+p}+T_{|n-p|}}{2}+\sigma\sum_{n=0}^{N}\widehat{(\bar{\tau}_{xy})}_nT_n\right)\\
+W\frac{2}{L}\sum_{n=0}^{N}\sum_{p=0}^{N}\frac{1}{c_n}\sum_{\substack{q=p+1\\ p+q\,\mathrm{odd}}}^{N}q\widehat{(\bar{v})}_n\widehat{\left(\tau_{xy_{\mathrm{B}}}\right)}_q\left(T_{n+p}+T_{|n-p|}\right)\\
-W\left(1-\frac{\xi}{2}\right)\frac{2}{L}\sum_{n=0}^{N}\sum_{p=0}^{N}\frac{1}{c_n}\sum_{\substack{q=p+1\\ p+q\,\mathrm{odd}}}^{N}q\widehat{(\tau_{xx_{\mathrm{B}}})}_n\widehat{(\bar{u})}_q\left(T_{n+p}+T_{|n-p|}\right)\\
-W\left(1-\frac{\xi}{2}\right)\frac{2}{L}\sum_{n=0}^{N}\sum_{p=0}^{N}\frac{1}{c_n}\sum_{\substack{q=p+1\\ p+q\,\mathrm{odd}}}^{N}q\widehat{(\bar{\tau}_{xx})}_n\widehat{(u_{\mathrm{B}})}_q\left(T_{n+p}+T_{|n-p|}\right)\\
+Wi\psi\frac{\xi}{2}\sum_{n=0}^{N}\sum_{p=0}^{N}\widehat{(\bar{v})}_n\widehat{(\tau_{xx_{\mathrm{B}}})}_p\frac{T_{n+p}+T_{|n-p|}}{2}-W\left(1-\frac{\xi}{2}\right)i\psi\sum_{n=0}^{N}\sum_{p=0}^{N}\widehat{(\bar{v})}_n\widehat{\left(\tau_{yy_{\mathrm{B}}}\right)}_p\frac{T_{n+p}+T_{|n-p|}}{2}\\
+\frac{W\xi}{2}\frac{2}{L}\sum_{n=0}^{N}\sum_{p=0}^{N}\frac{1}{c_n}\sum_{\substack{q=p+1\\ p+q\,\mathrm{odd}}}^{N}q\widehat{\left(\tau_{yy_{\mathrm{B}}}\right)}_n\widehat{(\bar{u})}_q\left(T_{n+p}+T_{|n-p|}\right)\\
+\frac{W\xi}{2}\frac{2}{L}\sum_{n=0}^{N}\sum_{p=0}^{N}\frac{1}{c_n}\sum_{\substack{q=p+1\\ p+q\,\mathrm{odd}}}^{N}q\widehat{(\bar{\tau}_{yy})}_n\widehat{(u_{\mathrm{B}})}_q\left(T_{n+p}+T_{|n-p|}\right)+\sum_{n=0}^{N}\widehat{(\bar{\tau}_{xy})}_nT_n\\
+\frac{\epsilon W}{m\left(1-\beta\right)}\left(\sum_{n=0}^{N}\sum_{p=0}^{N}\widehat{(\tau_{xx_{\mathrm{B}}})}_n\widehat{(\bar{\tau}_{xy})}_p\frac{T_{n+p}+T_{|n-p|}}{2}+\sum_{n=0}^{N}\sum_{p=0}^{N}\widehat{\left(\tau_{yy_{\mathrm{B}}}\right)}_n\widehat{(\bar{\tau}_{xy})}_p\frac{T_{n+p}+T_{|n-p|}}{2}\right)\\
+\frac{\epsilon W}{m\left(1-\beta\right)}\left(\sum_{n=0}^{N}\sum_{p=0}^{N}\widehat{\left(\tau_{xy_{\mathrm{B}}}\right)}_n\widehat{(\bar{\tau}_{xx})}_p\frac{T_{n+p}+T_{|n-p|}}{2}+\sum_{n=0}^{N}\sum_{p=0}^{N}\widehat{\left(\tau_{xy_{\mathrm{B}}}\right)}_n\widehat{(\bar{\tau}_{yy})}_p\frac{T_{n+p}+T_{|n-p|}}{2}\right)\\
=m\left(1-\beta\right)\left(\frac{2}{L}\sum_{n=0}^{N}\frac{1}{c_n}\sum_{\substack{p=n+1\\ n+p\,\mathrm{odd}}}^{N}p\widehat{(\bar{u})}_pT_n+i\psi\sum_{n=0}^{N}\widehat{(\bar{v})}_nT_n\right),
\end{aligned}
\tag{D.8}
$$

$$
\begin{aligned}
W\left(i\psi\sum_{n=0}^{N}\sum_{p=0}^{N}\widehat{(u_{\mathrm{B}})_n}\widehat{(\bar{\tau}_{yy})_p}\frac{T_{n+p}+T_{|n-p|}}{2}+\sigma\sum_{n=0}^{N}\widehat{(\bar{\tau}_{yy})_n}T_n\right)\\
+W\frac{2}{L}\sum_{n=0}^{N}\sum_{p=0}^{N}\frac{1}{c_n}\sum_{\substack{q=p+1\\ p+q\,\mathrm{odd}}}^{N}q\widehat{(\bar{v})_n}\widehat{\left(\tau_{yy_{\mathrm{B}}}\right)_q}\left(T_{n+p}+T_{|n-p|}\right)\\
-2W\left(1-\xi\right)\frac{2}{L}\sum_{n=0}^{N}\sum_{p=0}^{N}\frac{1}{c_n}\sum_{\substack{q=p+1\\ p+q\,\mathrm{odd}}}^{N}q\widehat{\left(\tau_{yy_{\mathrm{B}}}\right)_n}\widehat{(\bar{v})_q}\left(T_{n+p}+T_{|n-p|}\right)\\
-W\left(2-\xi\right)\frac{2}{L}\sum_{n=0}^{N}\sum_{p=0}^{N}\frac{1}{c_n}\sum_{\substack{q=p+1\\ p+q\,\mathrm{odd}}}^{N}q\widehat{\left(\tau_{xy_{\mathrm{B}}}\right)_n}\widehat{(\bar{u})_q}\left(T_{n+p}+T_{|n-p|}\right)\\
-W\left(2-\xi\right)\frac{2}{L}\sum_{n=0}^{N}\sum_{p=0}^{N}\frac{1}{c_n}\sum_{\substack{q=p+1\\ p+q\,\mathrm{odd}}}^{N}q\widehat{(\bar{\tau}_{xy})_n}\widehat{(u_{\mathrm{B}})_q}\left(T_{n+p}+T_{|n-p|}\right)\\
+W\xi i\psi\sum_{n=0}^{N}\sum_{p=0}^{N}\widehat{\left(\tau_{xy_{\mathrm{B}}}\right)_n}\widehat{(\bar{v})_p}\frac{T_{n+p}+T_{|n-p|}}{2}+\sum_{n=0}^{N}\widehat{(\bar{\tau}_{yy})_n}T_n\\
+\frac{\epsilon W}{m\left(1-\beta\right)}\left(\sum_{n=0}^{N}\sum_{p=0}^{N}\widehat{(\tau_{xx_{\mathrm{B}}})_n}\widehat{(\bar{\tau}_{yy})_p}\frac{T_{n+p}+T_{|n-p|}}{2}+\sum_{n=0}^{N}\sum_{p=0}^{N}\widehat{\left(\tau_{yy_{\mathrm{B}}}\right)_n}\widehat{(\bar{\tau}_{yy})_p}\left(T_{n+p}+T_{|n-p|}\right)\right)\\
+\frac{\epsilon W}{m\left(1-\beta\right)}\sum_{n=0}^{N}\sum_{p=0}^{N}\widehat{\left(\tau_{yy_{\mathrm{B}}}\right)_n}\widehat{(\bar{\tau}_{xx})_p}\frac{T_{n+p}+T_{|n-p|}}{2}\\
=2m\left(1-\beta\right)\frac{2}{L}\sum_{n=0}^{N}\frac{1}{c_n}\sum_{\substack{p=n+1\\ n+p\,\mathrm{odd}}}^{N}p\widehat{(\bar{v})_p}T_n. \quad \text{(D.9)}
\end{aligned}
$$

Appendix E

The Full Orr-Sommerfeld Equation for Giesekus Fluids

In this Appendix the method used to obtain the full Orr-Sommerfeld equation for Giesekus fluids is demonstrated. The derivation shown here is in a general form whereby the equations for the multiple fluid problems have been used with the omission of the subscripts denoting the fluids. Simplification to the case of one fluid is trivial (set $m = 1$). The linearized stability equations are repeated here (from equations (3.33)-(3.38)).

$$R\left(i\psi u_{\mathrm{B}} + \sigma\right)\bar{u} - m\beta\left(\bar{u}'' - \psi^2\bar{u}\right) + Ru'_{\mathrm{B}}\bar{v} = i\psi\left(\bar{\tau}_{xx} - \bar{p}\right) + \bar{\tau}'_{xy}, \tag{E.1}$$

$$R\left(i\psi u_{\mathrm{B}} + \sigma\right)\bar{v} - m\beta\left(\bar{v}'' - \psi^2\bar{v}\right) = i\psi\bar{\tau}_{xy} + \bar{\tau}'_{yy} - \bar{p}', \tag{E.2}$$

$$i\psi\bar{u} + \bar{v}' = 0, \tag{E.3}$$

$$W\left[\left(i\psi u_{\mathrm{B}}+\sigma\right)\bar{\tau}_{xx}+{\tau_{xx}}_{\mathrm{B}}'\bar{v}-2i\psi\left(\tau_{xx\mathrm{B}}\bar{u}+\tau_{xy_{\mathrm{B}}}\bar{v}\right)\right]+\bar{\tau}_{xx}$$
$$+2\frac{\epsilon W}{m\left(1-\beta\right)}\left(\tau_{xx\mathrm{B}}\bar{\tau}_{xx}+\tau_{xy_{\mathrm{B}}}\bar{\tau}_{xy}\right)=2i\psi m\left(1-\beta\right)\bar{u}, \quad \text{(E.4)}$$

$$W\left[\left(i\psi u_{\mathrm{B}}+\sigma\right)\bar{\tau}_{xy}+{\tau_{xy}}_{\mathrm{B}}'\bar{v}-\tau_{xx\mathrm{B}}\bar{u}'-u_{\mathrm{B}}'\bar{\tau}_{xx}-i\psi\tau_{yy\mathrm{B}}\bar{v}\right]+\bar{\tau}_{xy}$$
$$+\frac{\epsilon W}{m\left(1-\beta\right)}\left(\tau_{xy_{\mathrm{B}}}\left(\bar{\tau}_{xx}+\bar{\tau}_{yy}\right)+\left(\tau_{xx\mathrm{B}}+\tau_{yy\mathrm{B}}\right)\bar{\tau}_{xy}\right)=m\left(1-\beta\right)\left(\bar{u}'+i\psi\bar{v}\right), \quad \text{(E.5)}$$

$$W\left[\left(i\psi u_{\mathrm{B}}+\sigma\right)\bar{\tau}_{yy}+{\tau_{yy}}_{\mathrm{B}}'\bar{v}-2\tau_{yy\mathrm{B}}\bar{v}'-2\left(u_{\mathrm{B}}'\bar{\tau}_{xy}+\tau_{xy\mathrm{B}}\bar{u}'\right)\right]+\bar{\tau}_{yy}$$
$$+2\frac{\epsilon W}{m\left(1-\beta\right)}\left(\tau_{xy\mathrm{B}}\bar{\tau}_{xy}+\tau_{yy\mathrm{B}}\bar{\tau}_{yy}\right)=2m\left(1-\beta\right)\bar{v}'. \quad \text{(E.6)}$$

The disturbance streamwise velocity, $\bar{u}$, can be eliminated using equation (E.3) so that

$$\bar{u}=\frac{i\bar{v}'}{\psi},$$

and the disturbance pressure can be eliminated by subtracting $i\psi\times$(E.2) from the derivative of (E.1) with respect to y to give

$$\frac{mi\beta}{\psi}\bar{v}^{\mathrm{IV}}-\left(-Ru_{\mathrm{B}}+\frac{i\sigma R}{\psi}+2mi\beta\psi\right)\bar{v}''-\left(Ru_{\mathrm{B}}''+R\psi^2u_{\mathrm{B}}-iR\psi\sigma-im\beta\psi^3\right)\bar{v}$$
$$+i\psi\bar{\tau}_{xx}'+\psi^2\bar{\tau}_{xy}+\bar{\tau}_{xy}''-i\psi\bar{\tau}_{yy}'=0. \quad \text{(E.7)}$$

The disturbance stresses can be eliminated as follows: By rewriting equations (E.4)-(E.6) in

the form

$$\begin{aligned} f_{11}\bar{\tau}_{xx} &+ f_{12}\bar{\tau}_{xy} &&= g_1(\bar{v}), \\ f_{21}\bar{\tau}_{xx} &+ f_{22}\bar{\tau}_{xy} + f_{23}\bar{\tau}_{yy} &&= g_2(\bar{v}), \\ & f_{32}\bar{\tau}_{xy} + f_{33}\bar{\tau}_{yy} &&= g_3(\bar{v}), \end{aligned} \tag{E.8}$$

where

$$\begin{aligned} f_{11} &= W\left(i\psi u_{\mathrm{B}} + \sigma\right) + 1 + \frac{2\epsilon W}{m\left(1-\beta\right)}\tau_{xx\mathrm{B}}, \\ f_{12} &= \frac{2\epsilon W}{m\left(1-\beta\right)}\tau_{xy\mathrm{B}}, \\ f_{21} &= -W u'_{\mathrm{B}} + \frac{\epsilon W}{m\left(1-\beta\right)}\tau_{xy\mathrm{B}}, \\ f_{22} &= W\left(i\psi u_{\mathrm{B}} + \sigma\right) + 1 + \frac{\epsilon W}{m\left(1-\beta\right)}\left(\tau_{xx\mathrm{B}} + \tau_{yy\mathrm{B}}\right), \\ f_{23} &= \frac{\epsilon W}{m\left(1-\beta\right)}\tau_{xy\mathrm{B}}, \\ f_{32} &= -2W u'_{\mathrm{B}} + \frac{2\epsilon W}{m\left(1-\beta\right)}\tau_{xy\mathrm{B}}, \\ f_{33} &= W\left(i\psi u_{\mathrm{B}} + \sigma\right) + 1 + \frac{2\epsilon W}{m\left(1-\beta\right)}\tau_{yy\mathrm{B}}, \end{aligned}$$

and

$$
\begin{aligned}
g_1 &= g_A\bar{v} + g_B\bar{v}', & g_A &= -W{\tau_{xx_{\mathrm{B}}}}' + 2Wi\psi\tau_{xy_{\mathrm{B}}},\\
& & g_B &= -2W\tau_{xx_{\mathrm{B}}} - 2m\left(1-\beta\right),\\
g_2 &= g_C\bar{v} + g_D\bar{v}'', & g_C &= -W{\tau_{xy_{\mathrm{B}}}}' + Wi\psi\tau_{yy_{\mathrm{B}}} + im\psi\left(1-\beta\right),\\
& & g_D &= \frac{iW}{\psi}\tau_{xx_{\mathrm{B}}} + \frac{im}{\psi}\left(1-\beta\right),\\
g_3 &= g_E\bar{v} + g_F\bar{v}' + g_G\bar{v}'', & g_E &= -W{\tau_{yy_{\mathrm{B}}}}',\\
& & g_F &= 2W\tau_{yy_{\mathrm{B}}} + 2m\left(1-\beta\right),\\
& & g_G &= \frac{2iW}{\psi}\tau_{xy_{\mathrm{B}}}.
\end{aligned}
$$

Then the simultaneous equations (E.8) reduce to

$$\bar{\tau}_{xx} = \frac{g_1 - f_{12}\bar{\tau}_{xy}}{f_{11}}, \tag{E.9}$$

$$\bar{\tau}_{xy} = \frac{g_2 f_{11} f_{33} - f_{21} f_{33} g_1 - f_{11} f_{23} g_3}{f_{11} f_{22} f_{33} - f_{12} f_{21} f_{33} - f_{11} f_{23} f_{32}}, \tag{E.10}$$

$$\bar{\tau}_{yy} = \frac{g_3 - f_{32}\bar{\tau}_{xy}}{f_{33}}. \tag{E.11}$$

These terms are then differentiated as required and substituted into equation (E.7) to give the full Orr-Somerfeld equation. This results in a fourth-order ordinary differential equation for the perturbed cross-channel velocity, $\bar{v}$.

Appendix F

Branch Cuts of the Orr-Sommerfeld Equation for Giesekus Fluids

Here, the details of the calculations to find the continuous parts of the eigenspectrum for Poiseuille flow for Giesekus fluids is demonstrated. In order to find the continuous parts of the eigenspectra it is necessary to consider cases where the solutions to the Orr-Sommerfeld equations are not analytic functions of y and σ, that is at singular points, when the coefficient of the highest derivative vanishes. These are known as branch cuts. It has already been stated that the full Orr-Sommerfeld equation is cumbersome and a full analytical analysis would be time-consuming and unproductive. It is possible however, to find the coefficient to the highest derivative without explicitly stating the full equation. As for the derivation of the full Orr-Sommerfeld equations in Appendix E, equations for the multiple fluid problems are used here with the omission of the subscripts.

The highest derivative is known to be of the order four when equations (3.33)-(3.38) are combined to eliminate all variables except $\bar{v}$. Extracting coefficients from each of these equations gives contributions to the coefficient of the fourth order derivative of $\bar{v}$ as

$$\underbrace{m\beta}_{\star^1} + \underbrace{\frac{\left(\tau_{xx\mathrm{B}} W + m\left(1-\beta\right)\right) f_{11} f_{33} - 2W\tau_{xy\mathrm{B}} f_{11} f_{23}}{f_{11} f_{22} f_{33} - f_{12} f_{21} f_{33} - f_{11} f_{23} f_{32}}}_{\star^2} = 0$$

where

$\star^1$ From differentiating $\bar{u}''$ in the first Navier-Stokes equation and substituting continuity. The coefficient $\frac{i}{\psi}$ cancels with the other terms in the expression.

$\star^2$ From differentiating the term $\bar{\tau}'_{xy}$ in the first Navier-Stokes equation. The expression for $\bar{\tau}_{xy}$ is given by (E.10).

Here, the functions f_{ij} are defined as in Appendix E. Substituting for f_{ij} accordingly gives the cubic equation for σ

$$\begin{aligned}
&m\beta W^3\sigma^3 + \left[m\beta\left(\hat{f}_{11}+\hat{f}_{22}+\hat{f}_{33}\right) + W\tau_{xx\mathrm{B}} + m\left(1-\beta\right)\right] W^2\sigma^2 \\
&\quad + \left[m\beta\left(\hat{f}_{11}\hat{f}_{22} + \hat{f}_{11}\hat{f}_{33} + \hat{f}_{22}\hat{f}_{33} + \frac{4\epsilon W^2\tau_{xy\mathrm{B}}}{m\left(1-\beta\right)}\left(u'_{\mathrm{B}} - \frac{\epsilon\tau_{xy\mathrm{B}}}{m\left(1-\beta\right)}\right)\right)\right] W\sigma \\
&\quad + \left[\left(W\tau_{xx\mathrm{B}} + m\left(1-\beta\right)\right)\left(\hat{f}_{11}+\hat{f}_{33}\right) - \frac{2\epsilon W^2\tau_{xy\mathrm{B}}^{\,2}}{m\left(1-\beta\right)}\right] W\sigma \\
&\quad m\beta\left(\hat{f}_{11}\hat{f}_{22}\hat{f}_{33} + \frac{2\epsilon W^2\tau_{xy\mathrm{B}}}{m\left(1-\beta\right)}\left(u'_{\mathrm{B}} - \frac{\epsilon\tau_{xy\mathrm{B}}}{m\left(1-\beta\right)}\right)\left(\hat{f}_{11}+\hat{f}_{33}\right)\right) \\
&\quad + \left(W\tau_{xx\mathrm{B}} + m\left(1-\beta\right)\right)\hat{f}_{11}\hat{f}_{33} - \frac{2\epsilon W^2\tau_{xy\mathrm{B}}^{\,2}}{m\left(1-\beta\right)}\hat{f}_{11} = 0, \quad \text{(F.1)}
\end{aligned}$$

where

$$\begin{aligned}
\hat{f}_{11} =& Wi\psi u_{\mathrm{B}} + 1 + \frac{2\epsilon W}{m\,(1-\beta)}\tau_{xx\mathrm{B}},\\
\hat{f}_{22} =& Wi\psi u_{\mathrm{B}} + 1 + \frac{\epsilon W}{m\,(1-\beta)}\left(\tau_{xx\mathrm{B}} + \tau_{yy\mathrm{B}}\right),\\
\hat{f}_{33} =& Wi\psi u_{\mathrm{B}} + 1 + \frac{2\epsilon W}{m\,(1-\beta)}\tau_{yy\mathrm{B}}.
\end{aligned}$$

Solutions to this cubic are in the form

$$\sigma = x - \frac{p}{3x} - \frac{a_2}{3},$$

where

$$x = \quad \sqrt[3]{X}, \quad -\frac{1}{2}\sqrt[3]{X} + \frac{i\sqrt{3}}{2}\sqrt[3]{X}, \quad -\frac{1}{2}\sqrt[3]{X} - \frac{i\sqrt{3}}{2}\sqrt[3]{X},$$

$$X = Q \pm \sqrt{Q^2 + R^3}$$

and

$$\begin{aligned}
Q =& \frac{q}{2}, & R =& \frac{r}{3},\\
q =& \frac{9a_1a_2 - 27a_0 - 2a_2^3}{27}, & r =& \frac{3a_1 - a_2^2}{3}.
\end{aligned}$$

The terms a_j denote the coefficients of σ^j when equation (F.1) is expressed in the form

$$\sigma^3 + a_2\sigma^2 + a_1\sigma + a_0 = 0.$$

Explicit expressions of these solutions would be both overly complex and unnecessary, particularly since analytical solutions for the base flow variables are not available for the full Giesekus model. The numerical solutions for the base flow, however, have been substituted into the above expressions, and this method has yielded good results as is shown in Chapter 6.

Appendix G

The Full Orr-Sommerfeld Equation for Phan-Thien Tanner Fluids

The derivation shown here is similar to that for Giesekus fluids which was demonstrated in Appendix E. Again, the equations for the multiple fluid problems have been used with the omission of the subscripts denoting the fluids and they are repeated here (from equations (3.33)-(3.35) and (3.39)-(3.41)).

$$R\left(i\psi u_{\mathrm{B}}+\sigma\right)\bar{u}-m\beta\left(\bar{u}''-\psi^{2}\bar{u}\right)+Ru_{\mathrm{B}}'\bar{v}=i\psi\left(\bar{\tau}_{xx}-\bar{p}\right)+\bar{\tau}_{xy}', \tag{G.1}$$

$$R\left(i\psi u_{\mathrm{B}}+\sigma\right)\bar{v}-m\beta\left(\bar{v}''-\psi^{2}\bar{v}\right)=i\psi\bar{\tau}_{xy}+\bar{\tau}_{yy}'-\bar{p}', \tag{G.2}$$

$$i\psi\bar{u}+\bar{v}'=0, \tag{G.3}$$

$$W\left[\left(i\psi u_{\mathrm{B}}+\sigma\right)\bar{\tau}_{xx}+{\tau_{xx}}_{\mathrm{B}}'\bar{v}-2\left(1-\xi\right)i\psi\tau_{xx\mathrm{B}}\bar{u}-\left(2-\xi\right)i\psi\tau_{xy\mathrm{B}}\bar{v}+\xi\left(\tau_{xy\mathrm{B}}\bar{u}'+\bar{\tau}_{xy}u_{\mathrm{B}}'\right)\right]$$
$$+\bar{\tau}_{xx}+\frac{\epsilon W}{m\left(1-\beta\right)}\left(\tau_{xx\mathrm{B}}\left(\bar{\tau}_{xx}+\bar{\tau}_{yy}\right)+\bar{\tau}_{xx}\left(\tau_{xxB}+{\tau_{yy}}_{B}\right)\right)=2i\psi m\left(1-\beta\right)\bar{u}, \quad \text{(G.4)}$$

$$W\left[\left(i\psi u_{\mathrm{B}}+\sigma\right)\bar{\tau}_{xy}+{\tau_{xy}}_{\mathrm{B}}'\bar{v}\right]$$
$$-W\left[\left(1-\frac{\xi}{2}\right)\left(u_{\mathrm{B}}'\bar{\tau}_{xx}+\tau_{xx\mathrm{B}}\bar{u}'+i\psi\tau_{yy\mathrm{B}}\bar{v}\right)-\frac{\xi}{2}\left(u_{\mathrm{B}}'\bar{\tau}_{yy}+\tau_{yy\mathrm{B}}\bar{u}'+i\psi\tau_{xx\mathrm{B}}\bar{v}\right)\right]$$
$$+\bar{\tau}_{xy}+\frac{\epsilon W}{m\left(1-\beta\right)}\left(\tau_{xy\mathrm{B}}\left(\bar{\tau}_{xx}+\bar{\tau}_{yy}\right)+\bar{\tau}_{xy}\left(\tau_{xx\mathrm{B}}+\tau_{yy\mathrm{B}}\right)\right)=m\left(1-\beta\right)\left(\bar{u}'+i\psi\bar{v}\right), \quad \text{(G.5)}$$

$$W\left[\left(i\psi u_{\mathrm{B}}+\sigma\right)\bar{\tau}_{yy}+{\tau_{yy}}_{\mathrm{B}}'\bar{v}-2\left(1-\xi\right)\tau_{yy\mathrm{B}}\bar{v}'-\left(2-\xi\right)\left(\tau_{xy\mathrm{B}}\bar{u}'+u_{\mathrm{B}}'\bar{\tau}_{xy}\right)+\xi i\psi\tau_{xy\mathrm{B}}\bar{v}\right]$$
$$+\bar{\tau}_{yy}+\frac{\epsilon W}{m(1-\beta)}\left(\tau_{yy\mathrm{B}}\left(\bar{\tau}_{xx}+\bar{\tau}_{yy}\right)+\bar{\tau}_{yy}\left(\tau_{xx\mathrm{B}}+\tau_{yy\mathrm{B}}\right)\right)=2m\left(1-\beta\right)\bar{v}'. \quad \text{(G.6)}$$

As before, the Navier-Stokes equations for continuity of momentum and continuity of mass, equations (G.1)-(G.3) can be combined into a single expression, equation (E.7). Since the PTT constitutive equations are slightly more complex than the Giesekus constitutive equations a different approach is required to eliminate the disturbance stresses. Equations (G.4)-(G.6) are rewritten in an augmented matrix form,

$$\left(\begin{array}{ccc|c} f_{11} & f_{12} & f_{13} & g_1 \\ f_{21} & f_{22} & f_{23} & g_2 \\ f_{31} & f_{32} & f_{33} & g_3 \end{array}\right), \quad \text{(G.7)}$$

where

$$f_{11} = Wi\psi u_{\mathrm{B}} + W\sigma + 1 + \frac{\epsilon W}{m\left(1-\beta\right)}\left(2\tau_{xx\mathrm{B}} + \tau_{yy\mathrm{B}}\right),$$

$$f_{12} = W\xi u'_{\mathrm{B}},$$

$$f_{13} = \frac{\epsilon W}{m\left(1-\beta\right)}\tau_{xx\mathrm{B}},$$

$$f_{21} = -W\left(1-\frac{\xi}{2}\right)u'_{\mathrm{B}} + \frac{\epsilon W}{m\left(1-\beta\right)}\tau_{xy\mathrm{B}},$$

$$f_{22} = Wi\psi u_{\mathrm{B}} + W\sigma + 1 + \frac{\epsilon W}{m\left(1-\beta\right)}\left(\tau_{xx\mathrm{B}} + \tau_{yy\mathrm{B}}\right),$$

$$f_{23} = \frac{W\xi}{2}u'_{\mathrm{B}} + \frac{\epsilon W}{m\left(1-\beta\right)}\tau_{xy\mathrm{B}},$$

$$f_{31} = \frac{\epsilon W}{m\left(1-\beta\right)}\tau_{yy\mathrm{B}},$$

$$f_{32} = -W\left(2-\xi\right)u'_{\mathrm{B}},$$

$$f_{33} = Wi\psi u_{\mathrm{B}} + W\sigma + 1 + \frac{\epsilon W}{m\left(1-\beta\right)}\left(\tau_{xx\mathrm{B}} + 2\tau_{yy\mathrm{B}}\right),$$

and

$$
\begin{aligned}
g_1 = g_A\bar{v} + g_B\bar{v}' + g_C\bar{v}'', \qquad & g_A = -W{\tau_{xx_{\mathrm{B}}}}' + W\left(2-\xi\right)i\psi\tau_{xy_{\mathrm{B}}},\\
& g_B = -2W\left(1-\xi\right)\tau_{xx_{\mathrm{B}}} - 2m\left(1-\beta\right),\\
& g_C = \frac{-W\xi i}{\psi}\tau_{xy_{\mathrm{B}}},\\
g_2 = g_D\bar{v} + g_E\bar{v}'', \qquad & g_D = -W{\tau_{xy_{\mathrm{B}}}}' - \frac{W\xi}{2}i\psi\tau_{xx_{\mathrm{B}}}\\
& \quad + W\left(1-\frac{\xi}{2}\right)i\psi\tau_{yy_{\mathrm{B}}} + im\psi\left(1-\beta\right),\\
& g_E = \frac{iW}{\psi}\left(1-\frac{\xi}{2}\right)\tau_{xx_{\mathrm{B}}} - \frac{Wi\xi}{2\psi}\tau_{yy_{\mathrm{B}}}\\
& \quad + \frac{im}{\psi}\left(1-\beta\right),\\
g_3 = g_F\bar{v} + g_G\bar{v}' + g_H\bar{v}'', \qquad & g_F = -W{\tau_{yy_{\mathrm{B}}}}' - W\xi i\psi\tau_{xy_{\mathrm{B}}},\\
& g_G = 2W\left(1-\xi\right)\tau_{yy_{\mathrm{B}}} + 2m\left(1-\beta\right),\\
& g_H = W\left(2-\xi\right)\frac{i}{\psi}\tau_{xy_{\mathrm{B}}}.
\end{aligned}
$$

Expressions for the perturbed stresses can then be derived in terms of the disturbance cross channel velocity, $\bar{v}$, by using Gaussian elimination. The matrix (G.7) then reduces to,

$$
\left(\begin{array}{ccc|c}
f_{11} & f_{12} & f_{13} & g_1\\
0 & h_1 & h_3 & h_5\\
0 & 0 & h_1h_4 - h_2h_3 & h_1h_6 - h_2h_5
\end{array}\right) \tag{G.8}
$$

where

$$h_1 = f_{11}f_{22} - f_{12}f_{21}, \qquad h_2 = f_{11}f_{32} - f_{12}f_{31},$$

$$h_3 = f_{11}f_{23} - f_{13}f_{21}, \qquad h_4 = f_{11}f_{33} - f_{13}f_{31},$$

$$h_5 = f_{11}g_2 - f_{21}g_1, \qquad h_6 = f_{11}g_3 - f_{31}g_1.$$

The elements in the matrix (G.8) can be used to find expressions for the disturbance stress terms by back substitution. These terms are then differentiated as required and substituted into equation (E.7) to give the full Orr-Somerfeld equation in terms of the perturbed cross-channel velocity, $\bar{v}$. As for the Giesekus fluid model this is a fourth-order ordinary differential equation.

Appendix H

Branch Cuts of the Orr-Sommerfeld Equation for Phan-Thien Tanner Fluids

In this Appendix a sixth order polynomial equation for the eigenvalue σ is derived. The solutions for this equation have not been found, but are known to be the branch cuts of the Orr-Sommerfeld equation for Phan-Thien Tanner fluids. The polynomial is derived using the same method as was used to find the cubic equation (F.1), the solutions of which describe the branch cuts of the Orr-Sommerfeld equation for Giesekus fluids. The branch cuts which are sought occur when the coefficient of the highest derivative of $\bar{v}$ vanishes. For the Orr-Sommerfeld equation for Phan-Thien Tanner fluids the highest derivative is known to be of order four. Again, equations for the multiple fluid problems are used with the omission of

the subscripts.

Extracting coefficients from each of the linearized stability equations (3.33)-(3.35) and (3.39)-(3.41) gives contributions to the fourth order coefficient as

$$\underbrace{\frac{mi\beta}{\psi}}_{\star^3} + \underbrace{\frac{h_1 h_4 \left(f_{11} g_E - f_{21} g_C\right) + h_1 h_3 \left(f_{31} g_C - f_{11} g_H\right)}{h_1^2 h_4 + h_1 h_2 h_3}}_{\star^4} = 0$$

where

$\star^3$ From differentiating $\bar{u}''$ in the first Navier-Stokes equation and substituting continuity.

$\star^4$ From differentiating the term $\bar{\tau}'_{xy}$ in the first Navier-Stokes equation. The expression for $\bar{\tau}_{xy}$ is found by back substitution of the terms in matrix (G.7).

Here, the functions f_{ij}, g_K and h_m are defined as in Appendix G. Substituting for f_{ij}, g_K

and h_m accordingly gives the following sixth order polynomial for σ,

$$
\begin{aligned}
&\frac{mi\beta}{\psi}W^6\sigma^6 + \left[\frac{mi\beta}{\psi}\left(2h_1^1 + h_4^1\right) + g_E\right]W^5\sigma^5 \\
&+\left[\frac{mi\beta}{\psi}\left(h_4^0 + 2h_1^1h_4^1 + 2h_1^0 + \left(h_1^1\right)^2 + f_{23}f_{32}\right) + \hat{f}_{11}g_E + (h_1^1 + h_4^1)g_E - f_{21}g_C - f_{23}g_H\right]W^4\sigma^4 \\
&\quad + \frac{mi\beta}{\psi}\left[2h_1^1h_4^0 + 2h_4^1h_1^0 + (h_1^1)^2h_4^1 + 2h_1^0h_1^1 + f_{23}h_2^0 + h_3^0f_{32} + h_1^1f_{23}f_{32}\right]W^3\sigma^3 \\
&\quad + \left[\left(\left(h_1^1 + h_4^1\right)\hat{f}_{11} + h_4^0 + h_1^1h_4^1 + h_1^0\right)g_E + \left(f_{23}f_{31} - \left(h_1^1h_4^1\right)f_{21}\right)g_C\right]W^3\sigma^3 \\
&\quad - \left[f_{23}\hat{f}_{11} + h_3^0 + h_1^1f_{23}\right]g_HW^3\sigma^3 \\
&+\frac{mi\beta}{\psi}\left[2h_1^0h_4^0 + \left(h_1^1\right)^2h_4^0 + 2h_1^1h_4^1h_1^0 + \left(h_1^0\right)^2 + h_3^0h_2^0 + h_1^1h_2^0f_{23} + h_1^1h_3^0f_{32} + h_1^0f_{23}f_{32}\right]W^2\sigma^2 \\
&\quad + \left[\left(\left(h_4^0 + h_1^1h_4^1 + h_1^0\right)\hat{f}_{11} + h_1^1h_4^0 + h_4^1h_1^0\right)g_E + \left(h_3^0 + h_1^1f_{23}\right)f_{32}g_C\right]W^2\sigma^2 \\
&\quad - \left[\left(h_4^0 + h_1^1h_4^1 + h_1^0\right)f_{21}g_C + \left(\left(h_3^0 + h_1^1f_{23}\right)\hat{f}_{11} + h_1^1h_3^0 + h_1^0f_{23}\right)g_H\right]W^2\sigma^2 \\
&\quad + \frac{mi\beta}{\psi}\left[2h_1^1h_1^0h_4^0 + h_4^1\left(h_1^0\right)^2 + h_1^1h_3^0h_2^0 + h_1^0h_2^0f_{23} + h_1^0h_3^0f_{32}\right]W\sigma \\
&\quad + \left[\left(\left(h_1^1h_4^0 + h_4^1h_1^0\right)\hat{f}_{11} + h_1^0h_4^0\right)g_E + \left(h_1^1h_3^0 + h_1^0f_{23}\right)f_{31}g_C\right]W\sigma \\
&\quad - \left[\left(h_1^1h_4^0 + h_4^1h_1^0\right)f_{21}g_C + \left(\left(h_1^1h_3^0 + h_1^0f_{23}\right)\hat{f}_{11} + h_1^0h_3^0\right)g_H\right]W\sigma \\
&+\frac{mi\beta}{\psi}\left(\left(h_1^0\right)^2h_4^0 + h_1^0h_2^0h_3^0\right) + h_1^0h_4^0\hat{f}_{11}g_E + \left(h_3^0f_{31} - h_4^0f_{21}\right)h_1^0g_C - h_1^0h_3^0\hat{f}_{11}g_H. \quad \text{(H.1)}
\end{aligned}
$$

Here

$$\hat{f}_{11} = Wi\psi u_{\mathrm{B}} + 1 + \frac{2\epsilon W}{m\,(1-\beta)}\tau_{xx\mathrm{B}} + \frac{\epsilon W}{m\,(1-\beta)}\tau_{yy_{\mathrm{B}}}.$$

The terms h_i^j are the coefficients of $W^j\sigma^j$ in expansions of the expressions for h_i as given in

Appendix G. Thus

$$h_1 = W^2\sigma^2 + W\sigma h_1^1 + h_1^0, \qquad h_2 = W\sigma f_{32} + h_2^0,$$

$$h_3 = W\sigma f_{23} + h_3^0, \qquad h_4 = W^2\sigma^2 + W\sigma h_4^1 + h_4^0,$$

and

$$h_1^1 = \hat{f}_{11} + \hat{f}_{22}, \qquad h_1^0 = \hat{f}_{11}\hat{f}_{22} - f_{12}f_{21},$$

$$h_2^0 = \hat{f}_{11}f_{32} - f_{12}f_{31}, \qquad h_3^0 = \hat{f}_{11}f_{23} - f_{13}f_{21},$$

$$h_4^1 = \hat{f}_{11} + \hat{f}_{33}, \qquad h_4^0 = \hat{f}_{11}\hat{f}_{33} - f_{13}f_{31},$$

where

$$\hat{f}_{22} = Wi\psi u_{\mathrm{B}} + 1 + \frac{\epsilon W}{m\,(1-\beta)}\left(\tau_{xx\mathrm{B}} + \tau_{yy\mathrm{B}}\right),$$

$$\hat{f}_{33} = Wi\psi u_{\mathrm{B}} + 1 + \frac{\epsilon W}{m\,(1-\beta)}\left(\tau_{xx\mathrm{B}} + 2\tau_{yy\mathrm{B}}\right).$$

No solution has yet been found for this polynomial but it has been stated here for completeness.

Bibliography

[1] http://scienceworld.wolfram.com/physics/BoltzmannsConstant.html

[2] http://www.sizes.com/natural/Avogadro.htm

[3] http://en.wikipedia.org/wiki/Polymer_banknote

[4] http://en.wikipedia.org/wiki/Extrusion#Road_marking_compound

[5] NAG Library Mark 22, NAG, Oxford, UK.

[6] Alves M. A., Pinho F. T., Oliviera P. J. Study of steady pipe and channel flows of a single-mode Phan-Thien Tanner fluid. *J. Non-Newtonian Fluid Mech.* **101** pp. 55-76 2001.

[7] Anturkar N. R., Papanastasiou T. C., Wilkes J. O. Linear stability analysis of multi-layer plane Poiseuille flow *Phys. Fluids A* **2** pp. 530-541 1990.

[8] Bird R. B., Hassager O., Armstrong R. C., Curtiss C. F. Dynamics of Polymeric Liquids, Vol. II: Kinetic Theory. *Wiley*, New York 1977.

[9] Bogaerds A. C. B., Grillet A. M., Peters G. W. M., Baaijens F. P. T. Stability analysis of polymer shear flows using the eXtended Pom-Pom constitutive equations. *J. Non-Newtonian Fluid Mech.* **108** pp. 187-208 2002.

[10] Canuto C., Hussaini M. Y., Quarteroni A., Zang T. A. Spectral Methods in Fluid Dynamics. *Springer-Verlag*, Berlin 1988.

[11] Chen K. P. Elastic instability of the interface in Couette flow of viscoelastic liquids *J. Non-Newtonian Fluid Mech.* **40** pp. 261-267 1991.

[12] Cruz D. O. A., Pinho F. T. Fully-developed pipe and planar flows of multimode viscoelastic fluids. *J. Non-Newtonian Fluid Mech.* **141** pp. 85-98 2007.

[13] Cruz D. O. A., Pinho F. T., Oliviera P. J. Analytical solutions for fully developed laminar flow of some viscoelastic liquids with a Newtonian solvent contribution. *J. Non-Newtonian Fluid Mech.* **132** pp. 28-35 2005.

[14] Curtiss C. F., Bird R. B., Hassager O. Kinetic theory and rheology of macromolecular solutions. *Adv. Chem. Phys.* **35** pp. 31-117 1976.

[15] Curtiss C. F., Bird R. B. A kinetic theory for polymer melts. I. The equation for the single-link orientational distribution function. *J. Chem. Phys.* **74** pp. 2016-2025 1981.

[16] Curtiss C. F., Bird R. B. A kinetic theory for polymer melts. II. The stress tensor and the rheological equation of state. *J. Chem. Phys.* **74** pp. 2026-2033 1981.

[17] de Gennes P.-G. Reptation of a polymer chain in the presence of fixed obstacles. *J. Chem. Phys.* **5** pp. 572-579 1971.

[18] Doi M., Edwards S. F. The Theory of Polymer Dynamics. *Oxford University Press*, Oxford 1986.

[19] Doi M., Edwards S. F. Dynamics of concentrated polymer systems. Part 1 - Brownian motion in the equilibrium state. *J. Chem. Soc. Faraday Trans II* **74** pp. 1789-1801 1978.

[20] Doi M., Edwards S. F. Dynamics of concentrated polymer systems. Part 2 - Molecular motion under flow. *J. Chem. Soc. Faraday Trans II* **74** pp. 1802-1817 1978.

[21] Doi M., Edwards S. F. Dynamics of concentrated polymer systems. Part 3 - The constitutive equation. *J. Chem. Soc. Faraday Trans II* **74** pp. 1819-1832 1978.

[22] Doi M., Edwards S. F. Dynamics of concentrated polymer systems. Part 4 - Rheological properties. *J. Chem. Soc. Faraday Trans II* **75** pp. 38-54 1979.

[23] Edwards S. F. The statistical mechanics of polymerized material. *Proc. Phys. Soc.* **92** pp. 9-16 1967.

[24] Ferry J. D. Viscoelastic Properties of Polymers. *Wiley*, New York 1961.

[25] Giesekus H. Elasto-viskose Flüssigkeiten, für die in stationären Schichtströmungen sämtliche Normalspannungskomponenten verschieden gross sind. *Rheologica Acta* **2** pp. 50-62 1962.

[26] Giesekus H. Die rheologische Zustandsgleichung von elasto-viskosen Flüssigkeiten - insbensondere von Weissenberg-Flüssigkeiten - fü allgemeine und stationäre Fliessvorgänge. *Z. Angew. Math. Mech.* **42** pp. 32-61 1962.

[27] Giesekus H. Einige ergänzende Bemerkungen zur Darstellung der rheologischen Zustandsgleichung nach Weissenberg und Grossman. *Z. Angew. Math. Mech.* **42** pp. 259-262 1962.

[28] Giesekus H. Statistical rheolology of suspensions and solutions with special reference to normal stress effects. In *Second-Order Effects in Elasticity, Plasticity and Fluid Dynamics.* Eds. M. Reiner, D. Abir pp. 553-584. Macmillan, New York 1964.

[29] Giesekus H. A simple constitutive equation for polymer fluids based on the concept of deformation-dependent tensorial mobility. *J. Non-Newtonian Fluid Mech.* **11** pp. 69-109 1982.

[30] Gorodtsov V. A., Leonov A. I. On a linear instability of a plane parallel Couette flow of viscoelastic fluid. *J. Applied Math. Mech.-USSR* **31** pp. 289-299 1967.

[31] Grillet A. M., Bogaerds A. C. B., Peters G. W. M. and Baaijens F. P. T. Stability analysis of constitutive equations for polymer melts in viscometric flows. *J. Non-Newtonian Fluid Mech.* **103** pp. 221-250 2002.

[32] Guillopé C., Saut J.-C. Global existence and one-dimensional nonlinear stability of shearing motions of viscoelastic fluids of Oldroyd type. *Mathematical Modelling and Numerical Analysis - Modèlisation Mathèmatique et Analyse Numèrique* **24** pp. 369-401 1990.

[33] Han C. D. Rheology in Polymer Processing. *Academic Press*, New York 1976.

[34] Ho T. C., Denn M. M. Stability of plane Poiseuille flow of a highly elastic liquid. *J. Non-Newtonian Fluid Mech.* **3** pp. 179-195 1977/8.

[35] Hooper A. P. Long-wave instability at the interface between two viscous fluids: Thin layer effects. *Phys. Fluids***28** pp. 1613-1618 1985.

[36] Hooper A. P., Boyd W. G. C. Shear-flow instability at the interface between two viscous fluids. *J. Fluid Mech.* **128** pp. 507-528 1983.

[37] Joseph D. D., Renardy Y. Y. Fundamentals of Two Fluid Dynamics Part I: Mathematical Theory and Applications. *Springer-Verlag*, New York 1993.

[38] Khomami B., Renardy Y., Su K. C., Clarke M. A. An experimental/theoretical investigation of interfacial instabilities in superposed pressure-driven channel flow of Newtonian and well characterized viscoelastic fluids. Part II: Nonlinear stability. *J. Non-Newtonian Fluid Mech.* **91** pp. 85-104 2000.

[39] Khomami B., Su K. C. An experimental/theoretical investigation of interfacial instabilities in superposed pressure-driven channel flow of Newtonian and well characterized viscoelastic fluids. Part I: Linear stability and encapsulation effects. *J. Non-Newtonian Fluid Mech.* **91** pp. 59-84 2000.

[40] Kwon Y. On instability of the Doi-Edwards model in simple flows. *J. Non-Newtonian Fluid Mech.* **88** pp. 89-98 1999.

[41] Larson R. G. Instabilities in viscoelastic flows. *Rheologica Acta* **31** pp. 213-263 1992.

[42] Laure P., Le Meur H., Demay Y., Saut J. C., Scotto S. Linear stability of multilayer plane Poiseuille flows of Oldroyd B fluids. *J. Non-Newtonian Fluid Mech.* **71** pp. 1-23 1997.

[43] Leigh D. C. Non-Linear Continuum Mechanics. *McGraw-Hill*, New York 1968.

[44] Leslie F. M. The stability of Couette flow of certain anisotropic fluids. *Proc. Camb. Phil. Soc.* **60** pp. 949-955 1964

[45] Lodge A. S. Constitutive equations from molecular theories for polymer solutions. *Rheologica Acta* **7** pp. 379-392 1968.

[46] McLeish T. C. B., Larson R. G. Molecular constitutive equations for a class of branched polymers: The pom-pom polymer. *J. Rheology* **42** pp. 81-110 1998.

[47] Palmer A. S., Phillips T. N. Numerical approximation of the spectra of Phan-Thien Tanner liquids. *Num. Alg.* **38** pp. 133-153 2005.

[48] Palmer A. S., Phillips T. N. Numerical approximation of the spectra of Poiseuille flow of two Phan-Thien Tanner liquids. In *Proceedings of the Third MIT Conference on Computational Fluid and Solid Mechanics* Ed. K.-J. Bathe pp. 792-796. *Elsevier Science* 2005.

[49] Pearson J. R. A., Petrie C. J. S. On the melt flow instability of extruded polymers. *Proc. 4th Int. Cong. Rheol.* **Part 3** pp. 265-281 1965

[50] Pearson J. R. A., Petrie C. J. S. On melt flow instability of extruded polymers. In *Polymer Systems: Deformation and Flow* Eds. Wetton R. E., Whorlow R. W. pp. 163-187 *Macmillan*, London 1968

[51] Phan-Thien N. A nonlinear network viscoelastic model. *J. Rheology* **22** pp. 259-283 1978.

[52] Phan-Thien N., Tanner R. I. A new constitutive equation derived from network theory. *J. Non-Newtonian Fluid Mech.* **2** pp. 353-365 1977.

[53] Porteous K. C., Denn M. M. Linear stability of plane Poiseuille flow of viscoelastic liquids. *Trans. Soc. Rheology* **16** pp. 295-308 1972.

[54] Porteous K. C., Denn M. M. Nonlinear stability of plane Poiseuille flow of viscoelastic liquids. *Trans. Soc. Rheology* **16** pp. 309-319 1972.

[55] Renardy M., Renardy Y., Linear stability of plane Couette flow of an upper convected Maxwell fluid. *J. Non-Newtonian Fluid Mech.* **22** pp. 23-33 1986.

[56] Renardy Y. Instability at the interface between two shearing fluids in a channel *Phys. Fluids* **28** pp. 3441-3443 1985.

[57] Renardy Y. The thin-layer effect and interfacial stability in a two-layer Couette flow with similar liquids. *Phys. Fluids* **30** pp. 1627-1637 1987.

[58] Renardy Y. Stability of the interface in two-layer Couette flow of Upper Convected Maxwell liquids. *J. Non-Newtonian Fluid Mech.* **28** pp. 99-115 1988.

[59] Renardy Y. Weakly nonlinear behaviour of periodic disturbances in two-layer Couette Poiseuille flow. *Phys. Fluids A* **1** pp. 1666-1676 1989.

[60] Rouse P. E. Jr. A theory of linear viscoelastic properties of dilute solutions of coiling polymers. *J. Chem. Phys.* **21** pp. 1272-1280 1953.

[61] Scotto S., Laure P. Linear stability of three-layer Poiseuille flow for Oldroyd-B fluids. *J. Non-Newtonian Fluid Mech.* **83** pp. 71-92 1999.

[62] Su Y. Y., Khomami B. Purely elastic interfacial instabilities in superposed flow of polymeric fluids *Rheologica Acta* **31** pp. 413-420 1992.

[63] Verbeeten W. M. H., Peters G. W. M., Baaijens F. T. P. Differential constitutive equations for polymer melts: the extended pom-pom model. *J. Rheology* **45** pp. 823-843 2001.

[64] Wilson H. J., Rallison J. M. Short wave instability of co-extruded elastic liquids with matched viscosities. *J. Non-Newtonian Fluid Mech.* **72** pp. 237-251 1997.

[65] Wilson H. J., Renardy M., Renardy Y. Y. Structure of the spectrum in zero Reynolds number shear flow of the UCM and Oldroyd-B liquids. *J. Non-Newtonian Fluid Mech.* **80** pp. 251-268 1999.

[66] Yamamoto M. The visco-elastic properties of network structure I. General formalism. *J. Phys. Soc. Japan* **11** pp. 413-421 1956.

[67] Yamamoto M. The visco-elastic properties of network structure II. Structural viscosity. *J. Phys. Soc. Japan* **12** pp. 1148-1158 1957.

[68] Yamamoto M. The visco-elastic properties of network structure III. Normal stress effect (Weissenberg effect). *J. Phys. Soc. Japan* **13** pp. 1200-1211 1958.

[69] Yih C. S. Instability due to viscosity stratification. *J. Fluid Mech.* **27** pp. 337-352 1967.